Distinguishing flood frequency and magnitude in the morphodynamics and sedimentology of rivers: Insights from the South Saskatchewan River, Canada

by

Natalie Olwyn Parker

A thesis submitted to
The University of Birmingham
for the degree of
DOCTOR OF PHILOSOPHY

School of Geography, Earth and
Environmental Sciences
The University of Birmingham
February 2010

1st of 2 files

Introductory material and chapters 1 to 4

The remaining chapters are in an additional file

ABSTRACT

There is currently a lack of research surrounding the morphological impact and preservation potential of different flow events; for example, large floods versus more frequent, annual flood events. This research aimed to assess the impact of a 1 in 40 year flood on the morphology and sedimentology of the sandy braided South Saskatchewan River, Canada, and; therefore, to establish the relative importance of high-magnitude low-frequency flood events to the geomorphological and sedimentological evolution of sandy braided rivers.

A four year dataset (2004 to 2007) on subsurface sedimentology from extensive repeat GPR surveys of compound bars was analysed, coupled with the production of annual DEMs from aerial photographs. Comparison of GPR surveys, and the production of DEMs of difference allowed quantification of the initial and long-term 2005 flood impact on sedimentology and reach morphology.

The main results show that even though a significant initial morphological impact was caused due to the flood through net erosion throughout the reach and channel incision across compound bars, subsequent low-magnitude high-frequency floods were able to rework morphology, including net deposition of sediment 2005 to 2006, and the formation and migration of unit bars. This was thought to be due to the ability of low-magnitude floods to transport the medium sized sand bed load. In the subsurface, no distinct flood signature has been left. The 2005 flood deposits are similar to the scale and composition of deposits produced by low-magnitude high-frequency floods under conditions of bar overtopping. Furthermore, the 2005 flood deposits have a similar preservation potential to low-magnitude high-frequency flood deposits. Consequently, little evidence of such a flood event will be preserved in the sedimentary record.

In addition, research on the South Saskatchewan has highlighted some important key

findings with respect to linking morphological processes to sedimentary deposits. It has been suggested that depositional models may need revising in order to take into account the preservation of deposits more explicitly. Further detailed research on subsurface deposits will help to clarify which parts of bars and bedforms get preserved and thus provide a more robust analogue for ancient deposits. It has also been established that difficulties can exist in the reconstruction of flow depths from bedform dimensions in natural rivers due to factors such as dune lag, and that this can have implications for accurate reconstruction of flow conditions from ancient deposits.

The results from this thesis have wider applications to sand bed braided rivers that display similar channel characteristics. Such rivers include some of the largest channels in the world e.g. the Jamuna (Brahmaputra), Bangladesh and the Paraná, Argentina, and contribute to a large proportion of the sedimentological record. Thus, the findings presented here may aid interpretation and modelling of such deposits on a wider scale.

ACKNOWLEDGEMENTS

A huge thank you goes to my supervisor Greg for his encouragement, enthusiasm, and patience! Also thanks for introducing me to the wonders of Dropbox and Mumford and Sons, key factors in helping the write up! Thanks also goes to Stuart Lane, Rob Thomas and Penny Widdison for their invaluable help and advice on DEM processing and interpretation. One of the most enjoyable aspects of the PhD research was the fieldwork in Canada and Argentina. Thanks to all who took part, and made it such a memorable experience. Also, a big thank you to Kevin Burkhill at GEES for the unit bar diagrams and your help with printing!

A special thank you goes to my husband Matt who has supported me through the highs and lows of this PhD! I am looking forward to finally having lots of free time to spend with you. Mam and Dad, thanks for all your support, and for being so optimistic and enthusiastic about everything! Thanks to Nobby and Sue for taking us under your wing during the past few months of writing up, we are so grateful! Last but not least, thanks to Colin the cat who has been really good company whilst writing up!

CONTENTS

LIST OF FIGURES

a sandy braided river, based on the South Saskatchewan: i) a simple unit bar contains facies 1 deposits at the margins due to bar migration; ii) a simple compound bar formed from the amalgamation of 2 unit bars displays decreased percentages of facies 1 due to truncation at the converging unit bar margins, and production of facies 4 where a cross bar channel has formed between the unit bars; iii) a compound bar composed of numerous stacked unit bars displays minor percentages of facies 1 and facies 3 deposits below the bar surface due to unit bar truncation over time. Compound bars are therefore dominated by facies 2 deposits. The truncation of unit bars in this way is similar due to different magnitude-frequency flows and thus the impact of different flood events is not distinguishable in their sedimentology.

282-283

LIST OF TABLES

LIST OF EQUATIONS

[2.1] $$\Theta = \tau_0 / (\sigma-\rho)gD$$

Dimensionless shear stress (Θ) is a function of bed shear stress (τ_0), grain density (σ), fluid density (ρ), acceleration of gravity (g) and grain diameter (D). 27

[2.2] $$Re_b = U_* D/\nu$$

The boundary grain Reynolds number (Re_b) is a function of the threshold shear velocity (U_* ($= (\tau_0/\rho)^{0.5}$)), grain diameter (D) and the fluid's kinematic viscosity (ν). 27

[4.1] $$t = \frac{1000}{6f}$$

t is sampling interval (ns), f is centre frequency (MHz) (Sensors and Software, n.d, p.9). 59

[4.2] $$v_1 = \sqrt{\left[\left(x_2^2 - x_1^2\right)/\left(t_{x_2}^2 - t_{x_1}^2\right)\right]}$$

The average velocity for a reflection (v_1). x_1 and x_2 are antenna separations and t_{x1} and t_{x2} are the two-way travel times at the antenna separations (Robinson and Çoruh, 1988, p.89). 63

[4.3] $$D = V \times T/2$$

D is depth, V is velocity (m/ns) and T is two-way travel time (ns) (Sensors and Software, 2005). 63

[4.4] $$\begin{bmatrix} x \\ y \\ -c \end{bmatrix} = kM \begin{bmatrix} X - Xo \\ Y - Yo \\ Z - Zo \end{bmatrix}$$

The projective transformation. (X,Y,Z) are object point coordinates, (X_0,Y_0,Z_0) is the perspective centre of the lens, (x,y,z) is a point in the 2D image, -c is the cameras focal length, k is a scale factor, and M is a rotation matrix with elements m_{11}…m_{33} which are functions of ω, κ and φ (camera orientation parameters) (Lane *et al.*, 1993). 80

[4.5] $$x = \frac{-c\left[m_{11}(X - X_0) + m_{12}(Y - Y_0) + m_{13}(Z - Z_0)\right]}{\left[m_{31}(X - X_0) + m_{32}(Y - Y_0) + m_{33}(Z - Z_0)\right]}$$

A collinearity equation for image point x. See [4.3] for symbol definitions. 80

[4.6] $$y = -c\frac{[m_{21}(X - X_0) + m_{22}(Y - Y_0) + m_{23}(Z - Z_0)]}{[m_{31}(X - X_0) + m_{32}(Y - Y_0) + m_{33}(Z - Z_0)]}$$

A collinearity equation for image point *y*. See [4.3] for symbol definitions. 80

[4.7] $$\sigma_e{}^2 = \frac{1}{n-1}\sum_{i=1}^{n}(e_i - \bar{e}_i)^2$$

The variance of error (σ_e^2). σ_e is the standard deviation of error, n is the number of observations, *ei = zei – zci; zei* is the DEM estimated elevation of point *i, zci* is the independently measured elevation of point *i* (Lane *et al.*, 2004). 87

[4.8] $$\sigma_e = \left(\sigma_{e_1}^2 + \sigma_{e_2}^2\right)^{0.5}$$

The standard deviation of error (σ_e) of a DEM of difference. σ_{e1} and σ_{e2} are the standard deviations of error of individual DEMs (Lane *et al*.,1993). 88

[4.9] $$X_i = \ln L_i - Lw_{(i)}$$

Relationship between depth and light intensity. X_i is a parameter linearly related to the depth of water (in band *i*), L_i is water brightness and $Lw_{(i)}$ represents the deep water reflectance (Lyzenga, 1981). 90

[4.10] **Predicted depth = (G*ln(DN – extinction DN)) + I**

Predicted depth for DN values > extinction depth DN. DN is pixel digital number (or brightness), G is the gradient, and I is the intercept calculated from linear regression analysis between real depth and ln(DN – extinction depth). 98

[4.11] **Predicted depth = extinction depth**

Predicted depth for DN values <= extinction depth DN. See [4.9] for symbol definition. 98

ABBREVIATIONS

AGC	Automatic Gain Control
CMP	Common Mid Point
CO	Common Offset
DEM	Digital Elevation Model
DGPS	Differential Global Positioning System
DN	(pixel) Digital Number
GCP	Ground Control Point
GIS	Geographical Information System
GPR	Ground Penetrating Radar
GPS	Global Positioning System
IHS	Intensity Hue Saturation (colourspace)
LiDAR	Light Detection And Ranging
LPS	Leica Photogrammetry Suite
NAD83	North American Datum 1983
pdf	probability density function
RGB	Red Green Blue (colourspace)
RMSE	Root Mean Square Error
VA	Vertical Accuracy

1 INTRODUCTION

1.1 RESEARCH AREA BACKGROUND

Braided channels are prevalent across the globe and form some of the largest rivers in the world, e.g. the Jamuna (Brahmaputra), Bangladesh and the Paraná, Argentina. They are an important topic of research from a geomorphological perspective with respect to the dynamics of sediment transport processes (Bristow and Best, 1993). The varied depositional environment of braided rivers also has economical importance in the form of aquifers and hydrocarbon reserves (Martin, 1993). In order to exploit these resources, detailed knowledge is required on processes of braiding and their relationship to deposits preserved in the sedimentary record. Historically, research on braided rivers has been limited compared with other fluvial environments such as meandering rivers (Bristow and Best, 1993). Previous studies of braided rivers have often relied heavily on ground surveys to determine morphological change (Westaway *et al*, 2003) and bank exposures and trenches to observe sedimentary deposits (Lunt *et al*, 2004). However, these methods have associated temporal and spatial constraints, for example, observations and cross sectional surveys are often not carried out at frequent intervals to gain information on channel migration and bedform evolution (Westaway *et al*, 2003; Lunt *et al*, 2004). Likewise, observations of deposits are restricted to those above the water table (Lunt *et al*, 2004). In the past decade however, advances in technology such as digital photogrammetry and ground penetrating radar (GPR) have allowed the quantification of morphological change (Winterbottom and Gilvear, 1997; Lane *et al*., 2003), and the detailed 3-dimensional visualisation of subsurface deposits, including those under the water table (Bridge *et al*, 1998; Best *et al*, 2003; Skelly *et al*., 2003; Wooldridge and Hickin, 2005; Sambrook Smith *et al*, 2006b; Lunt *et al*, In prep.).

These techniques have provided the opportunity to carry out key research in many fields including braided rivers. For example, research is required into the specific links between formative processes of braided bedforms and preservation in the sedimentary record (Sambrook Smith *et al*, 2006b). This has been investigated by combining subsurface deposit GPR data with aerial photography of surface features (Lunt *et al*. 2004; Wooldridge and Hickin, 2005); however, surface morphological evolution has not been linked fully with subsurface deposition. Specifically, there is a lack of research surrounding the surface geomorphic impact and the preservation potential in the subsurface, of different flow events, for example, large floods versus more frequent, annual flood events. Research into the significance of different flood events using techniques such as sequential GPR surveys and digital photogrammetry would aid understanding of modern fluvial deposits, and would place greater confidence in the reconstruction of processes and depositional environments of ancient braided rivers.

1.2 AIMS AND OBJECTIVES

The main aim of this research is to establish the relative importance of high-magnitude low-frequency flood events to the geomorphological and sedimentological evolution of a sandy braided river. This will be achieved by assessing the impact of a 1 in 40 year flood on the morphology and sedimentology of the sandy braided South Saskatchewan River, Canada. To meet this aim this research has the following key objectives:

1. Quantify the nature of bar and channel evolution due to low-magnitude high-frequency flood events by the analysis of aerial photographs taken prior to the 2005 flood, and post-flood in 2006 and 2007.

2. Establish the signature of low-magnitude high-frequency flood events in the depositional record by linking the photogrammetric analysis with GPR surveys from 2004, 2006 and 2007.
3. Determine the immediate impact of the 2005 flood by a) developing digital elevation models (DEM) of difference from aerial photographs taken just before and after the flood and b) comparing repeat GPR surveys taken from the same surveys lines pre- and post-flood.
4. Characterise the longer-term impact of the 2005 flood by completing the same analysis as in objective 3 but several years after the flood event has passed.
5. Based on the analysis in objectives 1-4 above, fully identify the link between surface and subsurface evolution, and quantify the relative importance of different flood events to the evolution of the river, answering the fundamental question, what is preserved in the sedimentary record?

1.3 THESIS STRUCTURE

Chapter 2 gives a review of related literature on the subject. Chapter 3 presents an overview of the study site and places the research into context with previous work on the South Saskatchewan River, with Chapter 4 outlining the methodologies employed in this research. Chapter 5 presents results from photogrammetric analysis of DEMs, and identifies surface evolution of bedforms. Subsurface deposits identified from GPR, and their evolution, are quantified in Chapter 6. Chapter 7 places the results in to context within the wider field of braided rivers, and Chapter 8 concludes the thesis.

2 LITERATURE REVIEW

2.1 BRAIDED RIVERS

2.1.1 Braiding characteristics

Leopold and Wolman (1957) distinguished channel patterns based upon a simple classification of straight, meandering or braided channels. There has followed a number of different classification schemes, some focussing on the number of channels present, e.g. single thread (straight and meandering) or multiple thread (braided and anastomosing) (Rust, 1978a). Others, however, have differentiated between channel patterns by including type of bedload as a factor, for example, Schumm (1981) classified 14 different categories of channel, including transitional types.

Several authors have specified conditions that may be conducive to the development of a braided planform based upon the theory that there is a continuum of channel patterns dependent on factors such as sediment supply, slope and discharge (e.g. Leopold and Wolman, 1957; Schumm and Khan, 1972; Parker, 1976). Ashmore (1991a) divided the conditions into two categories, the first termed 'functional explanations', which relate braiding to certain external conditions. The most commonly suggested of these are an abundant bedload (Kirkby, 1980), erodible banks (Ferguson, 1987), a highly variable discharge, and a slope/discharge threshold (Leopold and Wolman, 1957). However, various laboratory and field studies have shown that some variables such as highly variable discharge are not always a solitary causal factor as braiding has developed under conditions of steady discharge (Schumm and Khan, 1972). However, Ferguson (1987) remarks that methodological discrepancies may have occurred in the field and laboratory studies, resulting in interpretational inaccuracies of the braiding process. The second category Ashmore

(1991a) defines is explanations pertaining to the stability of bedforms. An example of this is Parker (1976) who used a technique to introduce perturbations into a scale model, using a ratio of sediment transport to water transport as a parameter. Parker (1976) deduced that sediment transport is an essential factor for the occurrence of meandering and braiding in alluvial channels. Parker (1976) explained that aggradation often leads to an increase in slope and can force channels to spread out of their banks causing a meandering river to braid. Therefore braiding is favoured where slope and the width: depth ratio (at formative discharges) are of a value high enough to cross this braiding threshold, e.g. when the width: depth ratio is greater than 50 (Fredsøe, 1978).

The process of braiding involves a divergence of flow and bed load flux around alluvial bars (Ashmore, 1991a), thus producing a dynamic fluvial environment characterised by zones of confluence and diffluence (Figure 2.1). Various braiding indexes have been defined to measure the degree of braiding a river exhibits. For example, Hong and Davies' (1979) braiding index is calculated by dividing the total length of bankfull channels by the distance along the main channel (total sinuosity), whereas Ashmore (1991b) defined the index as the mean number of active channels per transect. However, braiding indexes are dependent on stage height and thus may not be a useful measure. Alternatively, ordering schemes defining bar and channel hierarchies have been proposed to reflect the dominance of features

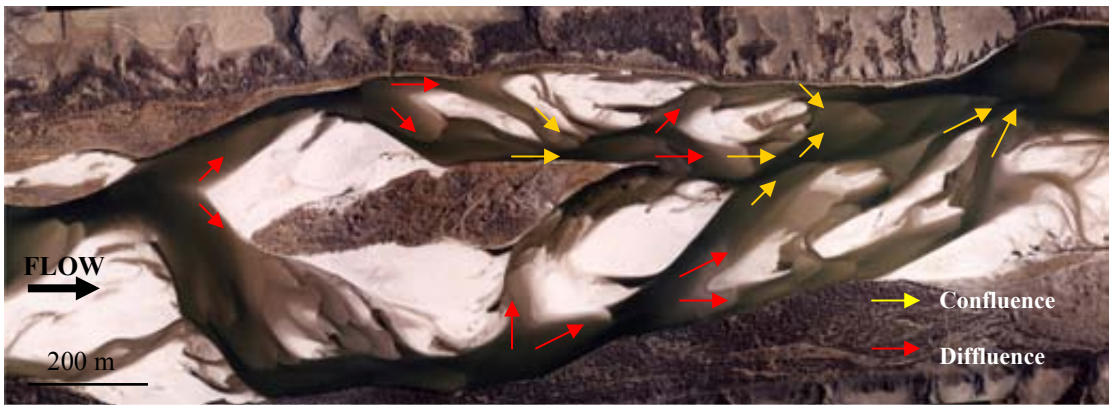

Figure 2.1. Aerial photo of South Saskatchewan River, Canada showing areas of confluence and diffluence.

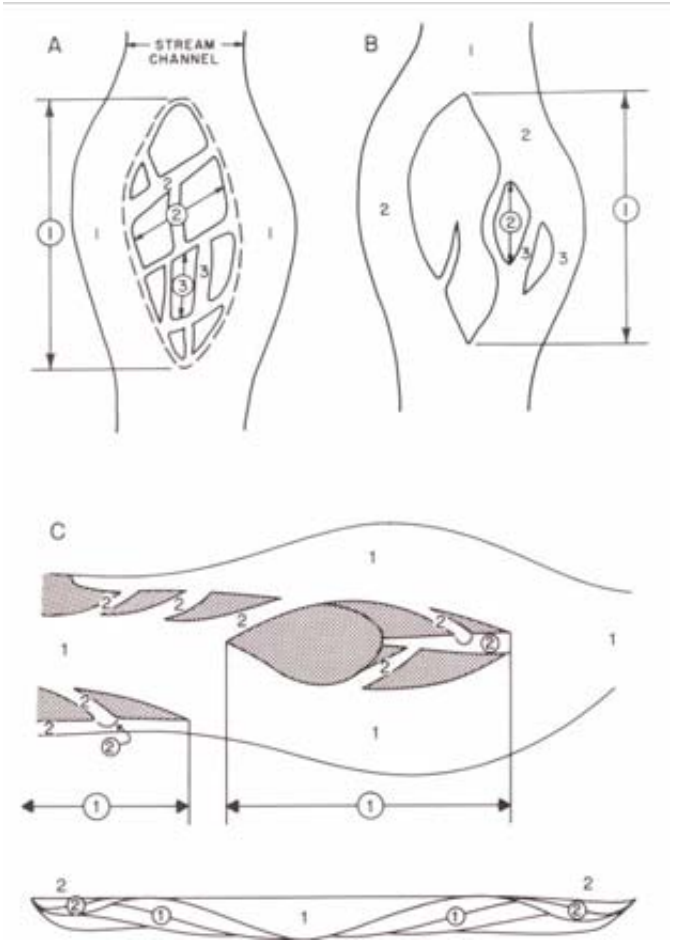

Figure 2.2. Bar and channel hierarchies a) Williams and Rust (1969), b) Bristow (1987) and c) Bridge (1993). Circled numbers refer to bar hierarchies and un-circled numbers refer to channel hierarchies. From Bridge (1993), p. 20, Fig. 3.

at different discharges in braided rivers. For example, Williams and Rust (1969) and Bristow (1987) classified bars and channels into three orders on the Donjek and Brahamuptra rivers respectively (Figure 2.2). However, Bridge (1993) has criticised these hierarchies as being difficult to apply and has suggested an alternative hierarchy system of two orders where second order channels are cross-bar channels and second order bars are formed within second order channels (See Figure 2.2). Hierarchies are also stage dependent so comparing different rivers based on braiding indexes or bar and channel hierarchies may be problematic.

Research has also been conducted on sediment size with respect to the differences between sand and gravel bed braided rivers. For example, Simons and Simons (1987) inferred

that channel patterns and bars are similar in both river types, and that it is only the smaller grain size dependent bedforms that vary (Bristow and Best, 1993). However, sand sized material responds more rapidly to fluctuations in discharge, with dynamic changes in bed elevation occurring through bar formation and channel migration (Simons and Simons, 1987). For gravel bed rivers, these processes may take longer at comparable flows since a higher stream power is required to entrain sediment; thus, there is possibly a distinction between sand and gravel bed rivers with respect to transience in sediment transport. This may have implications for the sedimentary record, with the preservation potential of bedforms depending on the amount of reworking that is possible.

2.1.2 Morphological features of braided rivers

Fluvial bedforms have been differentiated into three fundamental groups based on their size and processes of formation (Jackson, 1975, Allen, 1982a): microforms are the smallest bedforms such as ripples, mesoforms are bedforms such as dunes, and macroforms, the largest bedforms, are bars (Table 2.1). These bedforms are not exclusive to braided rivers however, as they are also found in other river planform types.

Table 2.1. Bedforms commonly found in sand and gravel bed rivers.

	Sand bed	Gravel bed
Microform	Ripples	Pebble clusters, bedload sheets & transverse ribs. Rippled sand ribbons (mixed sand & gravel)
Mesoform	Dunes	Dunes
Macroform	Bars	Bars

2.1.2.1 Microforms

The configuration of microforms such as ripples is controlled by turbulent structures near the bed (inner zone of turbulent boundary layer) (Jackson, 1975). Ripples are formed in fine sands (grain size less than 0.7 mm), with height and length dimensions under 40 mm and 600 mm respectively (Allen, 1982a; Bridge, 2003). Rippled sand ribbons are found in rivers with a heterogeneous bed load and can form with mixed sand and gravel bedloads where sand supply is limited, and flow is inadequate to transport the gravel component of bedload (Lunt *et al*., 2004). Allen (1982b) reported that rippled sand ribbons have wavelengths of approximately twice the depth of flow.

In rivers with gravel bedloads, bedforms such as pebble clusters, bedload sheets and transverse ribs can form. Pebble clusters are an arrangement of large grains closely stacked behind a dominant grain on the upstream face (Lunt *et al*., 2004). Typically, heights are equivalent to widths, and length is double that of the width (Lunt *et al*., 2004). A bedload sheet is a migrating accumulation of sediment (fine gravel or coarse sand) with coarse grains at the leading edge, which is typically up to 2 coarse grains high (Whiting *et al*., 1988). These bedforms may develop on dune stoss sides, therefore promoting dune migration with each subsequent sheet deposition (Whiting *et al*., 1988). Transverse ribs are gravel ridges composed of pebbles, cobbles or boulders, and are located perpendicular to flow direction (McDonald and Banerjee, 1971). They are relatively straight in planform, and no wider than a few clasts (Allen, 1982a). They are known to occur during low flows on bars and in channels (Lunt *et al*., 2004), and may exhibit sediment sorting, with the coarsest particles forming the top of the ridges (McDonald and Banerjee, 1971).

2.1.2.2 Mesoforms

The geometry of mesoforms such as dunes is determined by flow patterns in the outer area of the boundary layer (Jackson, 1975). Due to this, mesoforms have been found to scale with depth, for example, dune height increases with the depth of formative flow (e.g. Yalin, 1964). A range of depth: height ratios have been found ranging from 3 to 20 (Bridge, 2003). However, Bridge (2003) cautions that when measuring dune height in natural rivers, dune geometries may not be in equilibrium with the current flow conditions, as they may be lagging behind. Dunes often lag behind a change in flow due to the volume of sediment that must be moved for their geometries to adjust (Bridge, 2003). Additionally, dune height has been found to be a non-linear function of dimensionless shear stress in unsteady flows (Allen, 1978).

As transport rates increase, dunes are formed on ripple beds in sediments with a mean grain size larger than 0.1 mm (Bridge, 2003). Gravel dunes may develop from bedload sheets (Lunt *et al.*, 2004). The migration of dunes occurs in a downstream fashion, with erosion of sediment occurring on the stoss side of the sedimentary structure and subsequent deposition on the lee side. Dunes possess heights and lengths greater than 40 mm and 600 mm respectively (Allen, 1982a) (See Figure 2.3) and are dynamic features that evolve morphologically as a response to variation in stage heights (Carling *et al.*, 2000). A rising stage can promote an increase in crest height, due to sediment accumulation, whilst a falling or steady stage can generate rapid migration on the lee side and a reduction in dune height thus producing an extended crest (Carling *et al.*, 2000). Morphologically, dune crest lines are usually sinuous or linguoid in planform and stoss sides are planar. Ripples may develop in dune trough areas, between the lee and stoss slopes (Bridge, 2003) (See Figure 2.3). Parsons *et al.* (2005) remark on the importance of dunes in influencing local flow structure and hence

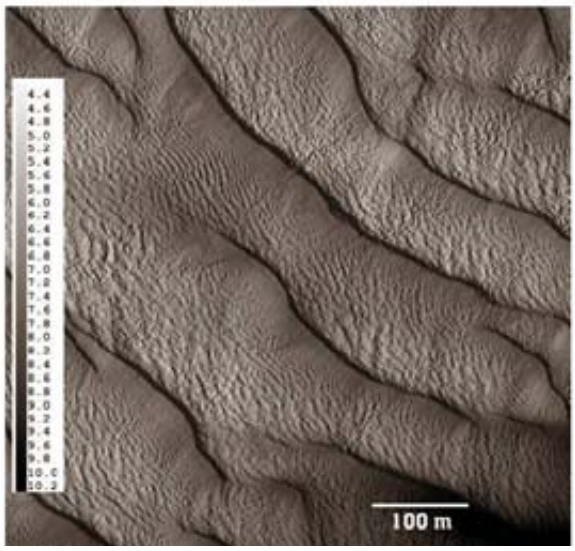

Figure 2.3. Bathymetric map of dunes in the Rio Paranà, Argentina. Note superimposed bedforms on dune surfaces. Flow is top right to bottom left and scale is depth in metres. From Parsons *et al.* (2005), p. 5, Fig. 4.

sediment transport and deposition.

2.1.2.3 Macroforms

Microforms and mesoforms are often superimposed upon the surface of macroforms (Sambrook Smith *et al.*, 2006a). Macroforms are larger morphological structures such as bars, which develop in response to the geomorphological regime of the environment (Jackson, 1974). Their geometry is controlled by local flow and sediment transport (Bridge, 2003). A bar will be defined herein as "a bedform whose length is proportional to channel width and whose height is comparable with the mean depth of the formative flow" (ASCE, 1966, p.53).

There are two principal bar types present in braided rivers: unit bars and compound bars (Lunt and Bridge, 2004; Lunt *et al*, 2004; Sambrook Smith *et al*, 2006a). Typically, unit bars have a lobate planform (See Figure 2.4), and a relatively simple history of formation (Smith, 1974). Flume experiments and theoretical models have attributed unit bar formation in straight channels due to the instability of flow and erodible beds, and the subsequent

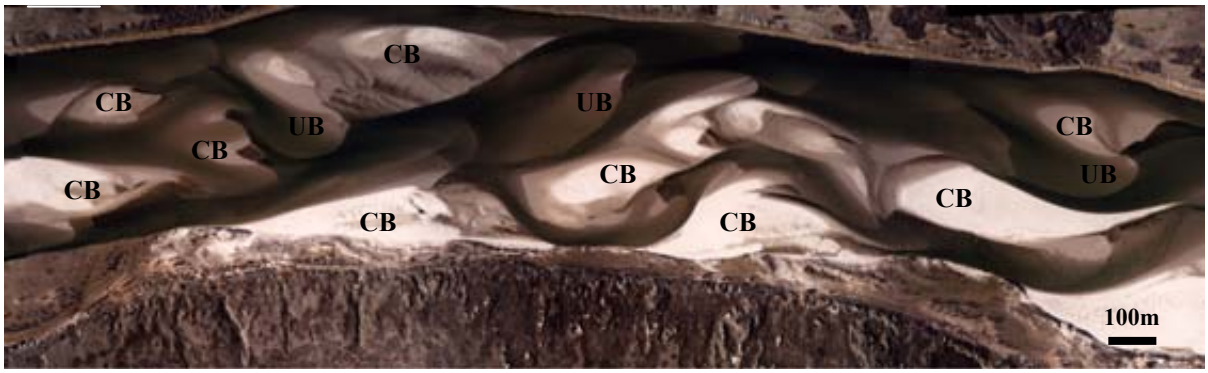

Figure 2.4. Unit and compound bars in the South Saskatchewan, Canada. Mosaic of 2006 aerial photographs.

creation of spontaneous perturbations on the bed which form deep (pool) and shallow (riffle) reaches (e.g. Callander, 1969; Engelund and Skovgaard, 1973; Parker, 1976; Tubino, 1991; Lanzoni, 2000). These alternate (unit) bars grow in length and height in equilibrium with flow and sediment conditions, and migrate downstream (Federici and Seminara, 2003). Smith (1974) distinguished between types of unit bar, based upon their orientation. Longitudinal, transverse and point bars all form parallel to the direction of flow but their direction of growth (either downstream or lateral) is controlled by localised flow properties and morphology of the channel (Smith, 1974). Alternatively, diagonal bars are formed such that the long axes of the bar are in a direction oblique to the flow (Smith, 1974). Tubino *et al.* (1999) also distinguished between types of unit bars depending on their location within a channel. Free bars are able to migrate in a downstream fashion, with their morphology controlled by channel depths and widths, whereas the location of fixed bars (or point bars) occurs only at certain positions on inner banks where a bend angle exists such that migration is prevented (Whiting and Dietrich, 1993; Tubino *et al.*, 1999).

Compound braid bars (see Figure 2.4) are formed from an amalgamation of unit bars, which have migrated and become attached to an initial core bar (Lunt and Bridge, 2004; Lunt *et al.*, 2004; Sambrook Smith *et al.*, 2006a), or from the chute cut-off of point bars (Lunt and Bridge, 2004). However, Ashworth *et al.* (2000) attributed braid bar formation in the large-

Figure 2.5. Compound bar with symmetrical limbs on the South Saskatchewan River, Canada. Arrows denote limbs. Bar is approximately 50 m long. Photo by P. Ashworth, 2007.

scale Jamuna River, Bangladesh to the accretion of large dunes which by forming a bar nucleus, promoted further dune accretion resulting in the formation of a braid bar. However, Bridge (2003) disputes the formation of the braid bar due to dunes and instead interprets the dune front to be the face of a lobate unit bar.

Through erosional and depositional events, compound bars are able to migrate upstream, laterally and downstream, with a wide range of planforms possible, including the formation of downstream limbs or horns (Smith, 1971; Cant and Walker, 1978; Skelly *et al.*, 2003; Bridge and Lunt, 2006; Sambrook Smith *et al.*, 2006a; Mumpy *et al*., 2007) (See Figure 2.5). Cant and Walker (1978) describe the formation of symmetrical and asymmetrical limbs in the South Saskatchewan River. Initially, a decrease in stage can result in the emergence of the highest part of the initial unit bar (nucleus). Sediment is then directed around the nucleus due to flow divergence, resulting in the deposition of unit bars just downstream of the nucleus (Cant and Walker, 1978). Asymmetrical horns develop on bars which are diagonal (using Smith's (1974) definition), whereas symmetrical horns develop on bars which are oriented

parallel to flow direction (Cant and Walker, 1978) (see Figure 2.5).

2.1.3 Braiding mechansisms

Bridge (1993) distinguished braiding mechanisms into two types: the "development and emergence of individual or rows of alternate bars", encompassing mechanisms of central bar formation and transverse bar conversion; and secondly the "formation of cross-bar channels", with chute cut-off and multiple bar dissection occurring (Bridge, 1993, p. 18). The dominant mechanism is dependent on sediment transport conditions and channel morphology (Knighton, 1998) though the central bar formation has been the most frequently identified braiding mechanism in the literature (Ashmore, 1991a). Initially a submerged unit mid-channel bar is formed due to deposition of bedload as a result of a decline in transport competence (Ashmore, 1991a). This forms a locus for further deposition, resulting in the emergence of a central compound bar which is enlarged by further deposition (Ashmore, 1991). Bridge and Tye (2000) explain that if erosion of bank material occurs rapidly and in an irregular fashion, then discrete unit scroll bars may be deposited, featuring avalanche faces on their leading edge (Figure 2.6a). However, if deposition is less rapid and continuous then bedload sheets or dunes will be deposited (Bridge and Tye, 2000).

Transverse bar conversion involves the conversion of unit transverse bars to mid channel compound braid bars (Ashmore, 1991a) (Figure 2.7). Flume experiments have revealed the process to initiate from bedload sheets migrating across a symmetrical unit bar (Ashmore, 1991a). This results in vertical accretion on the unit bar and subsequent flow diversion around the bar margin (Ashmore, 1991a). Though Ashmore's (1991a) flume experiments were scaled to simulate gravel bed rivers, it is thought that the mechanisms are similar in sand bed braided rivers.

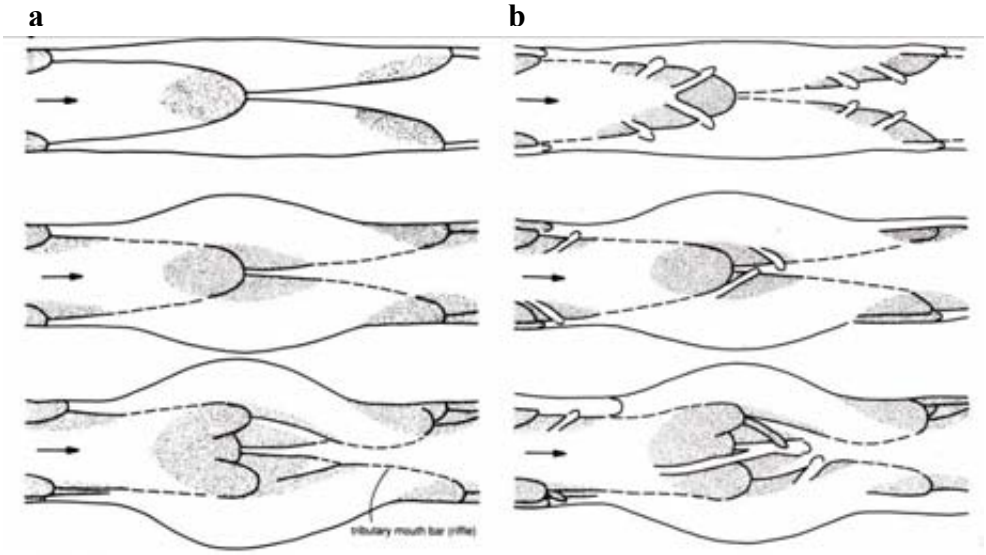

Figure 2.6. Formation of a braided channel including a) formation of double rows of unit bars developing into a braid bar and side bars and b) development of cross-bar channels and channel mouth bars. From Bridge (1993), p.16, Fig.1.

Chute cut-off is another common braiding process (Ashmore, 1991a) and involves the incision of a point (compound) or alternate (unit) bar, often exploiting low areas of bar between bar head lobes (Bridge, 1993). The original point or alternate bar then survives as a medial bar, and the original flow path is cut off. Another mechanism resulting in cross-bar channels is multiple bar dissection. This mechanism is said to be restricted to channels with high width-depth ratios (Ashmore, 1991a), and operates in a manner similar to chute cut-off but with multiple chutes creating corresponding channels (Bridge, 1993) (See Figure 2.6b for example of chute channel and cross-bar channel).

Even though many mechanisms of braiding exist, Ashmore (1991a) remarks that common to all the braiding processes is a loss of competence due to flow expansion laterally and aggradation locally. The variability of sediment transport in braided rivers therefore promotes ongoing channel changes, often resulting in the reworking of deposits.

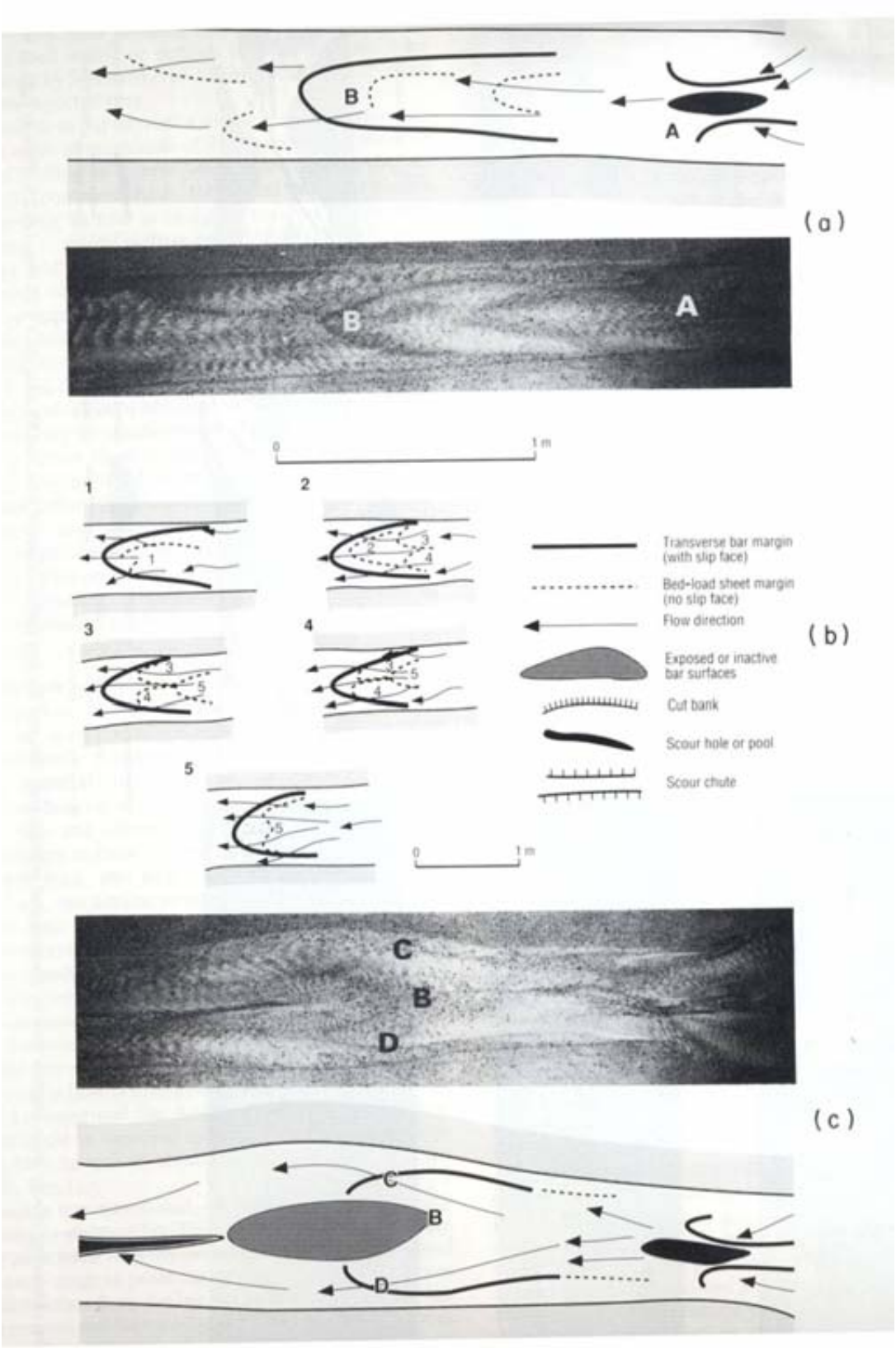

Figure 2.7. Transverse bar conversion. a) a symmetrical unit bar (A), formed downstream of a confluence scour (B), b) five bedload sheets migrating over the bar surface (1-5), c) flow has divided around the bar margin to form two diagonal bars (C & D) and resulting in deposition of coarse material in the centre of the channel (B). From Ashmore (1991a), p. 335, Fig. 6.

2.1.4 Depositional processes

The styles of deposition produced by braiding processes and bedforms have been well researched (e.g. Miall, 1978; Cant and Walker, 1978; Rust, 1978b; Blodgett and Stanley, 1980; Bridge *et al.*, 1986; Brierley, 1989; Bridge *et al.*, 1998; Best *et al.*, 2003; Skelly *et al.*, 2003; Sambrook Smith *et al.*, 2006a). Therefore, by examining the depositional record, braided processes and depositional history may be reconstructed.

Early models of braided river deposits were based on specific well known braided rivers, for example Coleman's (1969) work on the Brahmaputra. Miall (1978) classified six types of model based on braided rivers: the Trollheim, Scott, Donjek, South Saskatchewan, Platte and Bijou Creek models. They varied from gravel to sand dominated, and proximally or distally located with respect to the source, including rivers on alluvial fans (Miall, 1978). However, these models were vertical profiles and lacked information on the lateral variability and three dimensional aspects of deposits (Miall, 1978). Further research into braided river deposits by many authors (e.g. Hickin, 1993; Bridge *et al*., 1998, Skelly *et al*., 2003, Sambrook Smith *et al*., 2006a) has shed some light upon the continuity of deposits. Bridge (2003) has characterised four general scales of sedimentary deposits which can be applied to sand and gravel bed braided rivers (Figure 2.8):

1. A complete channel belt
2. Deposits of individual channel bars and channel fills (sets of large-scale inclined-strata, also known as storeys)
3. Depositional increments (large-scale inclined-strata) on channel bars and in channel fills formed during distinct floods
4. Depositional increments associated with the passage of discrete bed waves such as dunes, ripples and bedload sheets (sets of medium-scale and small-scale cross-strata

and planar-strata) (Bridge, 2003, p. 214).

The deposits will be discussed in the following sections.

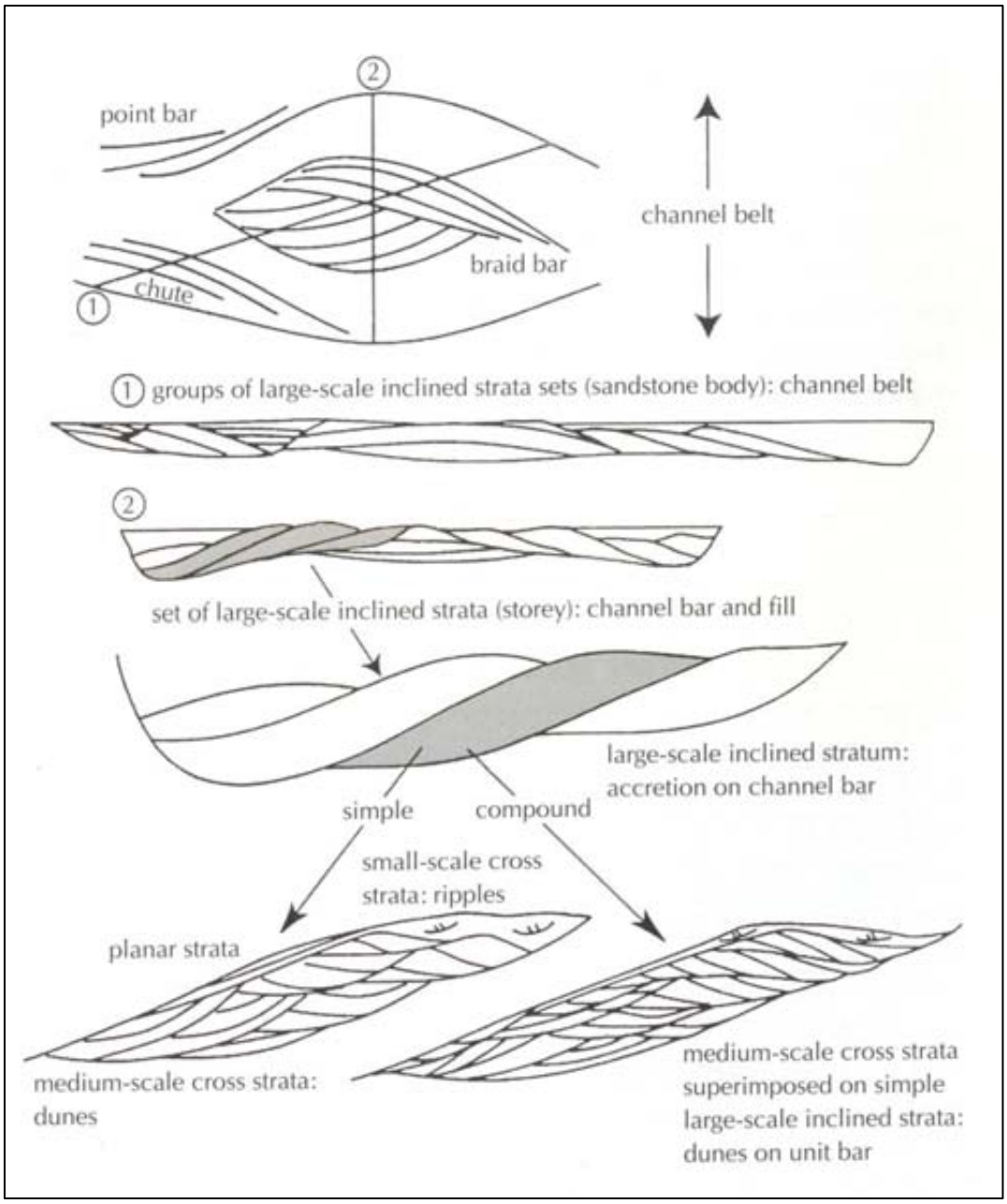

Figure 2.8. Fluvial deposit scales. Largest scale of deposition (complete channel belt) at top, followed by large-scale inclined strata, and medium- and small-scale cross-strata (at bottom). From Bridge (2003), p. 215, Fig. 5.42.

2.1.4.1 Small and medium-scale strata

The smallest depositional scale is concerned with cross-stratification produced from ripples in sand bed rivers. Medium-scale strata are produced by bedforms such as dunes and bedload sheets in both sand and gravel rivers (Bridge, 2003; Lunt *et al*., 2004). These accumulate on inclined surfaces of bedforms such as bars, with 3-dimensional geometry determined by the shape of the surface strata they accrete on (Bridge, 2003). For example, planar cross-stratification will result if sediment is deposited on straight crested ripples or dunes, whereas trough cross-stratification will be formed if deposition occurs on curve crested forms (Bridge, 2003).

The geometries of the resulting strata will also be determined by the depositional process with regards to grain sorting, rate of transport, and composition of bedload (Bridge, 2003; Kleinhans, 2004; Reesink and Bridge, 2007). Commonly, the coarsest grains in the bedload accumulate at the base and margin of the avalanche face, and due to kinematic sieving, the finer grains move into pore spaces (Bridge, 2003). In gravel bed rivers, coarse grains can accumulate at the base as a result of pebble clusters (Lunt *et al*., 2004). Grain flows occur infrequently during low sediment transport rates, and so will produce angular cross-strata (Figure 2.9; Reesink and Bridge, 2007). However, where sediment transport rates are

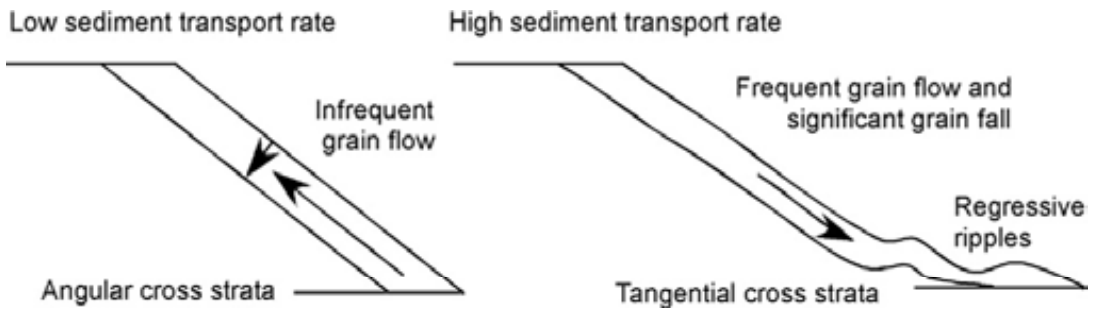

Figure 2.9. Geometry of cross-strata with respect to sediment transport conditions. From Reesink and Bridge (2007), p. 286, Fig. 9.

high, frequent grain flows may occur causing sediment to be deposited at the lower slope (Reesink and Bridge, 2007). Ripples may form in the recirculation zone which will produce tangential cross-strata, rather than angular (Figure 2.9). The texture of cross-strata will also vary due to the composition of bedload, for example, coarser and larger grains may be deposited during flood events, or due to passage of a superimposed bedform (Bridge, 2003). Conversely, fine bedload may be deposited during the passage of a bedform trough (Bridge, 2003).

The thickness of strata is related to the geometry of the associated bedform, with the strata length: thickness ratio corresponding to the wavelength: height ratio of the bedform (Figure 2.10) (Lunt *et al.*, 2004; Bridge and Lunt, 2006). This implies that the scale of

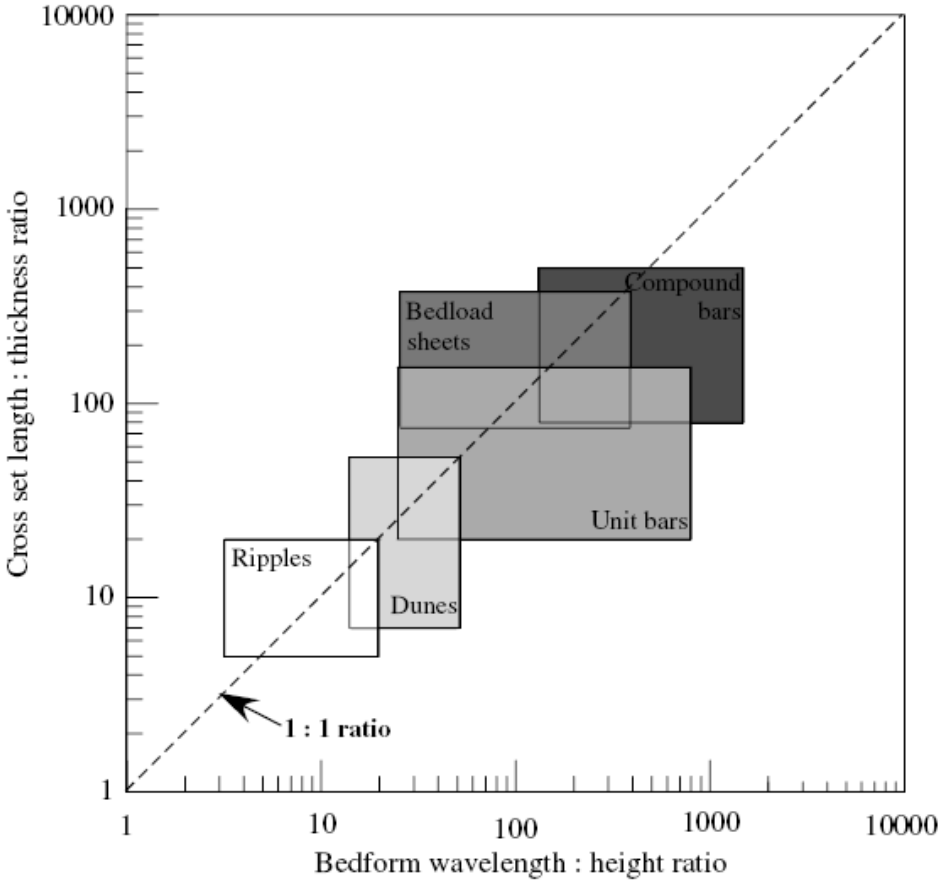

Figure 2.10. Ratio of strata length to thickness plotted against bedform wavelength to height ratio. From Lunt *et al.,* (2004), p. 409, Fig. 25.

strata set also varies with scale of river since channel depth and width dictate bedform scale (Lunt *et al.*, 2004). Paola and Borgman (1991) used probability density functions to investigate the relationship between bedform heights and strata thickness for random topography (Figure 2.11). In conditions of no aggradation, preserved strata thickness was found to scale in proportion to the ratio of the variance in bedform height to mean height (Paola and Borgman, 1991). Leclair *et al*. (1997) adapted the Paola and Borgman (1991) model and applied the theory to migrating dunes in non-aggrading and aggrading conditions. The preservation ratio (mean strata thickness: mean bedform height) was found to be equal to 0.3 in flume experiments, in non-aggrading conditions, therefore making this figure the lower limit, as aggradation was expected to increase the preservation ratio (Leclair *et al*., 1997).

However, an investigation into the effect of aggradation revealed no consistent increase in strata thickness occurring with an increase in aggradation (Leclair *et al*., 1997). It was thus concluded that the dominant control on preserved strata thickness is the variation in dune trough elevation (Leclair *et al*., 1997). Based on new experimental data, Leclair and Bridge (2001) approximated mean dune height to (2.9 (+/- 0.7)) x mean strata thickness, which equates to a preservation ratio (using Leclair *et al*. (1997) definition) between 0.28 and 0.45. This model was tested successfully with data from the Calamus and Mississippi rivers (Leclair and Bridge, 2001). Further experimental work by Leclair (2002) established that variations in variables such as velocity and flow depth, as well as aggradation, do not result in a systematic variation in the preservation ratio.

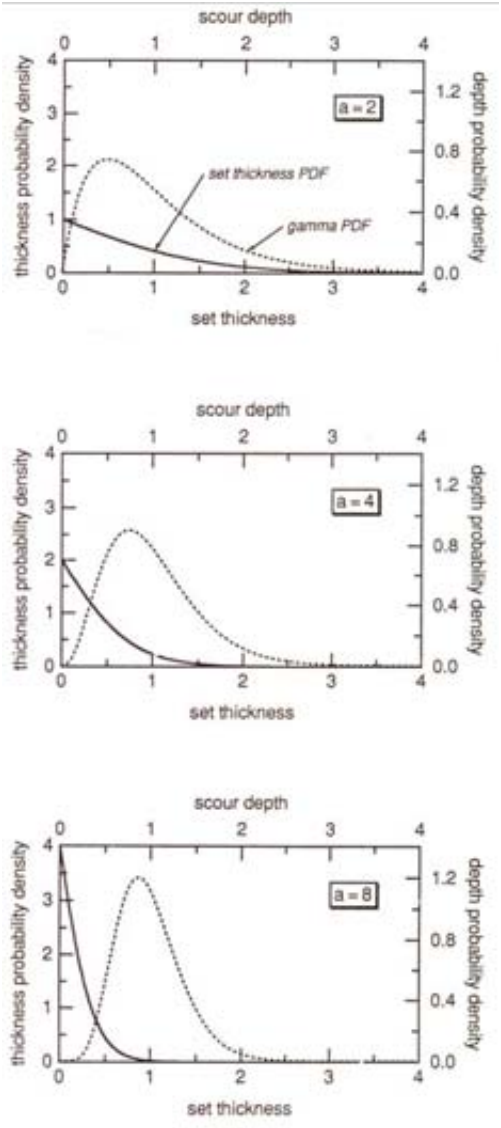

Figure 2.11. Probability density functions for set thickness (solid line) for three density functions for scour depth (dashed line). The mean height of topography is 1 in all panels; the changes in mean set thickness are controlled only by changes in the variance of the height of topography. 1/a = the mean value of the exponential tail of the probability density for topographical height. From Paola and Borgman (1991), p. 557, Fig. 3.

2.1.4.2 Large-scale strata

Bedforms such as unit and compound bars produce sets of large-scale inclined-strata which are present in both sand and gravel bed rivers (Bridge, 2003). However, the preservation potential of bars in gravel bed rivers has been questioned by Siegenthaler and Huggenberger (1993), who found only the bases of bar deposits preserved in the Rhine Valley gravels.

Elevated bar deposits were destroyed due to lateral shifting of channels in moderate

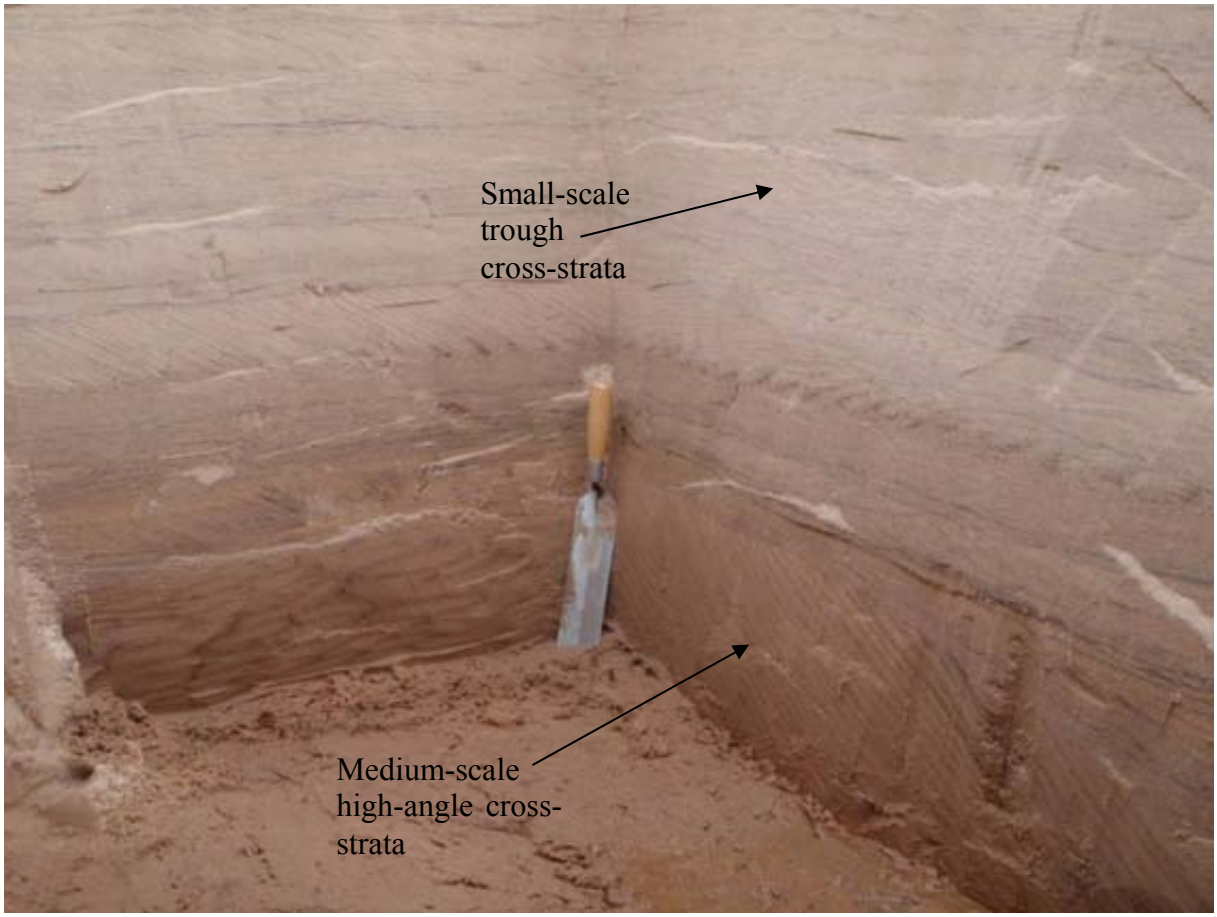

Figure 2.12. Unit bar deposits containing steeply dipping sets of medium-scale cross-strata, and small-scale sets of trough cross-strata in the Rio Paraná, Argentina. Photo by J. Best, 2008.

magnitude flows and higher magnitude floods (Siegenthaler and Huggenberger, 1993).

Large-scale strata (unit bars) are internally composed of sets of medium-scale strata (Figure 2.12) as a result of ripple, dune and bedload sheet migration, with size of strata often decreasing upwards within bars as a response to decreasing depth (Bridge and Lunt, 2006). Sediment sorting is often apparent in gravel bars, with the bases of unit bars composed of open framework gravel, then fining upwards to sand at the top (Lunt *et al*., 2004). As a result of variations in the lee-side slope of unit bars as they migrate, the inclination of large-scale inclined-strata may vary along a set length (Lunt and Bridge, 2004). Sambrook Smith *et al.* (2005) identified high-angle inclined deposits on bar margins in the South Saskatchewan and

Jamuna Rivers as being more frequent where bar overtopping occurs and where bars migrate into deep thalwegs. Inclinations may reach the angle of repose (30 - 40º) on bar margins (Bridge and Lunt, 2006). Bar growth processes may be deduced, for example, the upstream accretion of bedforms is often preserved as upstream dipping reflections of a low-angle, representing the stacking of forms along the channel (Skelly *et al.*, 2003). Similarly, the presence of horizontally bedded gravel deposits in unit bars may suggest bar accretion through the migration of bedload sheets (Rust, 1978b).

Compound bars are composed of stacked unit bars, therefore their composition may be identified by distinguishing different unit bar deposits by their sedimentary properties, for example upward fining of sediment in each unit bar, though this may be more apparent in mixed gravel-sand bed rivers.

Bar deposits can also shed light on the flow stage responsible for deposition. Skelly *et al.* (2003) distinguished between discontinuous-wavy and high-angle reflections produced by small dune migration in low flow secondary channels, and continuous low-angle reflections, of a planar form which represent larger dunes formed in high stage primary channels. However, the preservation of different flow stage deposits is not always complete, for example, low discharges may promote the exposure of braid bars and thus incision by secondary channels may occur (Skelly *et al.*, 2003).

2.1.4.3 Channel fills

The placement of channel fill deposits in the hierarchy varies depending on the channel size in which they are formed. For example, a small cross-bar channel fill would comprise smaller-scale deposits compared to a thalweg fill.

Unit bar deposits are often found in channel fills, particularly in the upstream and lower portions (Bridge and Lunt, 2006). Channel fills tend to fine upwards and down channel reflecting the loss of local transport competency, with laminated muds occurring in some downstream areas (Bridge and Lunt, 2006). However, Bridge (2003) explains that specific channel fill type is dependent on the particular process of abandonment with respect to flow and also the angle between the cut-off channel and the enlarging channel. For example, if the angle is relatively large then cut-off will occur quickly, so that the deposits will be mostly fine grained (Bridge, 2003). However, a smaller angle allows flow to be maintained initially so that bed load in the form of bars is deposited in the entrance (Bridge, 2003).

2.1.4.4 Channel belt

The largest scale of deposition, a complete channel belt, comprises large-scale inclined-stratas encompassing channel fills and smaller-scale strata sets (Fig. 2.8) (Bridge, 2003). Bridge and Lunt (2006) described the thickness of deposit scales in relative terms; "three to seven simple sets of large-scale strata (unit bar deposits) occur within the thickness of one compound large-scale set (compound bar deposit), and two to five compound large-scale sets (compound bars) occur within the channel belt thickness" (p. 40). However, the location and abundance of these deposit types in individual rivers is dependent on factors such as local sediment transport conditions, depositional processes and preservation potential (Bridge, 2003).

2.2 PRESERVATION OF FLUVIAL DEPOSITS

The degree of preservation of fluvial deposits can vary spatially and temporally in an individual river (Blodgett and Stanley, 1980), as it is influenced by factors such as basin sedimentation (tectonics, base level change, channel migration) (Ashworth *et al.*, 1999), and

sediment size. Fundamentally, the preservation potential of deposits may also be dependent on the type of flow events that produced them.

2.2.1 Sediment characteristics

2.2.1.1 Basin sedimentation

Factors such as the magnitude of channel migration, frequency of avulsion, basin aggradation rate, and type and magnitude of base level changes all have influences on the preservation and geometry of deposits (Ashworth *et al.*, 1999). For example, lateral migration of channels involves the reworking of sediments; thus with increased migration there is a decrease in the preservation of deposits (Bristow, 1996) (See Figure 2.13). Experimental modelling studies have shown that increases in sediment supply lead to increases in avulsion frequency (Ashworth *et al*., 2004; Ashworth *et al*., 2007). Coleman (1969) suggests that the rate and amplitude of channel migration is likely to be increased if factors such as a large flow variability and high bank and bed erosion susceptibility are present. With respect to alluvial architecture, floodplain fines will be deposited with every avulsion event so that channel

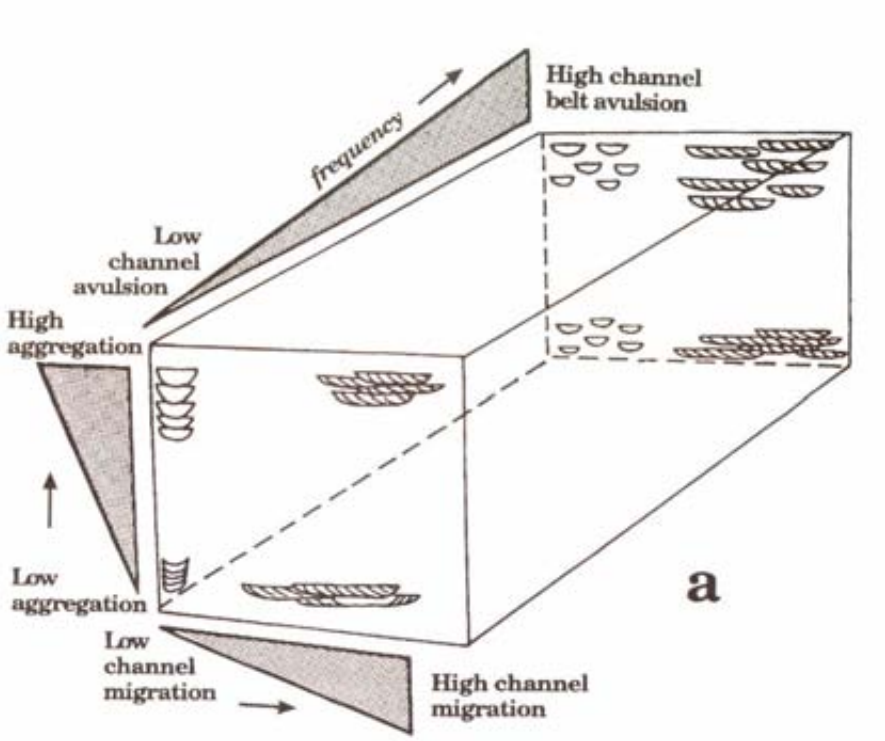

Figure 2.13. Preservation of deposits is dependant on aggradation rates, channel migration and avulsion. From Bristow (1996), p. 365, Fig. 10.9

deposits will be separated (Figure 2.13). Bristow (1996) and Ashworth *et al.* (1999) have suggested that higher aggradation rates result in better preserved deposits such as channel bodies as there is less opportunity for re-working. Skelly *et al.* (2003) remark that the geometry of the floodplain is a factor also, as there is increased potential for preservation with increased braid plain accommodation space.

Accommodation space can be viewed in terms of two timescales of accommodation: 'accumulation' space and 'preservation' space (Blum and Törnqvist, 2000). Accumulation space or real-time accommodation is the space available under present processes and is governed by the relationship between sediment load and stream power (Blum and Törnqvist, 2000). However, preservation space occurs when deposits are lowered below depths of incision by allogenic factors such as basin subsidence (Blum and Törnqvist, 2000). Dott (1983) suggested that deposits above the base level have a relatively low preservation potential. External triggers of aggradation and incision such as base level change and ground tilting can therefore heavily influence preservation potential. Due to sea level change, channels may either shorten or extend, as a response to a shoreline that is retreating or advancing (Blum and Törnqvist, 2000). Thus, the elevation of the channel base will change, along with the floodplain, resulting in either aggradation or incision (Blum and Törnqvist, 2000). For example, incision occurred on the Jamuna River, Bangladesh, as a response to base level fall (Best and Ashworth, 1997).

Furthermore, external factors such as tectonics may influence the type of deposits left in the sedimentary record. For example, depending on the rate of tilt, lateral ground tilting will either cause a channel to avulse, or to gradually migrate down dip (Peakall *et al*., 2000). This will result in either ribbon or sheet like channel deposits respectively (Peakall *et al*., 2000).

2.2.1.2 Sediment size

The size of the sediment transported may also be a significant factor with respect to preservation potential of flow events. Shields (1936) defined the threshold of transport as dependent on i) dimensionless shear stress (Θ):

$$\Theta = \tau_0 / (\sigma-\rho)gD \qquad [2.1]$$

where τ_0 is bed shear stress, σ is grain density, ρ is fluid density, g is acceleration of gravity and D is grain diameter, and ii) the boundary grain Reynolds number (Re_b):

$$Re_b = U_*D/\nu \qquad [2.2]$$

where U_* ($= (\tau_0/\rho)^{0.5}$) is the threshold shear velocity, and ν is the fluid's kinematic viscosity. Figure 2.14a demonstrates the relationship between these two variables with respect to thresholds of suspended load and bedload transport. The threshold curve can be simplified to τ_0 versus D (Figure 2.14b) where set values of fluid and grain densities are used (Komar, 1988; Bridge, 2003). Thus it can be seen that as grain size increases, increases in bed shear stress (Shields, 1936) are required to transport sediment. By taking Θ as a constant value of 0.045, the value of τ_0 required to entrain a particular grain size can be estimated (Komar, 1988). Wolman and Miller (1960) suggested that as the competency of flow required to transport sediment increases, so does the significance of the flood event that can generate such flows. This is because if high bed shear stresses are generated by a large flood, they enable the transportation of coarse sediment that may not be transported due to lower flows. Thus post-flood flows may lack the competency to modify the deposits to the extent that less coarse sediment can be eroded and deposited (Gupta, 1983). Therefore, coarser sediment flood deposits are more likely to persist over time (Stevens *et al.*, 1975) and thus may possess a higher preservation potential than sand deposits.

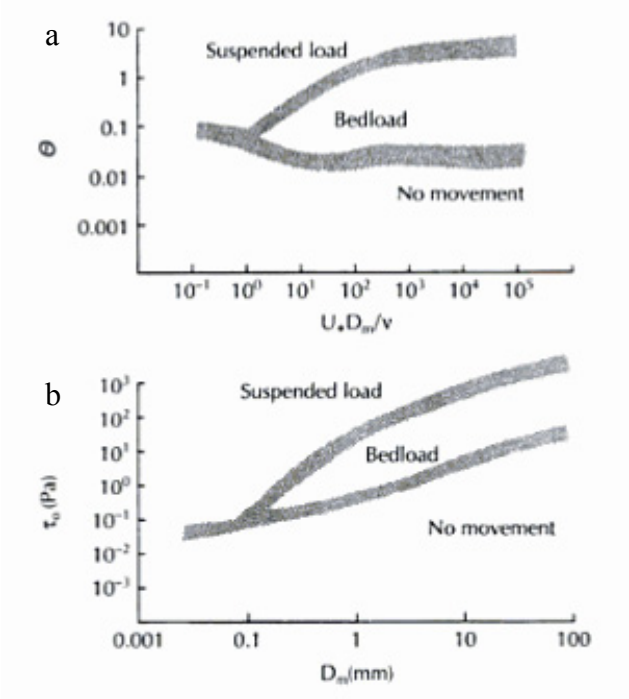

Figure 2.14. a) Shield's (1936) curve for the threshold of motion, b) Threshold of motion curve based on bed shear stress (τ_0) and grain diameter (D). See text for explanation. From Bridge (2003), p. 50, Fig. 3.7

2.2.2 Flow characteristics – which flow events will be preserved?

In order to establish which types of flow events are likely to be preserved in the sedimentary record, it is first necessary to assess the impact of different flow events on morphology and sediment transport. There has been considerable debate in fluvial geomorphology over the past several decades (Wolman and Miller, 1960; Wolman and Gerson, 1978; Gupta, 1983; Kochel, 1988; Magilligan *et al.*, 1998) surrounding the potential of different events to perform 'geomorphic work', and thus the potential for events to leave their signature in the sedimentary record. Importance has been assigned to a variety of factors for determining the impact of a flood, in particular, the flood characteristics, effective discharge of the river, and channel characteristics.

2.2.2.1 Flood characteristics: peak flow, rate of fall of flow, flow duration and periodicity

The characteristics of a particular flood event will influence the preservation potential of flood deposits (Stevens *et al.*, 1975; Gupta, 1983; Costa and O'Connor, 1995). The ratio of a flood's discharge peak to the mean annual discharge is a good indicator of the impact (Stevens *et al.*, 1975; Gupta, 1983). For example, a high ratio increases the likelihood of preservation of flood affected forms since post-flood flows may not have the ability to rework them (Gupta, 1983). High preservation potential of flood deposits often occurs in proglacial areas that experience 'catastrophic' high-magnitude floods, as the transportation of coarse material such as large boulders can only be carried out by flows which have a high transport competence such as jökulhlaups. For example, Carrivick *et al.* (2004), Russell *et al*. (2006) and Russell (2009) documented the deposition of large boulders including boulder ridges and clusters due to jökulhlaups. Similarly, Marren *et al.* (2002) reported of the formation of distinct jökulhlaup deposits in the form of large-scale bars, scaled to jökulhlaup channel widths and depths. Such bars remain relatively undisturbed by low-magnitude high-frequency flows, as the bar surfaces are above flow levels.

Such geomorphological and sedimentological impacts are also common in semi-arid areas that experience flash floods (Wolman and Gerson, 1978). For example, Laronne and Shlomi (2007) found that the preservation potential of deposits in braided channels in the Rift Valley, Israel, increased with flood magnitude and that deposits due to smaller floods were unlikely to be preserved in the long-term. Similarly, large floods in tropical areas can leave a long lasting geomorphic and sedimentological impact because in between floods, flows are very low or are absent, for example on the Burkedin River, Australia (Fielding *et al*., 2009).

Stevens *et al.* (1975) term channels that experience long-tern geomorphic impacts due to floods as possessing a 'non-equilibrium' form. However, this is more applicable in rivers

where sediment is coarse gravel and less so with sand sized material which is more easily transported. Conversely, where 'normal' discharge levels are relatively high, then any geomorphic work carried out by the flood discharge may be reworked. Smith *et al.* (2006) reported this on their study of the 1996 jökulhlaup on Skeiðaràrsandur**,** Iceland. 'Normal' flows post-flood are remobilising the surface sediment of flood deposits so that the geomorphic surface impact is of a short duration; however, deposits lower down in the sequence are expected to remain in the long-term (Smith *et al.*, 2006).

Blodgett and Stanley (1980) discuss the problem of using an inductive approach in interpreting ancient deposits using modern analogues, as this assumes the preserved deposits are representative of the river as a whole and therefore that preservation of deposits formed at different flow stages is constant. Blodgett and Stanley (1980) assessed the preferential preservability of low and high stage deposits on the Platte River, Nebraska. At bankfull flow, linguoid bars occupied channels of the Platte; however, when the stage dropped, these bars were modified by erosion and deposition (Blodgett and Stanley, 1980). Modification processes at low flow may involve:

1. "Erosion of bar flanks by active braid channels,
2. Planation of bar tops by shallow rapidly flowing water,
3. Dissection and scour of bartops by slack water channels (cross-bar channels), and
4. Bar front progradation by multi-lobate small-scale deltas" (Blodgett and Stanley, 1980 p. 999).

Blodgett and Stanley (1980) found evidence of preservation of both high flow deposits (large-scale planar cross-strata formed by linguoid bars) and low flow deposits (small-scale trough cross-strata formed by dune migration along bar top channels). However, the degree of preservation of stratification is dependent on the rate of fall of discharge (Blodgett and

Stanley, 1980). Where flood discharge falls rapidly, then bedforms may become abandoned above the water level (Jones, 1977; see Figure 2.15). This results in the divergence of flow around bedforms, which may initiate some erosion (e.g. on avalanche face) and the deposition of trough cross-beds (Jones, 1977). The bedforms abandoned in the falling stage are then reactivated during the next flood event and as such the avalanche face will be reformed (Jones, 1977).

However, at a slower rate of fall in discharge, small bedforms such as ripples and dunes may form on the back of inactive features forming convex upward surfaces (Jones, 1977). With a very slow fall in stage, bedforms may be dissected by channels such that surface erosion will take place and subsequent deposition of small bedforms in the channels may follow (Jones, 1977). However, Jones (1977) stresses that bedform response will vary spatially in a river due to differences in river bed topography, so that bedforms at a lower elevation with respect to flow stage will take longer to become emergent and thus, a higher degree of modification may occur compared to bedforms at higher elevations.

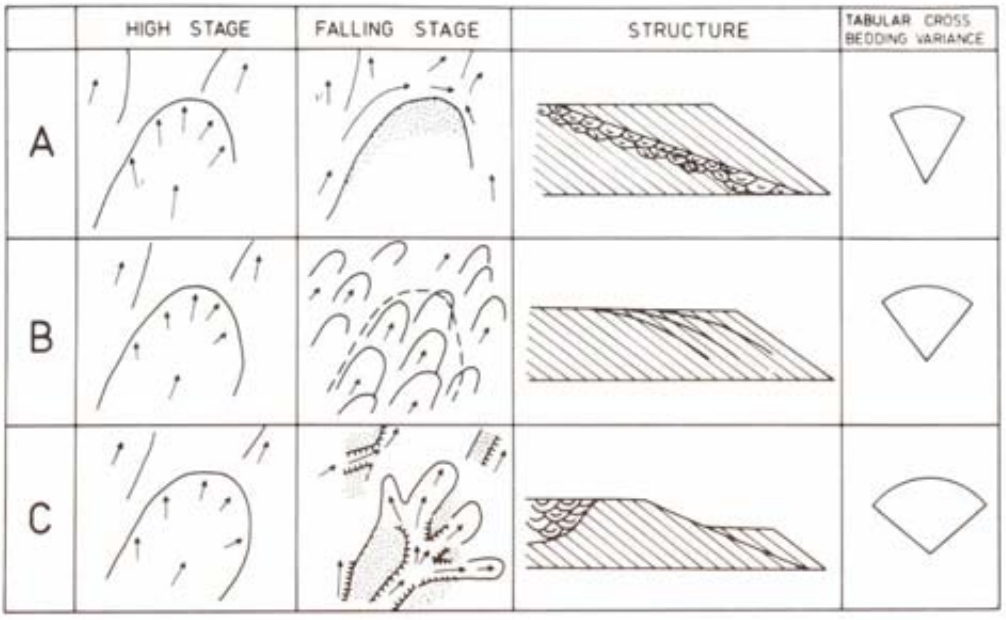

Figure 2.15. Bedform response to a) a rapid fall in discharge, b) a slower rate of fall in discharge and c) a small rate of fall. From Jones (1977), p. 569, Fig. 2.

The duration of a flood event also needs to be recognised as this is another significant factor with respect to geomorphic impact and hence may also influence sediment preservation (Costa and O'Connor, 1995). If the duration is of a short period of time, no matter how high the peak discharge is, a lesser geomorphic impact will be caused compared to a flood of longer duration (Costa and O'Connor, 1995). For example, a longer duration flood may saturate river banks therefore increasing their likelihood of failing, or may remove floodplain vegetation, increasing a floodplain's susceptibility to erosion by flood flow (Costa and O'Connor, 1995).

The periodicity of occurrence of flood events can also influence the preservation of flood deposits (Gupta, 1983; Kochel, 1988; Marren, 2005). Kochel (1988) explained that channels are adjusted to high flow states after a flood, so that lower flows will gradually reverse the flood effects and readjust the channel post-flood (Gupta, 1983). If subsequent floods then occur before the channel morphology has fully adjusted to low flows, then little geomorphic impact is caused by the subsequent flood (Kochel, 1988). However, this means that there may be a higher likelihood of preservation of flood events in the sedimentary record (Gupta, 1983). Gupta (1983) suggested that a flood with periodicity of once in every ten or twenty years would be favourable for preservation, based on field observations from Jamaica, Maryland (USA) and South East Asia. For example, Takagi *et al* (2006) investigated the geomorphic impact of a large flood on the Brahmaputra River from 1967-2002 and reported that the 1987 and 1988 large floods caused significant geomorphic change through braid belt widening; however, a flood of a similar magnitude occurring in 1998 caused little geomorphic impact. It was suggested that the modifications due to the previous floods which had not been subsequently reworked, facilitated the flood drainage (Takagi *et al.*, 2006). The preservation potential of sediments was not investigated however. Conversely, if the flood is a single

unique occurrence, then a more significant impact will be caused initially, but there is a longer time period available for reworking of flood deposits back to low flow conditions (Marren, 2005).

2.2.2.2 Effective discharge

Wolman and Miller (1960) argued that the effectiveness of an event with respect to 'geomorphic work', defined as sediment transport, was dependent on the frequency of the event as well as the magnitude. Based on field data, they suggested that the most effective discharges in this respect were of a moderate magnitude and occurred relatively frequently, instead of the rarer flood events. Their data showed these discharges occurred every year or every two years and was equivalent to bankfull discharge.

Nash (1994) revisited Wolman and Miller's (1960) hypothesis using a larger data set and determined that the effective discharge is highly variable ranging from weeks to decades such that no one recurrence interval is widely applicable. Nash (1994) also further investigated the effective discharge in terms of stream morphology. He suggested a correlation may exist between the effective discharge, in terms of sediment transport, and morphological features. Nash (1994) reviewed a number of studies investigating this, for example, Pickup and Warner (1975), and deduced that all found the effective discharge for stream morphology recurs more frequently than once a year. Such findings have implications for the preservation potential of sediments as if most geomorphic work is due to flows of a lower magnitude and a high frequency then rarer events may not have much control over long-term stream morphology.

2.2.2.3 Channel characteristics

Channel characteristics such as the channel gradient, bank material and the availability of sediment present can all influence the impact of flow events on the morphology of a river channel and thus may also contribute to the preservation potential of a particular flood.

Kochel (1988) compiled data on the impact of several 'catastrophic' floods and noted that rivers that experienced significant erosion and deposition had higher gradients than those that experienced only minor change. This is because steeper gradients mostly occur in bedrock channels and thus in large floods are able to transport coarse material due to the increased velocity of the flow (Kochel, 1988). Similarly more confined valleys generate higher shear stresses compared to wide valleys as more of the flow volume is concentrated in the channel (Magilligan, 1992). Because valley shape and stream gradient change spatially in a river, this means the impact of a flood with respect to sediment transport and storage can vary downstream (Magilligan, 1992). Thus, the preservation potential of sediment due to different flow events may also vary through the river system.

With respect to bank material, in order for erosion or scour to occur in a flood event, the stream power generated has to exceed the threshold of the bank material. Gomez *et al.* (1997) reported of a flood on the Upper Mississippi which had a greater than 100 year recurrence interval and was above flood stage for 101 consecutive days, but caused little channel change. Even though levees failed and the flood plain was inundated, Gomez *et al*. (1997) concluded that the cohesive soils that made up the floodplain had resisted the erosive flood forces.

The timing of the flood event with respect to sediment availability is also an important factor. Magilligan *et al.* (1998) argue that the sequence of flood events may be as significant as the magnitude of flow with respect to geomorphic and sedimentological impact. A large

magnitude flood in the upper Mississippi deposited only minor amounts of sediment on the floodplain as little sediment was available for transportation at the time of the flood (Magilligan *et al*., 1998). Thus even though the flood was a rare flow event, little evidence of it is likely to be preserved in the sedimentary record (Magilligan *et al.,* 1998).

The variation in preservation of flow events has implications for the interpretation of ancient sedimentary sequences, which traditionally rely on modern analogues. It is paramount that factors such as the magnitude and frequency hypotheses, effective discharge, and channel characteristics are incorporated into models of alluvial architecture in order to improve the representational accuracy of braided sedimentary deposits (Bridge and Lunt, 2006).

2.3 MODELLING OF BRAIDED RIVER DEPOSITS

Braided river deposition is commonly viewed with respect to two different timescales: deposits produced due to braided morphology processes in the short-term (decades to hundreds of years), and deposits influenced by longer-term processes (over thousands of years) including extrinsic factors such as basin subsidence (Miall, 2006). Short-term processes can only be directly examined when looking at modern river dynamics and deposits, whilst the effect of longer-term factors on preservation can only be inferred from looking at what is preserved in the sedimentary record. However, there is much debate about the suitability of either approach when constructing depositional models and determining preservation potential of braided deposits. There are arguments for the importance of modern processes for modelling and a criticism of using ancient sediments because of the limited data available (Bristow, 1996; North, 1996). Conversely, the importance of the ancient record for inclusion in modelling is stressed due to the understanding that can be gained of long-term preservation (Miall, 2006).

2.3.1 Facies models

Over the past three decades, research on braided rivers has attempted to typify braided river deposits through the construction of depositional or facies models. Cant and Walker's (1978) influential sandy braided river model based on the South Saskatchewan describes three main components of the braided environment: channel (medium-scale cross-strata), sandflat (high-angle inclined deposits) and mixed influence deposits (Figure 2.16). This model was incorporated by Miall (1978) in to his classification of 6 braided river models based on sediment size and environmental location (Figure 2.17). Miall (1973) also pioneered the use of statistics to identify facies associations through Markov chain analysis. This technique has been employed in deriving facies models e.g. Brierley (1989) on the Squamish River, Canada; however, its usefulness has been questioned (Miall, 1985; Brierley, 1989). The facies

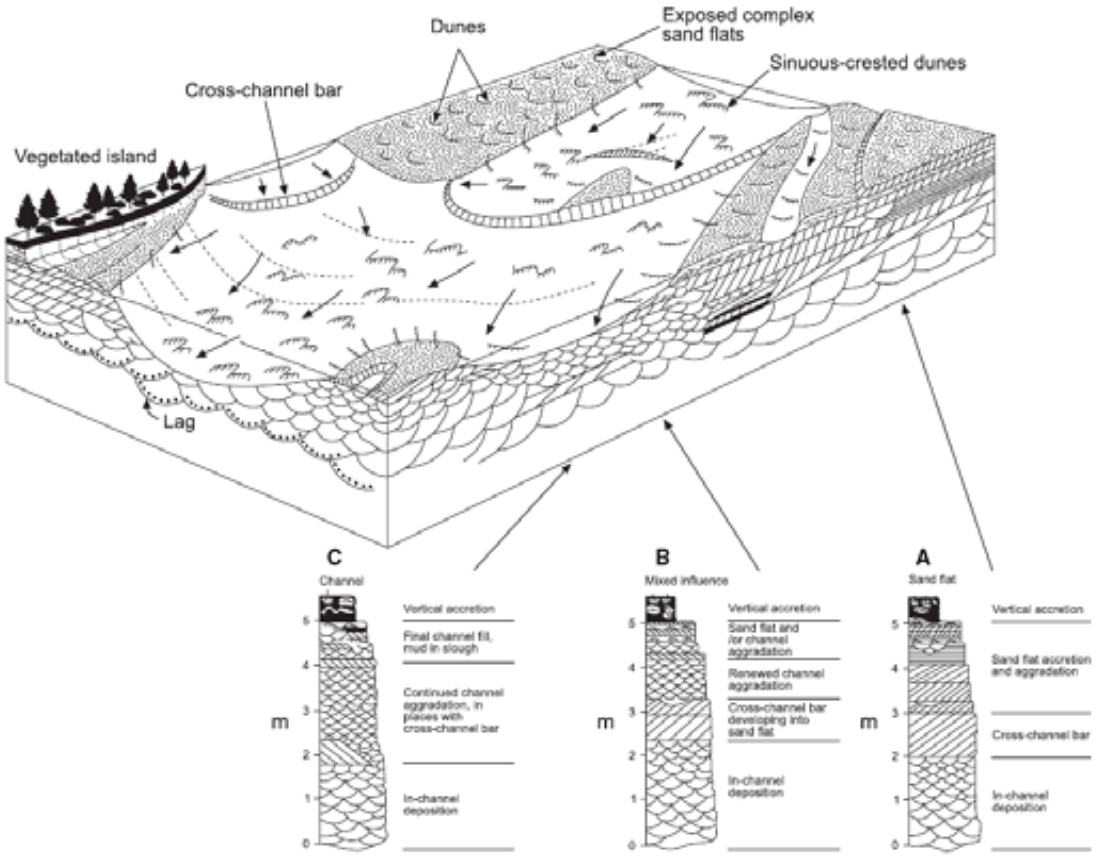

Figure 2.16. Cant and Walker's (1978) depositional model and vertical facies profiles of the South Saskatchewan. Redrawn by Sambrook Smith *et al.* (2006b), p. 414, Fig. 1.

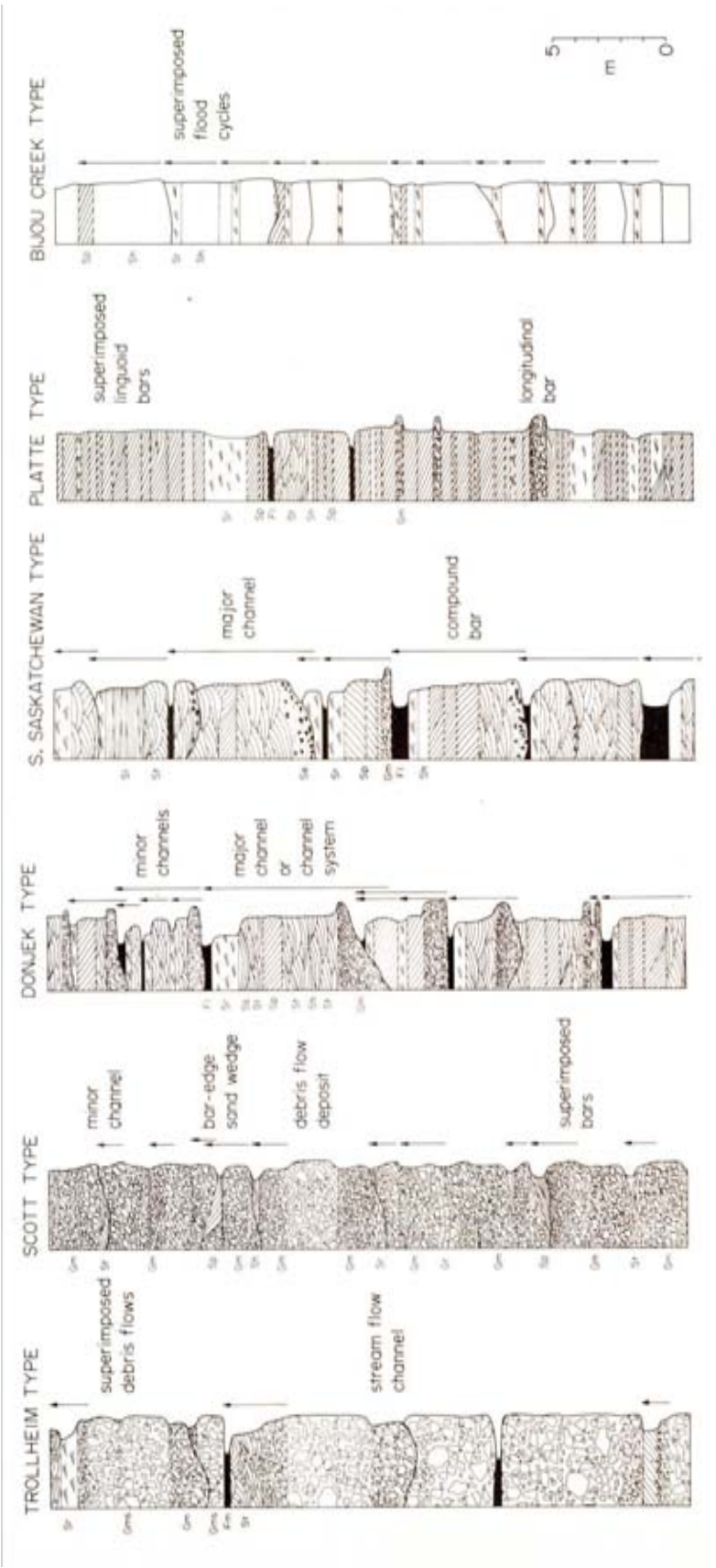

Figure 2.17. Six types of vertical profile models for braided deposits based on well studied rivers. From Miall (1978), pp. 5 - 6, Fig. 1.

transitions predicted using this method were described as "meaningless synthesised sequences" as they were found to be unrepresentative of those observed in the field (Brierley, 1989, p.32). Thus, the Markov chain analysis approach was irrelevant with respect to understanding processes of deposition (Brierley, 1989).

Depositional models have faced criticism due to use of inadequate data (Hickin, 1993) such as limited sediment sampling. For example, Sambrook Smith *et al.* (2006a) revisited Cant and Walker's (1978) work on the South Saskatchewan, using GPR techniques which enabled subsurface sedimentology to be imaged on a 50 metre grid spacing. Sambrook Smith *et al.* (2006a) noted a variability in deposit types, for example in bar deposits, that was not adequately represented in Cant and Walker's (1978) model. In addition, Brierley and Hickin (1991) studied the sedimentology of the Squamish River which displays braided, wandering and meandering planforms. They discovered that there were no predictable variations in sedimentology between the three planforms in bedform and event-scale facies (Brierley and Hickin, 1991). Thus, they questioned the scale of exposure that is needed to be representative of a planform type, and suggested that samples as large as a valley cross-section may be required in order to reveal distinct facies assemblages (Brierley and Hickin, 1991).

More recently, Sambrook Smith *et al.* (2005) investigated the applicability of depositional models to different rivers with respect to upscaling. Research on the Calamus, South Saskatchewan and Jamuna rivers revealed that morphological features such as scour depth and the bar width to depth ratio do upscale. However, comparisons of subsurface sedimentology revealed a contrast in facies type within and between the rivers. Sambrook Smith *et al*. (2005) explained that the sedimentology was influenced by factors such as discharge regime and bar stability, and thus when applying models to rivers with similar morphologies, the variability in sedimentology due to such factors has to be taken into

consideration.

2.3.2 Can we predict what will be preserved in the sedimentary record?

The modelling and prediction of sedimentary deposits and their characteristics are especially important for reservoir exploitation (North, 1996). Miall (2006) argues that the only way to assess preservation is by studying the ancient rock record, undermining the importance of modern river studies in this respect. However, the ancient rock record is not readily accessible, and even with well exposed rock outcrops, only a small portion of the subsurface can be sampled (North, 1996). North (1996) suggests that quantifying the rock record is therefore predictive rather than descriptive. Such models, based on the end sedimentary product, are termed 'object' based, whereas 'process' based models are those that simulate the processes that generate the sedimentary deposit (Miall, 2006).

North (1996) argues that in order to improve modelling techniques used in reservoir exploitation, more work is needed on present river deposits. Bunch *et al.* (2000) created a numerical model to simulate the geomorphological development and sedimentary facies of drylands, in order to assess the lateral variability of permeability in UK Triassic sandstone aquifers. The process based model utilised empirical flow and sediment transport equations and applied storm events in order to model the development of sedimentary facies.

For the modelling of present day rivers, techniques such as GPR are enabling the link between process and deposit to be investigated in detail (Best *et al*., 2003; Skelly *et al*., 2003; Lunt *et al*., 2004; Bridge and Lunt, 2006; Sambrook Smith *et al.*, 2006a). For example, Lunt *et al.* (2004) developed a 3D depositional model of a gravel braided river based on data from the Sagavanirktok River, Alaska. Deposits were described using GPR, cores, wire line logs and trenches, and the link with their formative process made through observations of channel

and bar evolution. However, Miall (2006) criticises 'process' based models as they do not account for evolution over a geologic timescale where allogenic factors such as base level rise will effect the preservation of deposits. Furthermore, applying modern analogues to the rock record results in an underestimation of time span since the rock record is incomplete and represents only net change over a period of time (Sadler, 1981; Van Andel, 1981, Sadler, 1983).

2.4 SUMMARY AND RESEARCH GAPS

From a review on literature of braided river morphology, it has been established that the main morphological units are dunes and unit and compound bars. Studies have shown that dune and unit bar geometries adjust to changes in the flow environment. Dune height has been thought to increase with flow depth (e.g. Yalin, 1964), but it has also been recognised that a complex relationship exists between dune height and flow depth due to factors such as the influence of dimensionless shear stress (Allen, 1978), and dune geometry lag (Bridge, 2003). Less research has been conducted on unit bars; however, it is commonly thought that unit bar heights are comparable with the mean depth of formative flow, and that unit bar lengths vary in proportion to channel width (ASCE, 1966).

Experimental work has been carried out to investigate the preservation of deposits due to dune migration (Paola and Borgman, 1991; Leclair *et al.,* 1997; Leclair and Bridge, 2001 and Leclair, 2002). With respect to unit bars, little research has been carried out on their preservation potential in present day deposits. However, there has been research into bar deposits over longer time-scales, for example, Siegenthaler and Huggenberger (1993) who found that only the bases of bar deposits remained preserved due to reworking of the elevated deposits by subsequent channel formation.

Preservation of fluvial deposits can be defined over short timescales (decadal) where preservation is influenced by present day processes (sediment supply and flow regime), or over long timescales (geological), where it is affected by allogenic factors such as base level change (Blum and Törnqvist, 2000). There are examples in literature surrounding the geomorphic and sedimentological work done by floods of different magnitudes. It appears that the significance of a flood event in this sense is due to a complex combination of factors such as flood characteristics (i.e. peak discharge, duration), the effective discharge of the river (in terms of sediment transport), and channel characteristics (e.g. slope, bed material, bank cohesion) (Wolman and Miller, 1960; Gupta, 1983; Kochel, 1988 and Magilligan, 1992). Unfortunately, many studies focussing on large flood events have limited data on pre-flood morphology and sedimentology and therefore are not able to fully determine the impact of the flood in context with the geomorphic and sedimentological work carried out by lesser flood events.

There are clearly gaps in research with respect to

- The type of present processes that are preserved in the subsurface at a short-term scale (i.e. which bedforms and flood events?),
- How deposits are preserved (i.e. completeness of deposit and whether there is differential preservation of different flood events), and
- If deposits can be clearly distinguished by the magnitude-frequency of their formative flows.

In order to establish the relationship between process form and deposit in sandy braided rivers, and to assess the preservation potential of different flood events, it is necessary to establish the signature of flood events in both surface morphology and subsurface deposits.

Only by looking at these issues with respect to short-term deposition, can advances be made on predicting what is likely to be preserved in the long-term.

3 SOUTH SASKATCHEWAN RIVER

3.1 LOCATION

The South Saskatchewan River is a sandy braided river, originating in the Alberta Rockies, Canada. The South Saskatchewan flows in a north-eastern direction through Saskatchewan and drains into Lake Winnipeg, Manitoba, as the Saskatchewan River. The study reach is located near the town of Outlook on the South Saskatchewan, approximately 25 km downstream of Lake Diefenbaker (Figure 3.1). The study reach is approximately 1.2 km long, and displays typical braiding characteristics.

Figure 3.1. Location of study site.

Figure 3.2. Across stream view of Study reach in 2007. A compound bar is situated mid-river, with channels either side. Sub-aqueous dunes can be seen in channel. Downstream is to right of picture.

3.2 CHARACTERISTICS

The River has a braided planform ~0.6 km wide that incises into Quaternary deposits and Cretaceous shales and sandstones. Bed material is sand with average grain size 0.3 mm. The main channels are ~50 to 150 m wide and 2 to 5 m deep (Figure 3.2) with an average bed slope of 0.0003. A braiding index was calculated for a 13 km length of the reach for October 2006 (2.2) and July 2007 (2.4), based on Ashmore's (1991b) definition. The higher index in 2007 is attributed to higher discharges dissecting bar tops. Channels contain a range of bedforms including sand dunes and unit and compound bars (as defined in Chapter 2) (Figures 3.2 & 3.3). Typical mean dimensions of unit bars in the South Saskatchewan River include heights, lengths and widths of 1.0 m, 132.4 m and 77.7 m respectively. The mean height for dunes located on the channel bed is 0.25 m, with individual heights typically

ranging between 0.1 and 0.6 m. The bars consist of medium-scale cross-strata formed by dune migration (see Chapter 2 for sedimentology). Cant and Walker (1978) measured compound bar dimensions (defined as 'sandflats') and found lengths to range between 50 and 2000 m, and widths to vary between 30 and 450 m.

The River derives its stream flow from snowmelt and precipitation. Mean annual discharge of the South Saskatchewan River is approximately 197 m^3s^{-1} (1968 - 2004). The Gardiner Dam is located 25 km upstream and has altered the hydrological regime of the river since its instatement in 1967 (1911 - 1963 mean annual discharge 281 m^3s^{-1}) (see Figure 3.4) but there has been no statistically significant change in mean bed elevation post-dam on the study reach at ~ 25 km downstream (Phillips, 2003).

Figure 3.3. View of study reach in 2007, looking downstream. Picture shows the front of a unit bar with ripples present on surface.

3.3 2005 FLOOD

3.3.1 Flood characteristics

A flood event occurred on the River in June 2005 due to heavy rainfall. A total of 157.2 mm precipitation fell in Outlook in June 2005, peaking at 32.6 mm on 17th June (Environment Canada). On average June rainfall in Outlook (1971 - 2000) is 63.7 mm (Environment Canada). Flood discharge peaked at 1830 m^3s^{-1} on the 22nd June, and remained above 1000 m^3s^{-1} for 19 consecutive days (Figure 3.4). Bars were overtopped on the study reach for approximately 60 consecutive days (overtopping at ~230 m^3s^{-1}). Thomas (2006) performed recurrence interval analysis using a log-Pearson Type III distribution on the annual mean series of discharge records for Saskatoon, and estimated that the 2005 flood had a post-dam recurrence interval of 1 in 40 years. Therefore the June 2005 flood can be classified as a high-magnitude low-frequency flood event.

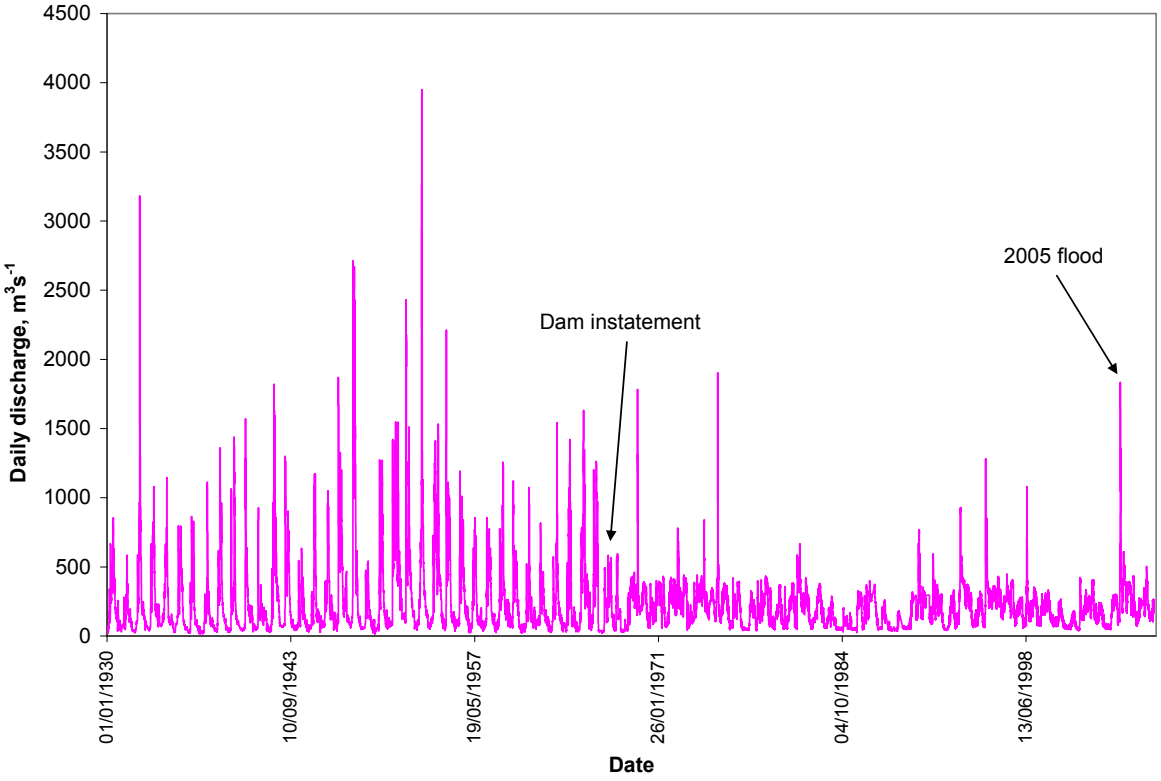

Figure 3.4. Daily discharge series 1930 - 2007 for South Saskatchewan at Saskatoon. Data obtained from Environment Canada.

3.3.2 Geomorphic significance

3.3.2.1 Frequency

The flood has a recurrence interval of 1 in 40 years, with the last flood of a similar magnitude occurring in June 1975. Kochel (1988) discussed periodicity of flood events and explains that if there has been sufficient recovery time from a prior flood, then a large impact will be caused by a new flood. However, this impact may be temporary depending on whether flows after the flood can rework and re-adjust to pre-flood conditions prior to another high-magnitude flood event (Marren, 2005). In the case of the June 2005 flood, it was a low-frequency event so that any previous flood's work (e.g. 1975) will have been reworked by post-flood low-magnitude high-frequency floods. This increases the likelihood of a large initial impact of the 2005 flood on the river's morphology. However, post-flood flows (2005 - 2007) have remained low-magnitude high-frequency flood events so that re-working of bar forms and deposits back to initial pre-flood conditions may have occurred. The possible re-working of deposits decreases the likelihood of the June 2005 flood leaving a long-term geomorphic impact. The initial impact and long-term impact of the flood will be assessed in Chapters 5, 6 and 7.

3.3.2.2 Flow characteristics

With respect to flow characteristics, Gupta (1983) stresses the importance of the ratio between peak flood discharge and mean annual discharge for determining the geomorphic significance of a flood event. Peak discharge for the June 2005 flood is 1830 m^3s^{-1}, thus compared with a mean annual discharge of 197 m^3s^{-1}, the ratio is high (9.3). Gupta (1983) explains that a 'high' ratio increases the preservation potential since re-working of material deposited by the flood will be restricted under lower discharges; however, this theory can

only really apply to coarse material such as gravel. The South Saskatchewan carries a medium size sand bedload, thus low-magnitude high-frequency floods may have the ability to re-work deposits produced by the flood.

Jones (1977) explains that the preservation of flood forms is also dependent on the rate of fall of flood discharge. A rapid fall increases the likelihood of preservation as there is less time for re-working, and bedforms may become abandoned. The June 2005 flood hydrograph (Figure 3.5) shows that initially, discharge fell quite rapidly. Furthermore, a second flood peak occurred 14 days after the peak discharge, with discharge falling rapidly afterwards. However, because the South Saskatchewan has a low variation in relief (~469 to 473 m, NAD83), the critical time to assess the rate of fall in discharge is perhaps when the flow drops to just below bar overtopping stage since this is when bedforms may be abandoned. Bars are overtopped when discharge reaches ~230 m^3s^{-1} so that the critical period is between the 6th and 7th August (flow drops from 283 m^3s^{-1} to 220 m^3s^{-1}).

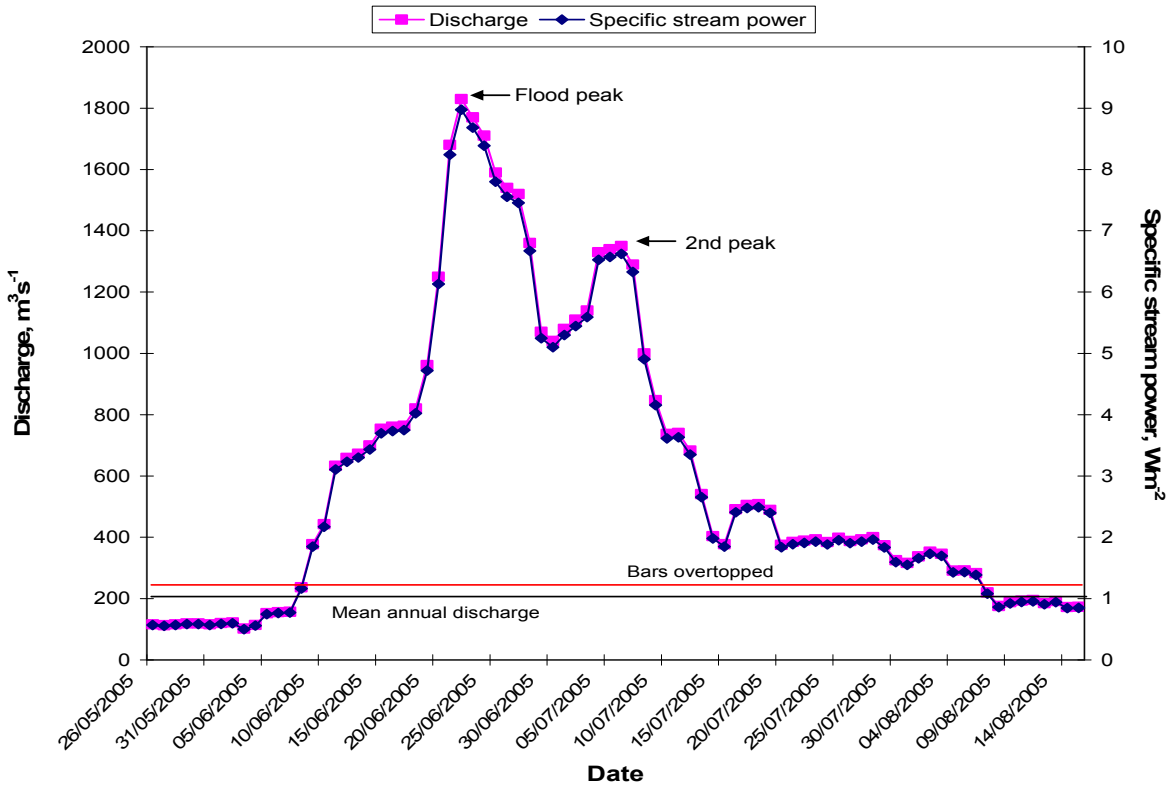

Figure 3.5. June 2005 flood daily discharge and specific stream power. Discharge data obtained from Environment Canada.

Unfortunately no stage heights are available for this period, but based on the width of the river (~0.6 km), it may be that a drop in discharge of 63 m^3s^{-1} in 24 hours could have occurred fairly rapidly. The preservation of deposits produced due to the June 2005 flood will be assessed in Chapters 6 and 7.

3.4 PREVIOUS WORK

The South Saskatchewan has been subject to regular monitoring since the construction of the Gardiner Dam. In 1964, the Saskatchewan Water Resources Commission set up 27 cross-sections downstream of the dam as a way of assessing the impact of the dam on bed elevations. In addition, the Saskatchewan Water Corporation and the Water Survey of Canada have monitored the cross-sections. Phillips (2003) assessed the impact of the dam using the cross-section information and has concluded that bed degradation occurred up to 12.9 km downstream of the dam and perhaps up to 23.7 km (study reach is 25 km downstream). A seasonal reversal of the hydrological regime has also occurred (Phillips, 2003). Pre-dam, the South Saskatchewan's hydrological regime featured increased flows in summer months due to snowmelt, and decreased flows in winter (Figure 3.6), however, post-dam flows have increased in winter months and reduced in summer months, reducing the seasonality of the regime (See Figures 3.4 & 3.6). This has resulted in a 27% reduction in mean annual discharge and a 60% decrease in annual peak discharge (Phillips, 2003). Even though the discharge regime has been altered, the braided channels are active for the majority of the year, and the flows are able to entrain sediment, enabling migration and growth of unit and compound bars (Sambrook Smith *et al*., 2006a). Thus, post-dam, the South Saskatchewan River still displays characteristics typical of a temperate sand bed braided river.

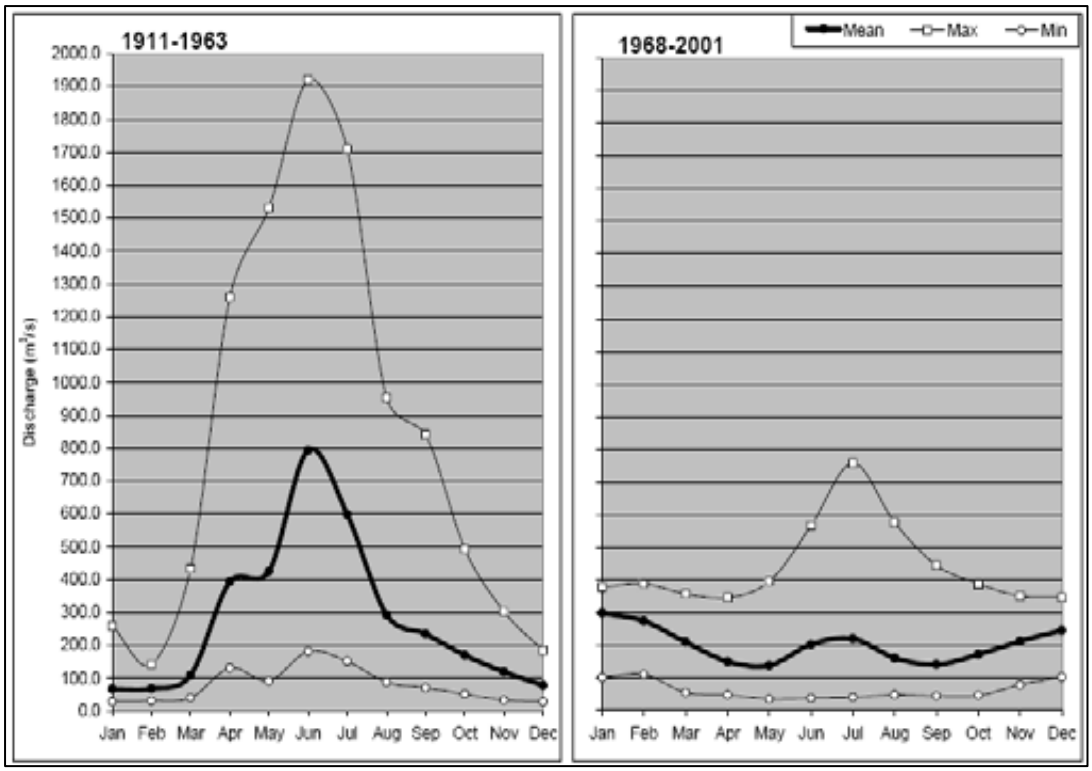

Figure 3.6. a) Daily discharge at Saskatoon, South Saskatchewan 1911 - 2006. Data from Environment Canada. b) Change in seasonal flow regime after dam construction. From Phillips, 2003, p.16, Fig. 11.

The South Saskatchewan has been a focus of sedimentological research since Cant and Walker's (1978) influential documentation of the River's morphological units and sedimentary deposits using techniques of trenching and box coring, and their proposition of a facies model for sandy braided rivers. In brief, the facies model suggested three types of facies; channel, mixed influence, and sand flat. Cant and Walker (1978) suggested channel facies are dominated by medium-scale cross-strata formed by migrating dunes, and that sand flat (bars) facies are comprised of mainly high-angle inclined deposits.

Thomas' (2006) PhD research on the South Saskatchewan focused on the development of a methodology for creating high resolution DEMs of the river bed to assess morphological change 1944 - 2005. Thomas (2006) also numerically modelled flow and sediment transport equations to assess flow processes and braiding mechanisms in the South Saskatchewan and found that unit bars are a key component of the braided morphology.

Sambrook Smith *et al.* (2006a) sought to re-evaluate Cant and Walker's (1978) facies model using data collected from GPR surveys and aerial photography on the same study reach of the South Saskatchewan in 2000. GPR surveys of both compound and unit bars identified four different types of radar facies in the bar deposits; medium-scale cross-strata formed by dune migration, high-angle inclined deposits due to bar migration into thalwegs, low-angle planar-stratification formed by low-amplitude dunes migrating over accretion surfaces, and also channel cut and fill features (Sambrook Smith *et al*., 2006a). These facies were present on different bar types but to a varying extent with respect to percentage of composition and location within bar deposits. Further research by Sambrook Smith *et al*. has extended the record of subsurface and surface data on the study reach 2004 - 2007. This period includes the June 2005 flood, and so has provided the opportunity to place the impact of the flood into context with previous morphological and sedimentological evolution on the reach.

This PhD research utilises the GPR data and aerial photographs collected 2004 - 2007 (see Table 3.1) to assess the impact of the June 2005 flood on the surface morphology and subsurface sedimentology on a sub-reach of the original study site. Thus, it uses a range of new and secondary data sources and analysis, and builds upon previous work by Sambrook Smith *et al*. (2006a). Table 3.1 details the data used in this thesis.

Table 3.1. Data used in PhD: recognition of source, processing and interpretation.

Data	Collection	Raw data processing	Analysis and interpretation
GPR 2004	SS *et al*	SS	**NOP**
GPR 2005	SS *et al*	SS	**NOP**
GPR 2006	SS *et al*	**NOP**	**NOP**
GPR 2007	**NOP**	**NOP**	**NOP**
DEM 2004	N/A	RT	**NOP**
DEM 2005	N/A	SL PW	**NOP**
DEM 2006	N/A	**NOP**	**NOP**
DEM 2007	N/A	**NOP**	**NOP**
SS = Greg Sambrook Smith	SL = Stuart Lane (Durham)	PW = Penny Widdison (Durham)	RT = Rob Thomas (Durham)

4 METHODOLOGY

In order to completely understand the evolution of subsurface deposits, there is a need to link subsurface deposit evolution with surface morphological dynamics. This will help clarify the relationship between surface and subsurface processes and will aid understanding into which types of processes are preserved in the sedimentary record. Recent studies of subsurface deposits using GPR have been supplemented with aerial photography of surface features (Lunt *et al.*, 2004 and Wooldridge and Hickin, 2005) in order to explore this. This PhD research goes further and links sequential GPR data with digital elevation models of the reach created from aerial photographs. This will enable quantification of both surface and subsurface evolution for comparison with each other.

4.1. GROUND PENETRATING RADAR

4.1.1 Theory

4.1.1.1 Introduction

Traditional methods of investigating subsurface sediments such as boreholes, coring, trenching and cut banks are often invasive and time consuming, and present a spatially restricted sample of deposits (Jol and Smith, 1991). GPR, which has become increasingly popular in the last few decades, is a non-invasive technique which uses electromagnetic radiation to detect subsurface discontinuities (Neal, 2004). GPR has been used in a wide variety of applications in sedimentology including glacial, coastal, lacustrine and fluvial research (Jol and Smith, 1991; Bridge *et al.*, 1995; Smith and Jol, 1995; Bridge *et al*., 1998, Skelly *et al.*, 2003; Lunt and Bridge, 2004; Lunt *et al*., 2004; Wooldridge and Hickin, 2005; and Sambrook Smith *et al.,* 2006a), and has also been used to assess the impacts of high-magnitude low-frequency floods in proglacial environments (Russell *et al.*, 2001; Cassidy *et*

al., 2003).

GPR transmits pulses of electromagnetic energy (typically 10 to 1000 MHz) from a transmitter into the subsurface (Jol and Smith, 1991). The electromagnetic energy is radiated in a 3D cone, so that the reflected energy may originate from any point on the wave front (Neal, 2004). The electromagnetic pulse is reflected back to a receiver if there is a significant discontinuity with respect to subsurface properties of dielectric permittivity, magnetic permeability or electric conductivity (Neal, 2004). Dielectric permittivity has been defined as "a measure of the material's ability to store electrical charge" (Neal, 2004, p. 268) whereas electrical conductivity is the ability to transport electrical charges on receipt of an electrical field (Neal, 2004). Magnetic permeability is similar to dielectric permittivity but involves the storage and loss of magnetic field energy (Neal, 2004). Discontinuities can be due to changes in the subsurface sediment/air/freshwater ratio, so that changes in sediment properties such as size sorting, orientation, lithology and porosity may produce prominent reflections in the radar profile (Neal, 2004). The strength of the reflected signal varies in proportion to the difference in electrical properties between surfaces (Jol and Smith, 1991). Therefore, the reflections can be related to sedimentary structures (Jol and Smith, 1991).

The electrical properties of the subsurface material also determine the depth of penetration and resolution of data. High values of dielectric permittivity, magnetic permeability and electric conductivity in subsurface material causes strong signal attenuation and thus decreased penetration depth (Schrott and Saas, 2008). Examples of such subsurfaces in sedimentological investigations include those containing a high clay content, silt content, or saline water (Smith and Jol, 1995; Schrott and Saas, 2008). A good resolution and penetration depth can be attained in sediments that are relatively dry and electrically resistive, for example sands, gravels and quartzose rich sediments (Smith and Jol, 1995).

4.1.1.2 Data collection

4.1.1.2.1 Types of data collection

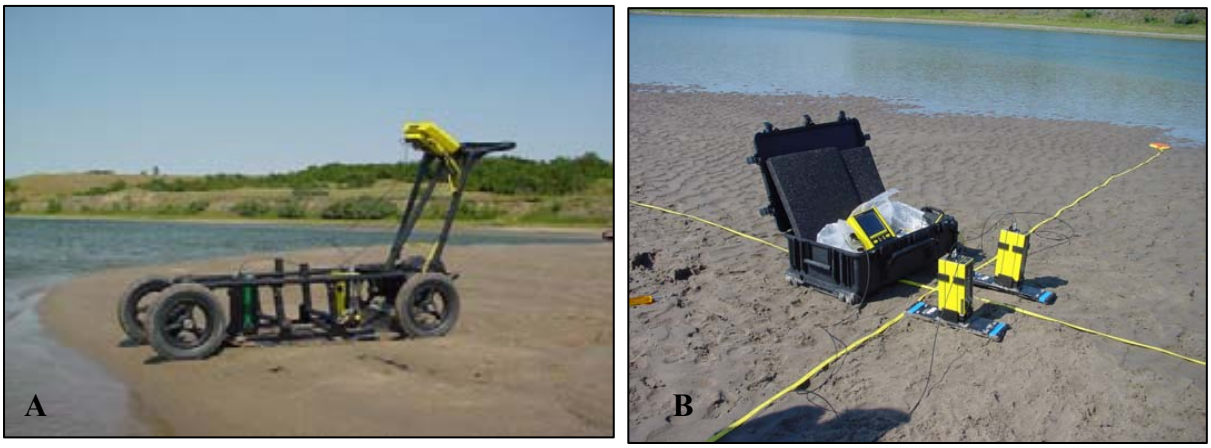

Figure 4.1. GPR investigations using A) a common offset method (antenna separation here is 0.5 m), B) a common mid point method. GPR system used is Sensors and Software PulseEKKO PRO.

There are four main types of data collection with respect to transmitter and receiver positions; common offset, common mid point, common source and common receiver. The most commonly used for sedimentological investigations is the common offset (CO) method where there is either a single transmitter and receiver in one unit or where separate antennas are separated by a fixed distance (Neal, 2004) (Figure 4.1A). This method has the benefit of allowing data collection to be carried out in a shorter time period when compared to the other methods; however, for each point surveyed it only collects one near offset trace, i.e. only one snapshot of the subsurface (Berard and Maillol, 2007). The common mid-point (CMP) method requires the transmitter and receiver to be moved apart horizontally at fixed distances (Figure 4.1B). Two-way travel times can be obtained from this method, which can be converted into radar wave velocities which subsequently can be used to estimate depths (Neal, 2004). The remaining methods, common source and common receiver, rely on the transmitter or the receiver (respectively) remaining stationary whilst the other antenna moves (Neal, 2004). The use of these methods means that multiple snapshots are taken of the subsurface

from different angles so that an improved image can be achieved when compared with the common offset method (Berard and Malliol, 2007). For example, increased depths of penetration can be attained without decreasing resolution, and reflector continuity is often improved; so that these methods are preferable where improved data quality is required over a surface of interest (Berard and Malliol, 2007). However, data collection is slower than the common offset method, and more post-processing is required (Neal, 2004).

4.1.1.2.2 Modes of data collection

Data can be collected in two modes: continuous mode or step mode (Neal, 2004). Continuous mode is where the antennas are pulled across a surface and the distance covered is converted from time or ground markers (Woodward *et al*., 2003). In step mode, the transmitter and receiver are moved progressively at set distances so that the exact location of each trace on a radar profile is known (Woodward *et al.,* 2003). The characteristics of the surface and the size of project need to be taken into account when deciding on the mode of data collection. For example, the continuous mode may be less time demanding on a large study site, however, if the terrain is rough, the quality of data may be impaired (Woodward *et al*., 2003).

4.1.1.2.3 Radar parameters

When the method and mode of data collection has been decided upon, the radar parameters are chosen. These include the choice of antenna frequency, antenna separation, station spacing, sampling interval, stacking and transmitter power.

Antenna frequency: A linear relationship exists between maximum depth of penetration and antenna frequency (MHz) (Smith and Jol, 1995) so that higher frequencies yield shallower penetration (Figure 4.2). However, an increase in antenna frequency yields

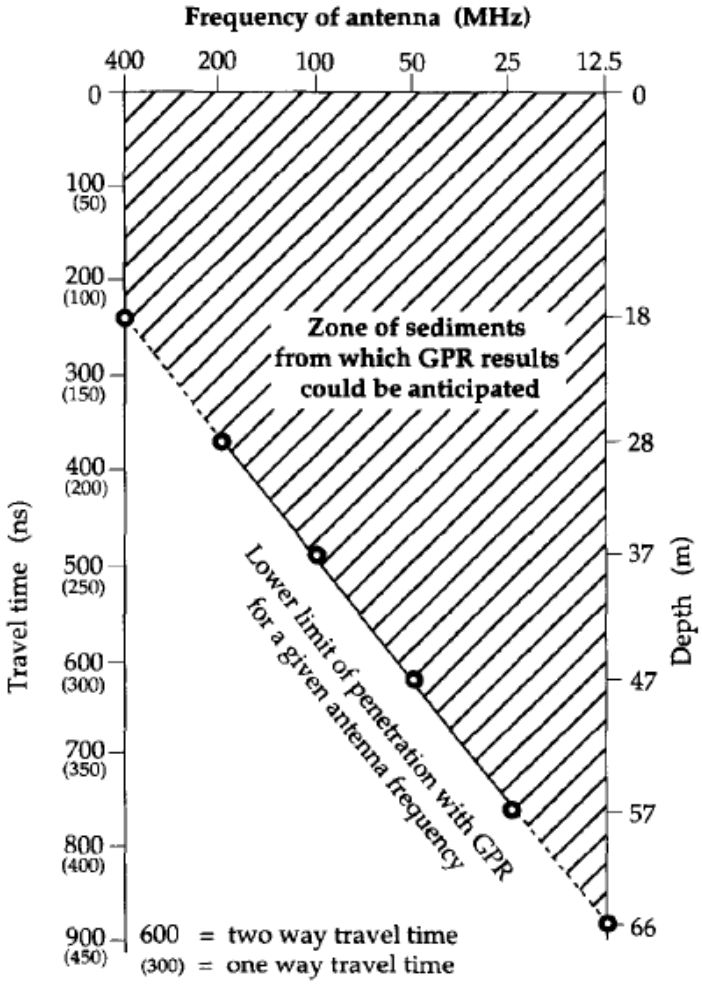

Figure 4.2. Relationship between antenna frequency and probable penetration depth in Quaternary sediments. From Smith and Jol (1995), p. 99, Fig. 7.

an increase in data resolution (Jol *et al*., 2002) (Figure 4.3). Thus, with increased penetration there will be a loss in resolution, so that a compromise has to be obtained between depth and detail of data. Alternatively, if there is enough time, a survey could be repeated with a different frequency.

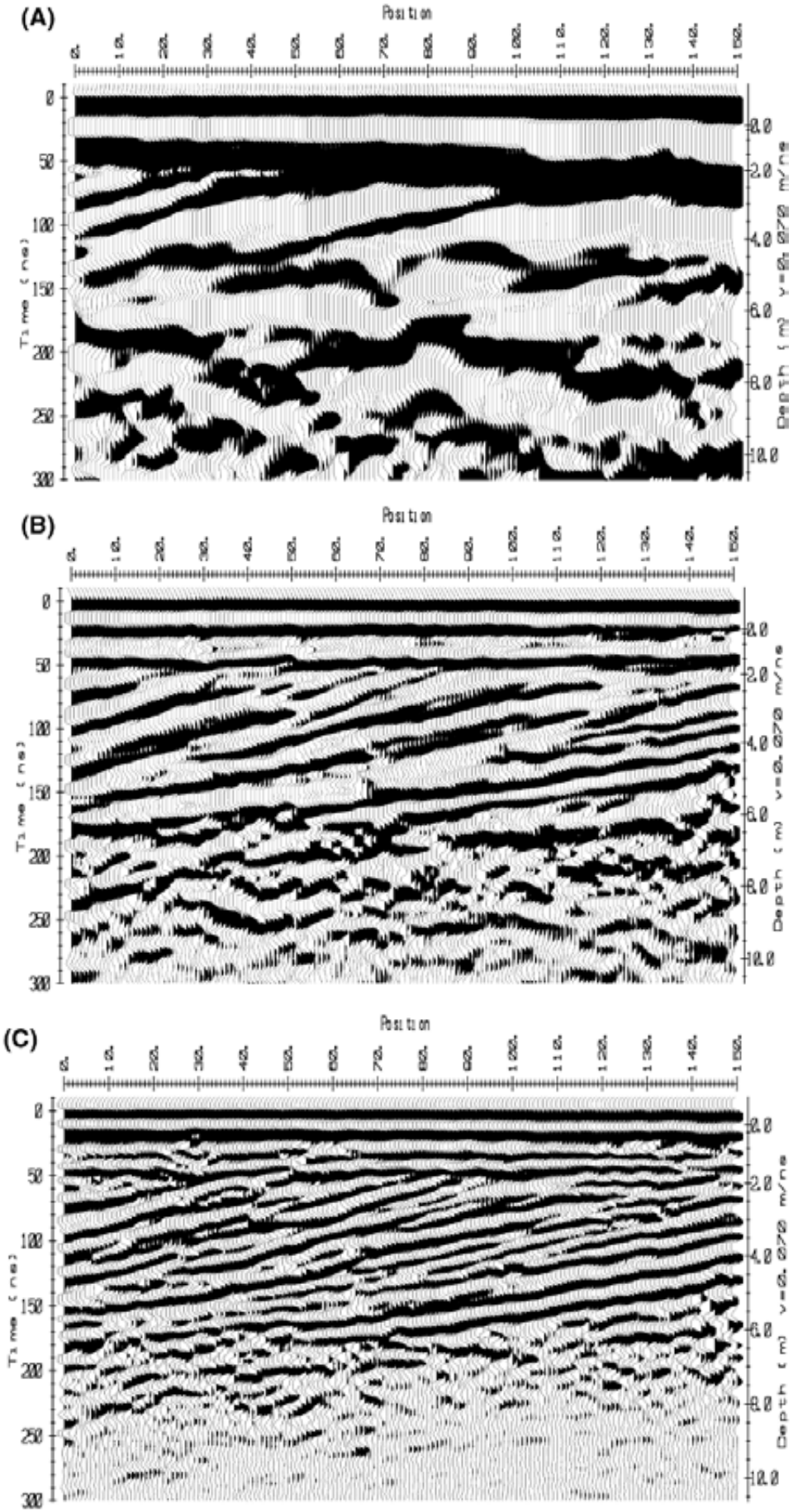

Figure 4.3.
Increasing resolution of GPR data and decreasing penetration depth with increasing antenna frequency a) 12.5 MHz antenna b) 50 MHz antenna c) 100 MHz antenna. From Jol *et al*. (2002), pp. 170-171, Fig. 5(a)(b)(c).

Antenna separation: Antenna separation is determined by the antenna frequency used. As a general rule minimum spacing should equal antenna length (Sensors and Software, 2005) (Table 4.1). If separation distance is too short, data may be lost due to overloading of the receiver electronics (Sensors and Software, 2005).

Table 4.1. Minimum antenna spacing for different frequencies. Adapted from Sensors and Software (2005), p. 71.

Frequency (MHz)	Minimum antenna separation (m)
12.5	8
25	4
50	2
100	1
110	1
200	0.5
250	0.38
500	0.225
1000	0.15

Station spacing: Station spacing (or antenna step size) is the spacing between each trace collected, and is also frequency dependent with larger station spacings used for smaller frequencies. For example, for 100 MHz and 500 MHz antenna, step sizes would typically be 0.25 m and 0.025 m respectively (Sensors and Software, 2005). The spacing is also determined by the nature of the reflections. For example, where reflections are relatively unchanging and continuous, a larger step size will suffice. However, if they are more varied or steeply dipping, a smaller step size is needed in order to detect the detail.

Sampling interval: Sampling interval (ns) is the time between points sampled on a trace. The sampling interval should generally be less than half the period of the highest frequency, so that sample interval decreases with increasing frequency (Sensors and Software, n.d). Sampling intervals are calculated using the formula

$$t = \frac{1000}{6f} \qquad [4.1]$$

Where t is time (ns) and f is centre frequency (MHz) (Sensors and Software, n.d, p.9). The equation assumes that the maximum frequency is 1.5 times the antenna centre frequency, and applies a safety margin of two to this. Table 4.2 lists maximum sampling intervals for antenna frequencies.

Table 4.2. Maximum sampling intervals for specified antenna frequencies. Data taken from Sensors and Software (n.d), p. 9.

Antenna centre frequency (MHz)	Maximum sampling interval (ns)
10	16.7
20	8.3
50	3.3
100	1.67
200	0.83
500	0.33
1000	0.17

Stacking: The number of stacks used is the number of traces collected and averaged at each position. Increasing the number of stacks can improve the signal to noise ratio where there is much interference present. A stacking of 8 may be used when collecting data in fairly remote areas where little electrical interference is present, however, if devices such as mobile phones, radio transmitters and television transmitters are present, then background noise may be introduced into the data (for example Figure 4.4) (Olhoeft, 2000; Neal, 2004), and increasing the number of stacks, for example to 64, may be able to reduce this (Neal, 2004). However, increasing the number of stacks will also increase the survey time (Neal, 2004).

Transmitter voltage: Increasing the transmitter voltage increases the energy supplied to the antennas and hence can increase the depth of penetration, as well as reflection continuity (Jol *et al*., 2002). However, increasing transmitter voltage results in faster

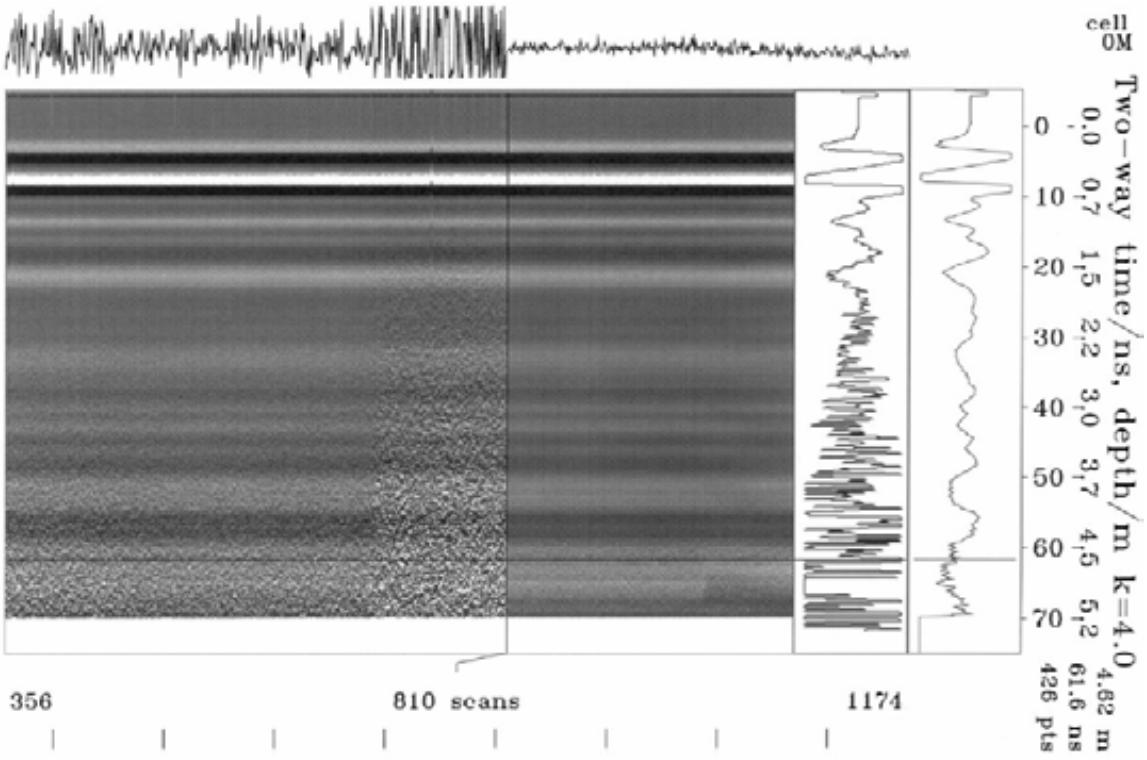

Figure 4.4. A GPR profile showing differing interferences from a mobile phone; the left side of the image resulted from a mobile that is switched on but with no active voice communication, the middle resulted from voice communication using the mobile phone, and the right resulted from the mobile phone being switched off. The interference affects the clarity of image, and inhibits identification of reflections and quantification of layer thicknesses, particularly when the mobile is in active use. From Olhoeft (2000), p.184, Fig. 11.

depletion of battery energy, and thus needs to be taken into consideration when planning data collection.

4.1.1.3 Data processing

Data processing is carried out to enhance radar reflections, and therefore to improve subsurface representation. Typical processing carried out in GPR software packages includes:

Time-zero-drift correction: This corrects for misalignment of the air wave and reflections beneath by moving traces up or down according to two-way travel time, and is usually applied automatically in GPR software packages (Neal, 2004).

Signal saturation correction: Signal saturation of the receiver can occur due to the large amounts of energy received from the ground and air waves and the near surface

reflectors. This introduces a low frequency wow into the data which can be suppressed by applying a high pass filter, for example a dewow (Neal, 2004).

Application of gains: Gain application increases signal strength at depth in the profile, where signal is often decreased due to increasing attenuation at depth. Often AGC (automatic gain control) is used whereby a gain is applied that is inversely proportional to the signal strength, resulting in equalised signal strength through the profile (Neal, 2004). However, this can also enhance any unwanted background noise.

Application of filters: Filters are applied to GPR data in an attempt to increase interpretation of data. Horizontal and vertical running-average filters have been used to reduce high-frequency or random noise, however the averaging effect also decreases data resolution (Neal, 2004). Band pass filtering is an alternative type of filtering which only removes a specific frequency band from the data (Neal, 2004). It is particularly useful where there is ambient noise to be removed (see Figure 4.5), and has the advantage of preserving the main features of the data (Neal, 2004).

Migration: Migration is another processing technique which removes structural distortions and corrects for reflector and dip displacement due to the antenna transmitting and receiving electromagnetic energy from a 3D cone, rather than 2D (Neal, 2004; Hugenholtz *et al*., 2007). This can result in an increase in the clarity and representation of the reflections (Hugenholtz *et al.*, 2007) (see Figure 4.6).

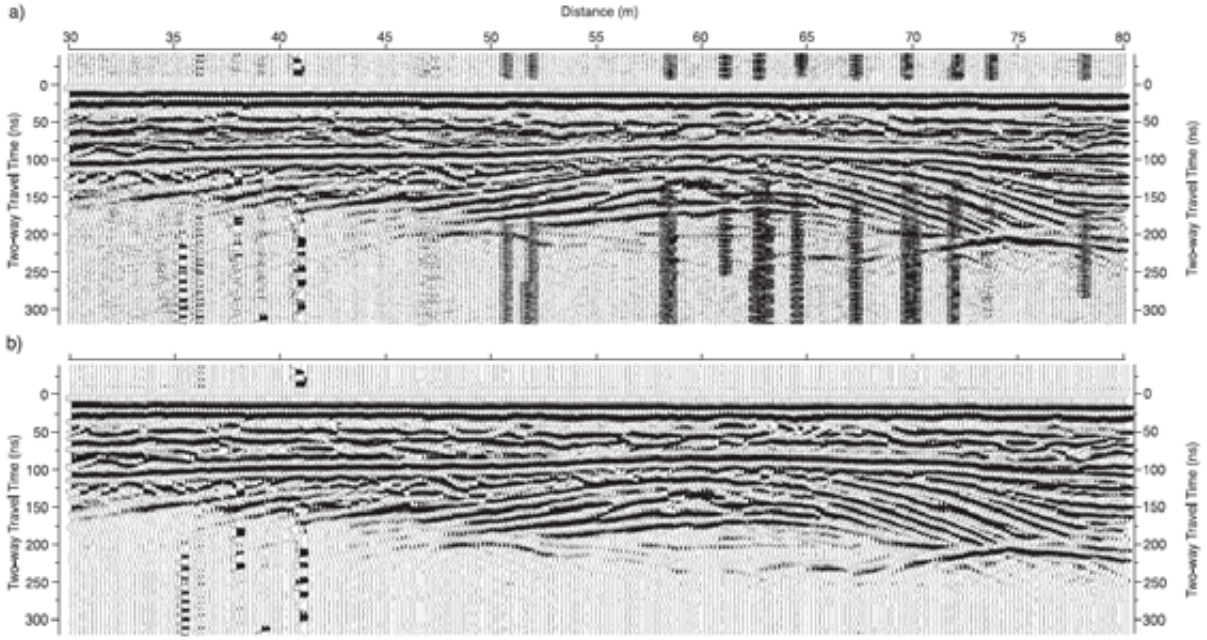

Figure 4.5. a) Unfiltered GPR profile showing interference from ambient noise b) Removal of most of the ambient noise after frequency filtering. From Neal (2004), p.287, Fig. 16.

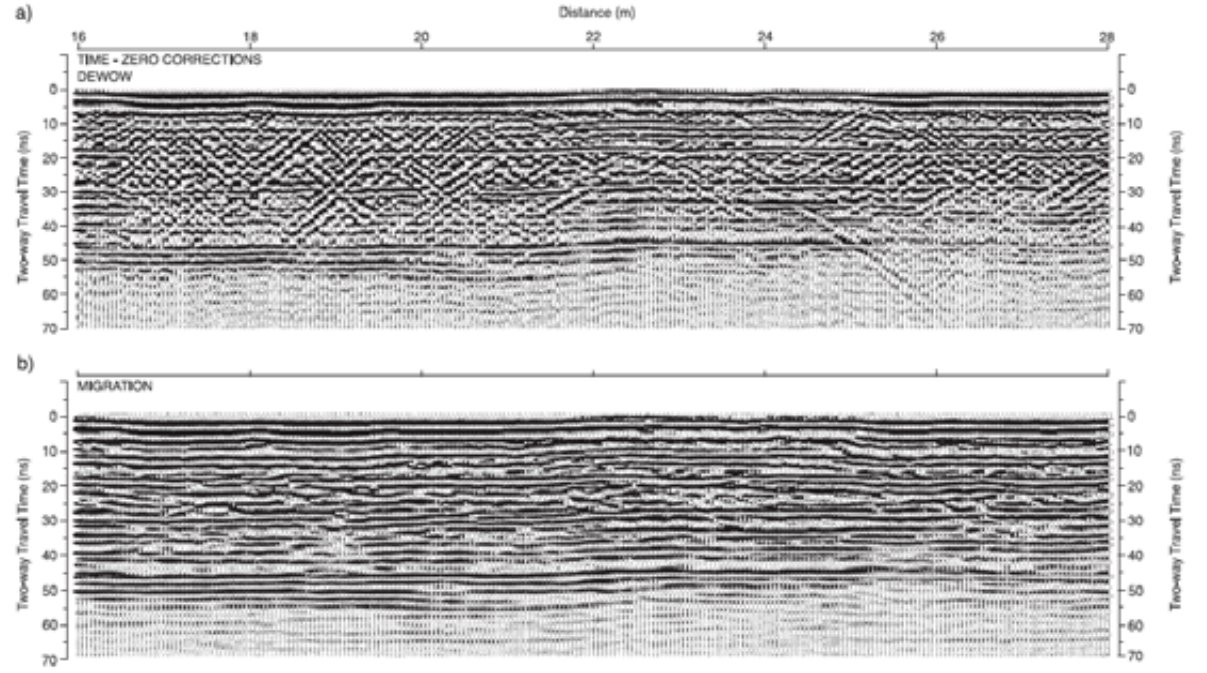

Figure 4.6. a) Un-migrated GPR profile showing horizontal reflections cross cut by diffraction hyperbolae b)Migrated profile showing improvement in subsurface representation: diffraction hyperbolae have been collapsed and so lateral continuity of reflectors is increased. From Neal (2004), p. 303, Fig. 21.

Depth conversion: Velocities need to be estimated in order to apply depth conversion. Velocities vary with subsurface type (Table 4.3) and can be estimated by several methods, for example by calculating the travel time between wells using borehole radar, or measuring the two-way travel time to a subsurface object or feature at a known depth (ground truthing), or by using CMP surveys on horizontal reflection surfaces (Neal, 2004). The CMP method is the most commonly used as it does not cause any subsurface disturbance (Greaves *et al*., 1996). From CMP analysis, two-way travel times can be obtained (see Figure 4.7), and the average velocity (v_1) for a reflection can be calculated using:

$$v_1 = \sqrt{\left[\left(x_2^2 - x_1^2\right)/\left(t_{x_2}^2 - t_{x_1}^2\right)\right]} \qquad [4.2]$$

where x_1 and x_2 are antenna separations and t_{x1} and t_{x2} are the two-way travel times at the antenna separations (Robinson and Çoruh, 1988, p.89).

Depth (D) then can be calculated with the following formula:

$$D = V \times T/2 \qquad [4.3]$$

Where V is velocity (m/ns) and T is two-way travel time (ns) (Sensors and Software, 2005).

Table 4.3. Typical velocities for different subsurface materials. Adapted from Sensors and Software (2005), p.73.

Material	Velocity (m/ns)
Air	0.30
Ice	0.16-0.17
Dry sand	0.15
Dry rock	0.12
Concrete	0.08-0.12
Shales	0.09
Wet sand	0.06
Clays	0.06
Fresh water	0.033

Topographic correction: If the survey surface is not level then topographic correction needs to be applied to the radar data during post-processing. The GPR presumes the surface is level, so in order to improve the accuracy of the geometry of the subsurface reflectors,

elevation data can be applied. This may be obtained via a topographic survey (e.g. using GPS). Line lengths may also need to be adjusted to the correct length to correct for any skipped traces or errors in line measurement.

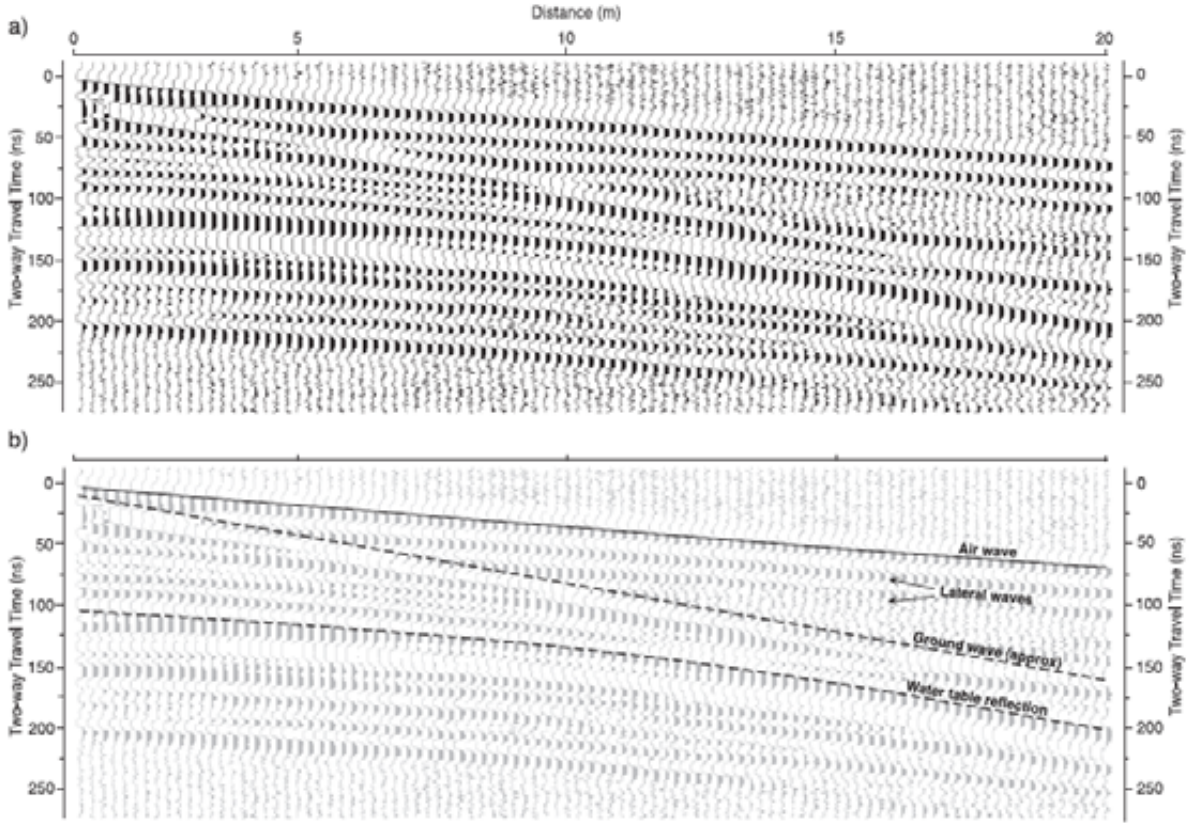

Figure 4.7. a) CMP profile with b) interpretation of reflections. From Neal (2004), p. 299, Fig. 19.

4.1.1.4 Data interpretation

The first reflections in a GPR profile are the airwave and groundwave (Figure 4.8) which travel from the transmitter to the receiver, and through the ground between the transmitter and receiver, respectively (Neal, 2004). In sedimentological investigations, radar reflections below the air and ground waves are interpreted to represent sedimentary structures (Beres and Haeni, 1991). Beres and Haeni (1991) applied seismic facies analysis methods to interpret

radar reflections based on configuration, continuity and amplitude of the reflections. Similar to seismic reflection studies (e.g. Sangree and Widmier, 1979), similar types of radar reflection can be grouped as a particular radar facies and may relate to a deposit type or a deposit produced under similar formational processes. It is therefore possible to reconstruct the depositional and erosional history of sedimentary deposits using radar profiles (Jol and Smith, 1991; Neal *et al*., 2008)).

In order to correctly interpret GPR profiles, ground truthing is imperative. A trench or core can be made over a GPR line and compared to the GPR data so that reflections can be matched up with subsurface features and radar facies identified for specific deposits; depths estimated from two-way travel times can be verified; and limitations of the GPR can be ascertained, for example, it can be established which scales of deposit can be identified by the radar, and which are too small to be represented.

When interpreting deposits from radar profiles, it is important to remember that the resolution of reflections is dependent on the frequency of the GPR antenna used, so that with

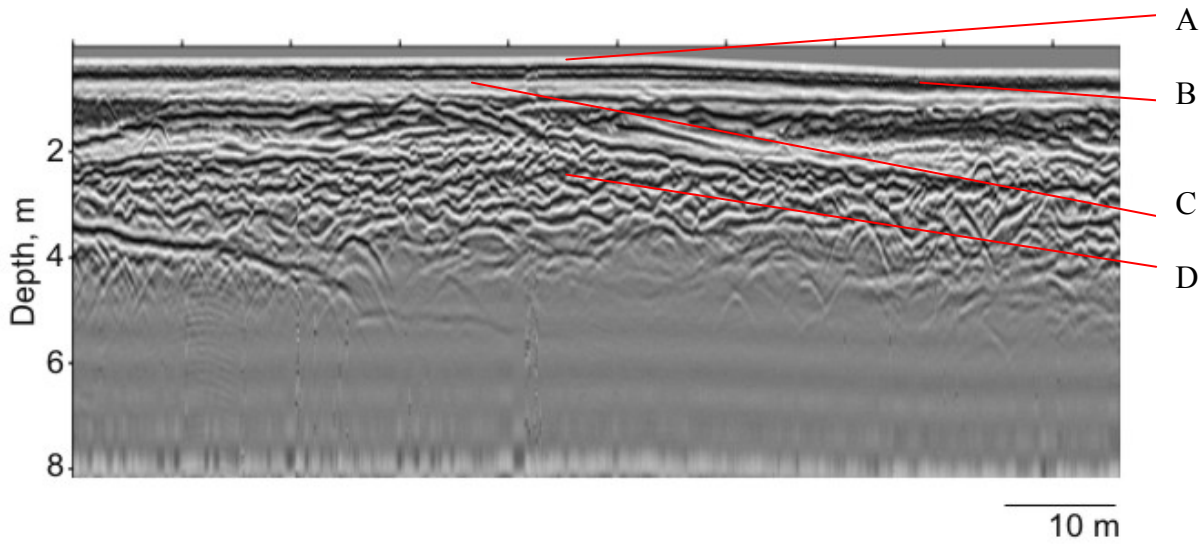

Figure 4.8. GPR profile showing A) the air wave, B) the ground wave, C) small-scale horizontal reflectors showing a decreased resolution compared with reflectors at depth, D) trough shaped reflectors. GPR of 25 line w-e, Bar E, 2006, processed by NOP.

lower frequencies the deposits of some small scale bedforms such as ripples may not be determined, only the bounding surfaces of such deposits can be identified (Sambrook Smith *et al.*, 2006a). Similarly at the top of GPR profiles, where deposits are often smaller in scale, reflections may lack detail. For example, small dune deposits may lack their distinct trough shape reflections and instead, horizontal or sub-horizontal reflections may be present which represent the bounding surfaces of planar and trough cross strata (see Figure 4.8, C) (Sambrook Smith *et al*., 2006a).

The orientation of the radar profile with respect to the deposit can also affect the clarity of the preserved feature as the degree of concavity of a reflection can vary with this, for example, concave reflections associated with channel cut features, are more distinct in radar when profiled perpendicular to flow direction (Sambrook Smith *et al*., 2006a). Lunt and Bridge (2004) also noted that variations in reflections inclinations may be either due to a change in the true dip of the deposit, or may be produced if the GPR profile varies in orientation with respect to the subsurface feature being imaged. Thus in order to accurately interpret the reflectors, many sedimentological GPR surveys are carried out using a grid system so that the subsurface can be imaged at different orientations (e.g. Figure 4.9).

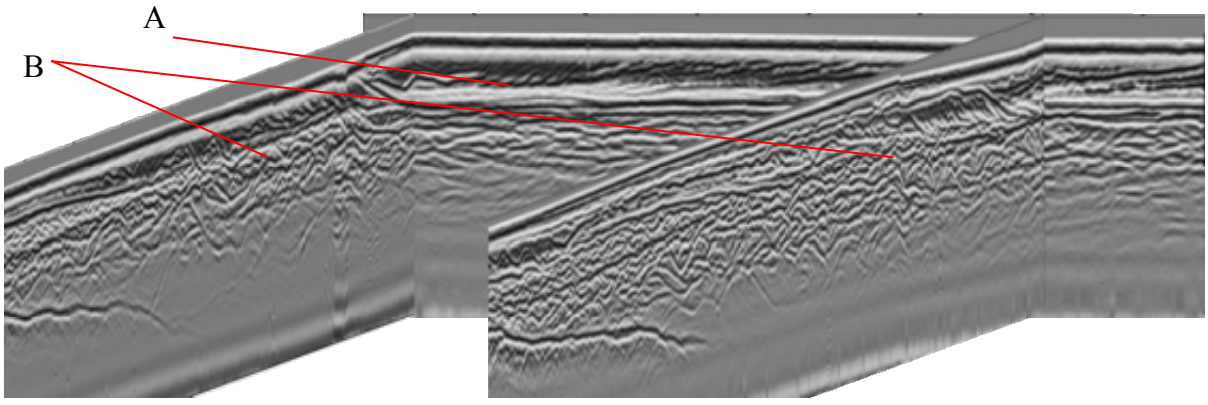

Figure 4.9. GPR profiles taken at opposite directions. Note the difference in reflectors between profiles: A) steep down-dipping reflectors, compared with B) an abundance of trough-shaped reflectors. GPR of 75 line s-n, and 100 & 150 lines w-e, Bar E, 2006, processed by NOP.

4.1.2 Methodology

4.1.2.1 Data collection

GPR surveys were conducted on a reach of the South Saskatchewan for consecutive years 2004 - 2007 using Sensors and Software PulseEKKO GPR models. Data collection methods broadly followed those of previous studies on the river in 2000 to ensure comparability of results. Survey parameters are listed in Table 4.4, and an outline of the data collection is presented in Figure 4.10.

The 100 MHz and 200 MHz antenna frequencies were tested but it was found that resolution was poor with the 100 MHz. The 200 MHz allowed penetration to a depth of ~6.0

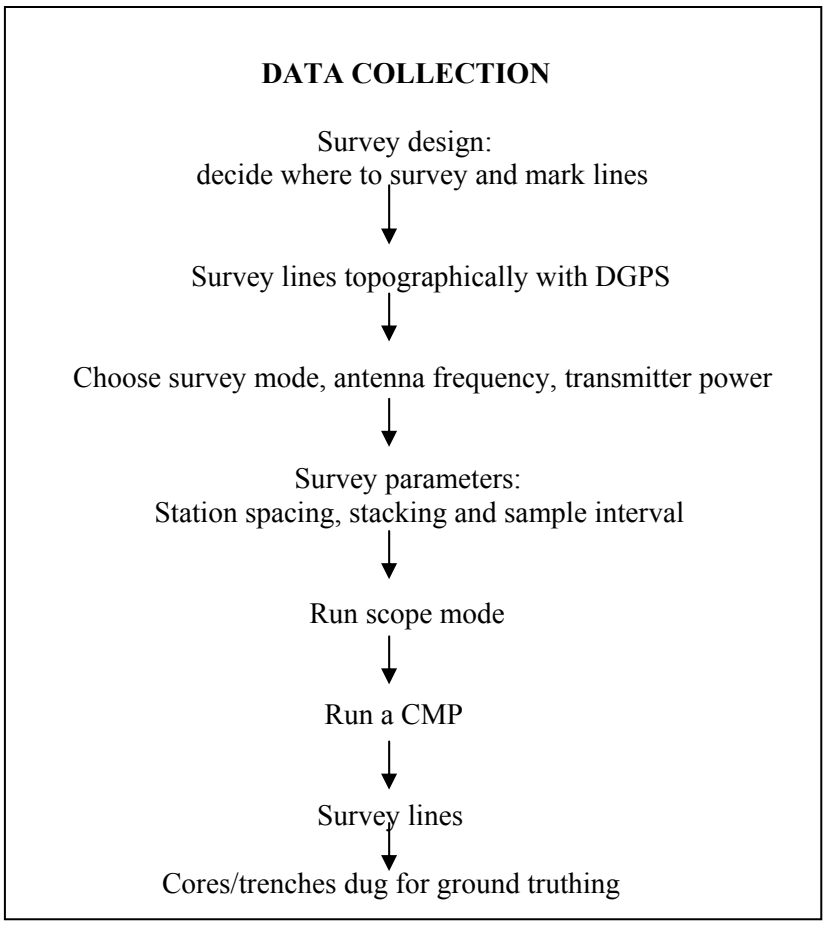

Figure 4.10. Stages of data collection.

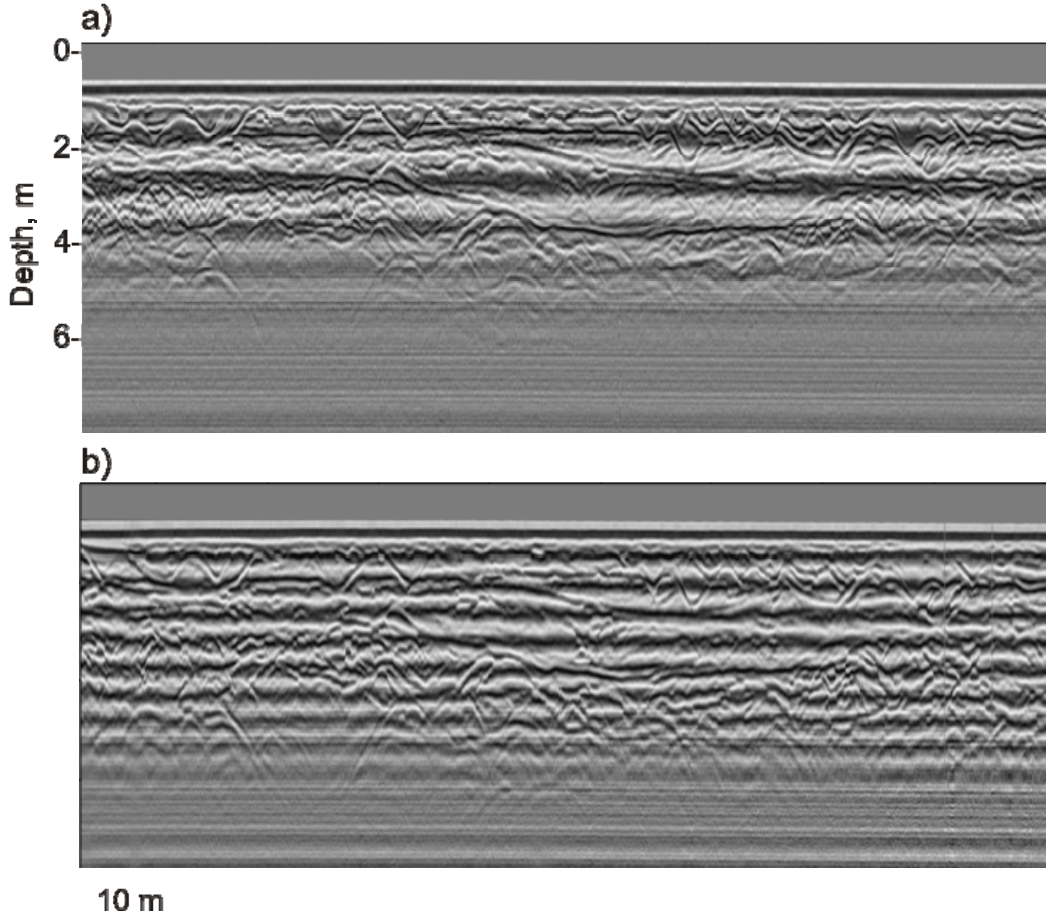

Figure 4.11. GPR profiles taken along the same line using a) 200 V transmitter and b) 1000 V transmitter. GPR of 350 line w-e, Bar A, 2007, processed by NOP.

m which captured the modern channel base so was deemed suitable for the study aims. The depth and scale were ideal for data collection needs as the enabled profiling of deposits ranging from large dunes to unit bars to channel depths. Different transmitter voltages were compared, however, the higher voltage transmitter did not significantly increase data clarity or depth of penetration (Figure 4.11). The 200 V transmitter was therefore used as it has a longer battery life than the 1000 V.

Data were collected using a common offset method in continuous mode with transmitter and receiver fixed perpendicular to the survey line for all surveys. Continuous mode was chosen as it is more time efficient than step mode, and tests indicated that data quality would not be impaired since the survey areas are relatively flat. A calibrated

Figure 4.12. A) sled mounted antenna for surveys 2004 - 2006 B) SmartCart™ used for 2007 surveys C) Leica GPS 1200 system used for surveying topography and marking out grid lines.

odometer wheel was used to control station spacing which was set at 0.1 m (Table 4.4) as this was optimum for data volume and also data quality, as it enabled the imaging of dipping reflectors. Minimum antenna separation for 200 MHz antenna is 0.5 m. Surveys conducted 2004 - 2006 used a sled to mount the antennas at a separation of 0.75 m (Figure 4.12A) and in 2007, a Sensors and Software SmartCart™ was used with a 0.5 m separation bar (Figure 4.12 B). A low number of stacks was chosen (8 or 16, Table 4.4) as the study site is fairly remote and tests revealed the GPR did not suffer from significant electrical interference. The data from all surveys are directly comparable.

After the data parameters are set, the GPR is run in scope mode prior to data collection. Scope mode has two purposes: firstly it tests the GPR to make sure all connections and parameters are correct so that data will be collected successfully, and secondly it enables time zero to be set, which is the first arrival of the radar wave (Sensors

Table 4.4. GPR survey parameters.

Year	GPR system	Antenna frequency (MHz)	Station spacing (m)	Antenna separation (m)	Stacks	Sample interval (ns)
2004	Sensors & Software PulseEKKO 100	200	0.1	0.75	16	0.4
2005	Sensors & Software PulseEKKO 100	200	0.1	0.75	16	0.4
2006	Sensors & Software PulseEKKO 100	200	0.1	0.75	8	0.4
2007	Sensors & Software PulseEKKO PRO	200	0.1	0.5	8	0.4

and Software, 2005). Setting time zero ensures that data will be recorded correctly, with no reflectors being lost at depth.

A grid system was implemented for the survey lines using DGPS (Leica GPS 1200 system), (Figure 4.12C) allowing precise resurvey of lines in each year, and thus a direct comparison of a sequence of GPR profiles (see Figure 4.13). The grid system is based on lines running downstream (south to north) and across stream (west to east), with origin at the south west (See Figure 4.14 for Reach A grids 2004 - 2007). A grid of survey lines allows different views of the subsurface to be attained, and thus an accurate representation of the subsurface derived from two directions. The Reach A grid (Bars A and A2) is based on a 50 metre spacing, allowing unit bars to be captured. A 25 metre spacing was used on Bar E to capture detail on the two small unit bars composing it. The grid size was also a compromise between data volume and survey time expenditure.

CMP surveys were conducted in 2004 and 2007 on the study reach in order to calculate a depth conversion velocity. Surveys were carried out on an area of ground displaying strong horizontal reflectors (see Figure 4.15). Measuring tapes were laid over the

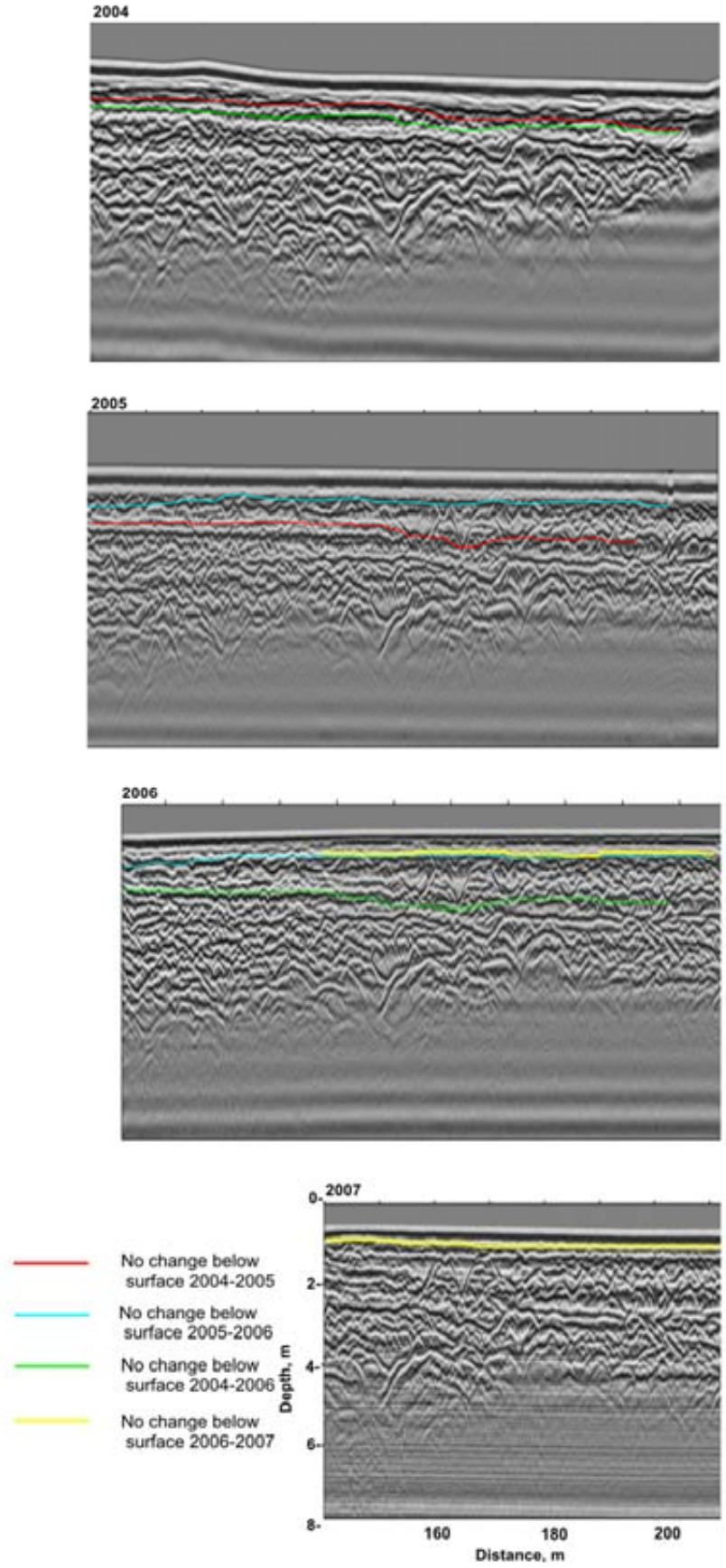

Figure 4.13. Repeat survey of 450 line w-e on Bar A in 2004, 2005, 2006 and 2007. Coloured lines identify surfaces of no change across the years. Processed by NOP.

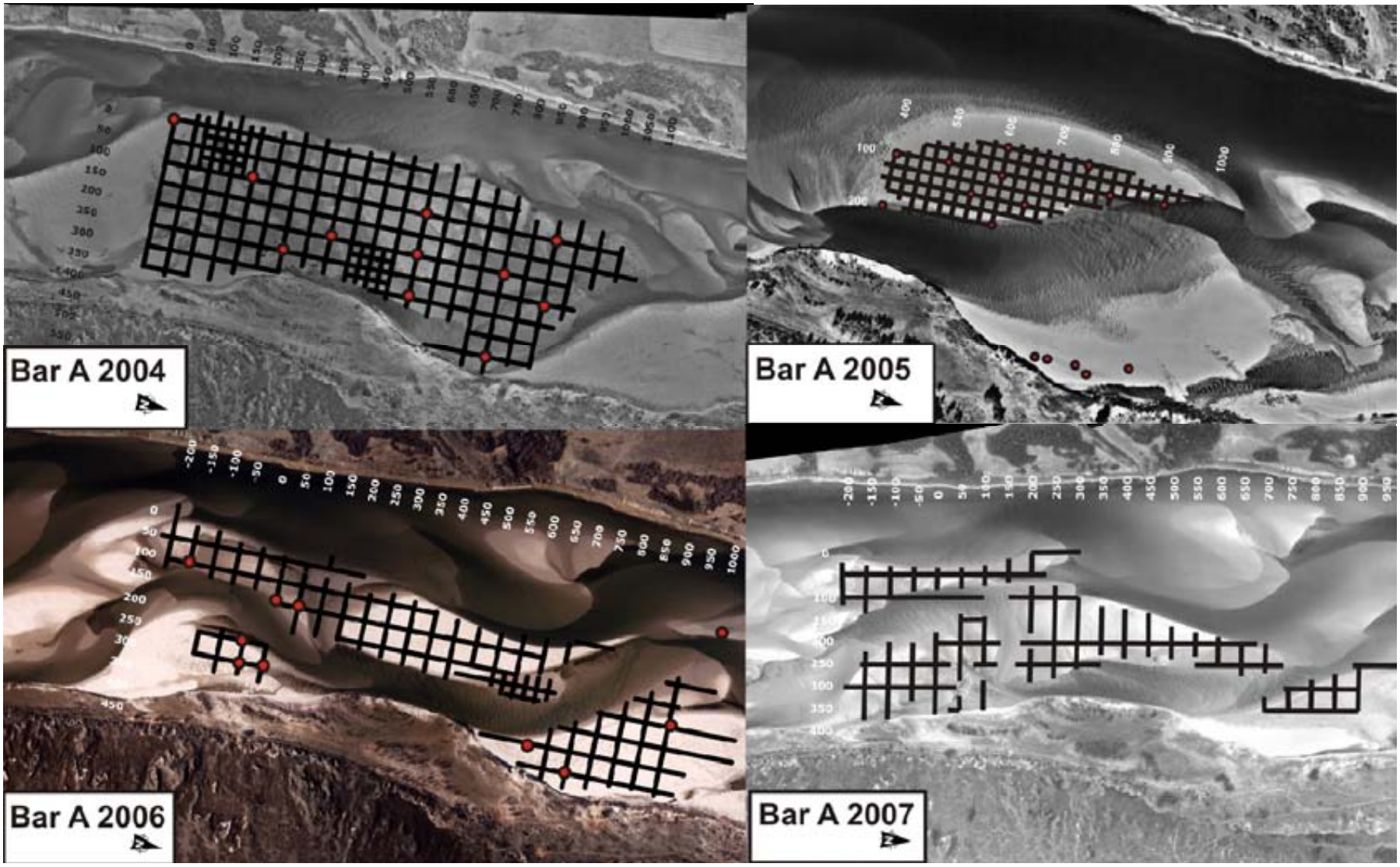

Figure 4.14. GPR lines surveyed 2004 - 2007. Black lines represent GPR lines and red circles are core locations.

area in across and downstream directions to enable two CMPs to be carried out perpendicular to each other. For each, the transmitter and receiver were initially separated 0.5 m (usual separation distance for 200MHz) and centred over the tape origin. They were then moved an interval of 0.05 m out from each other (as step size is 0.1 m), and a trace was recorded using a manual trigger on the console. This step was continued until the reflections on the CMP

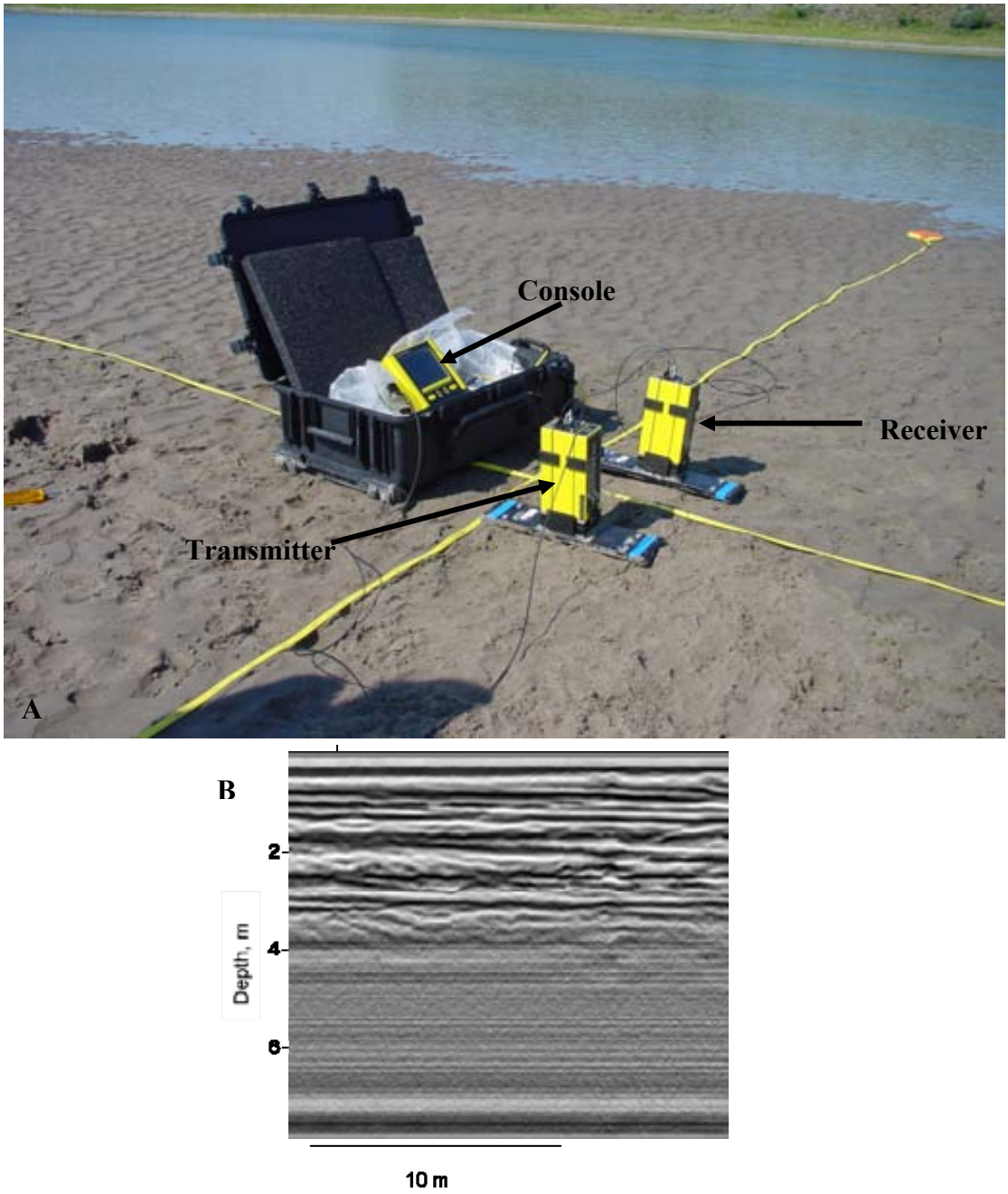

Figure 4.15. a) CMP profile conducted in 2007 on reach A b) relatively flat reflectors at this location made it an ideal choice for CMP analysis. Processed by NOP.

profile showed weak amplitudes. Vibracoring was carried out in 2004 (11 cores), and suction coring was carried out in 2005 (16 cores) and 2006 (15 cores) for the purpose of ground truthing the GPR data.

4.1.2.2 Processing

Figure 4.16 identifies processing procedures used. Raw GPR data required initial processing using Sensors and Software EKKO View Enhanced software to ensure any gaps in the traces were filled (*Fill gap* function). The line lengths were also adjusted to take into account any error arising from skipped traces (*reposition traces* function). The percentage of error was calculated from comparing lengths derived from DGPS data with that of the GPR odometer wheel. Topographic data files were then created for each line using DGPS data. Elevations for each trace were calculated by interpolating DGPS elevations at each grid node. Data were then imported into Seismic Unix, along with files of topographic data. Seismic Unix processing enabled time zero correction, signal saturation correction (dewow filter), band pass filtering and the application of gains using automatic gain control (Table 4.5). The band pass filter and dewow are determined by the frequency of the returned radar signal (see Figure 4.17) and so will vary due to the attenuation properties of the subsurface. For example, if wet sand or clay is present then a weaker signal will be returned compared to dry sand. Velocity determined from CMP analysis (see Figure 4.18) was applied for depth conversions. GPR lines were also topographically corrected in Seismic Unix using the elevation files. Migration was not applied on the data as did not significantly improve the radar signal (see Woodward *et al*., 2003).

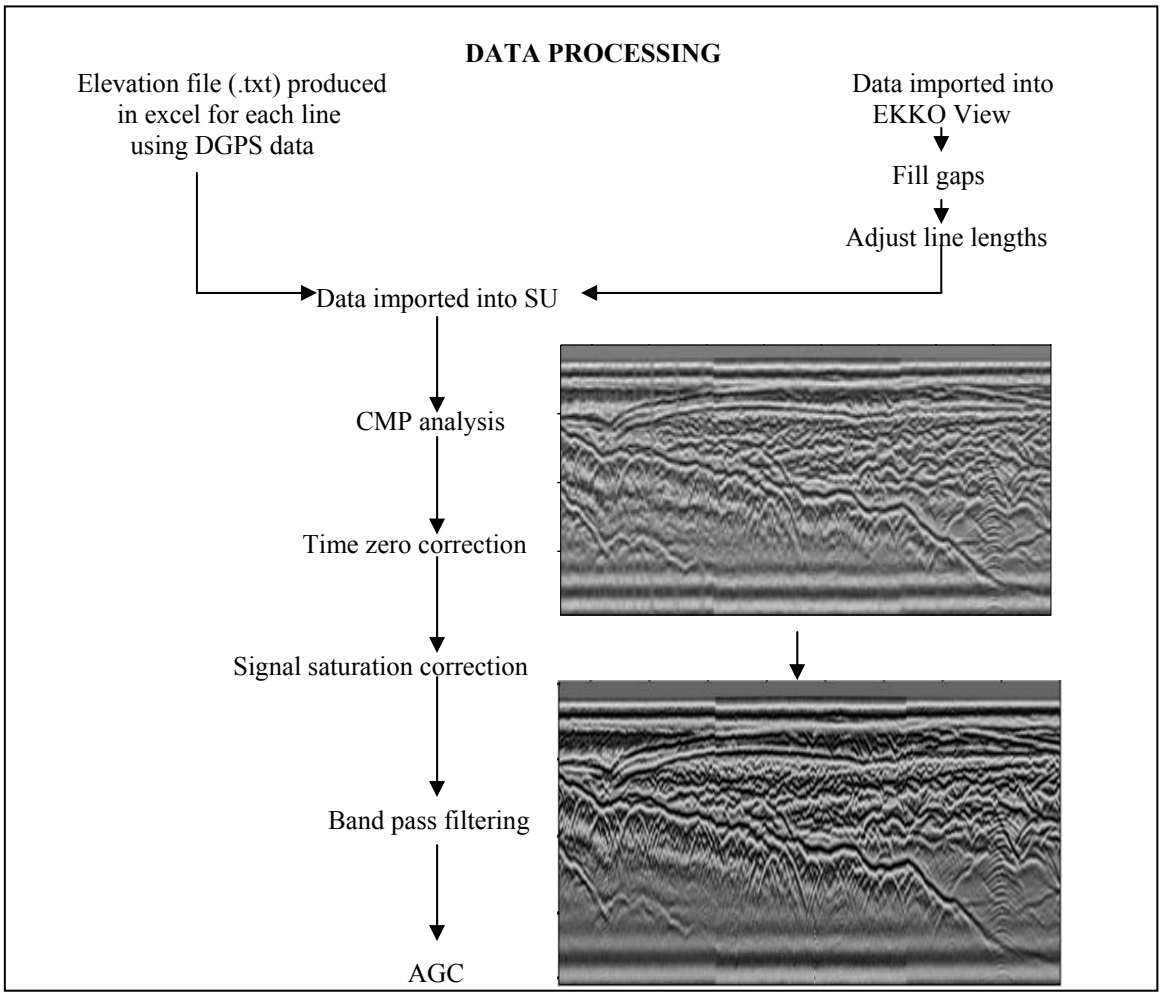

Figure 4.16. Procedure used for processing PhD data. GPR profiles at top and bottom show data before and after processing respectively. Note improvement in clarity and removal of vertical lines.

Table 4.5. GPR processing parameters. Depth conversion velocity is mean +/- 1 standard deviation.

Year	Bandpass filter (MHz)	Dewow (MHz)	Set time zero	Depth conversion velocity (mns^{-1})	AGC window (ns)	No. of CMPs	Kilometres of data processed
2004	Trapezoidal with gates at 21-40-150-300	20	Yes	0.06+/-0.012	10	6	13.46 (A)
2005	Trapezoidal with gates at 21-40-150-300	20	Yes	0.05	10	0	4.32 (A)
2006	Trapezoidal with gates at 20-40-150-300	14	Yes	0.05	10	0	8.34 (A) 2.10 (E)
2007	Trapezoidal with gates at 20-30-140-500	30	Yes	0.05+/-0.002	10	2	6.66 (A) 2.94 (E)

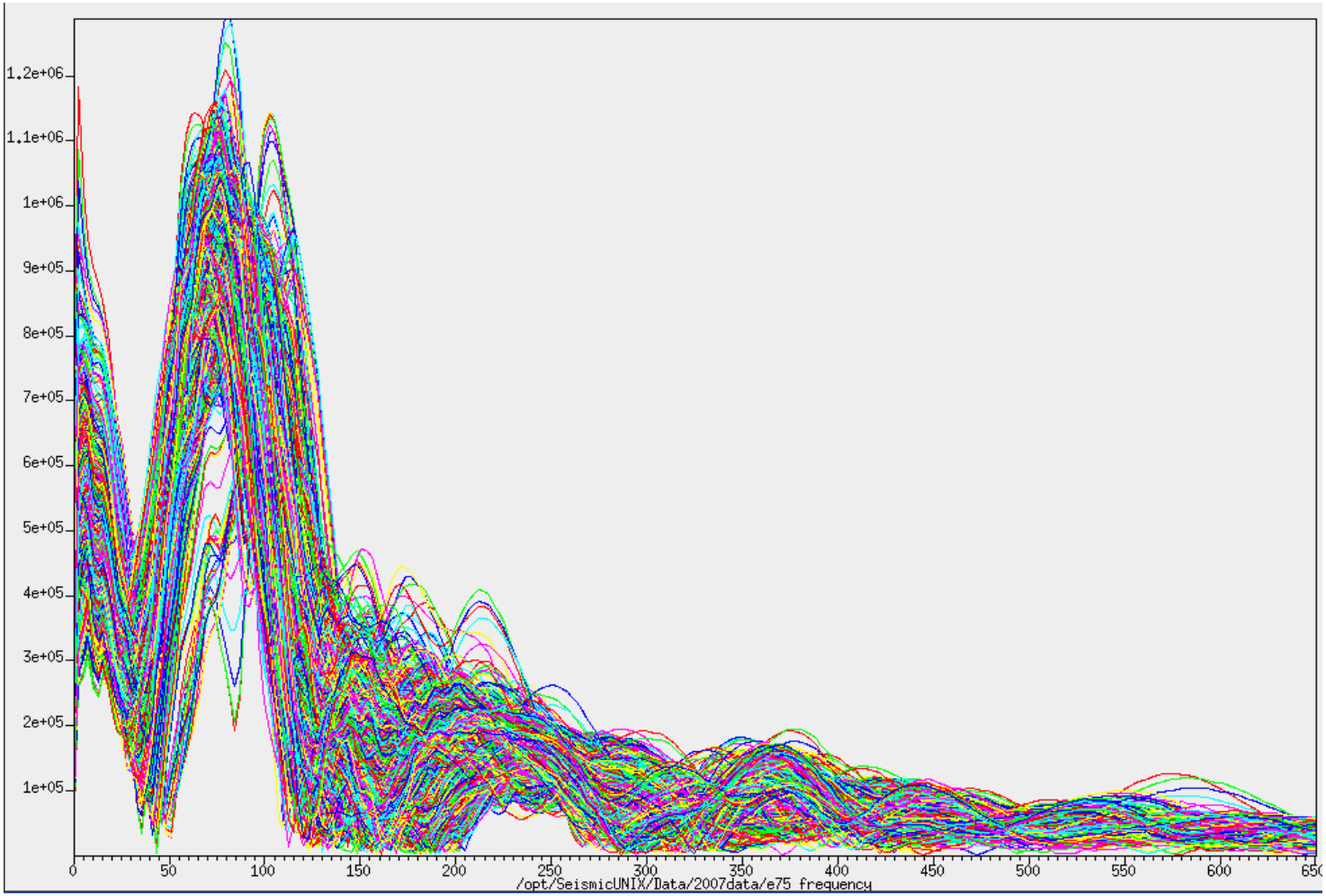

Figure 4.17. Frequency distribution of the radar signal. From this frequency distribution, a bandpass filter of 20,30,140,500 and a dewow of 0,30,40,100 were used. The bandpass filter consists of four frequencies which are chosen to compliment the amplitudes (0,1,1,0) so that: the filter removes data below the first frequency, progressively increases the proportion of data it keeps between the first and second, keeps everything between the second and third frequency, progressively reduces the proportion of data it keeps between the third and fourth and removes all data above the fourth frequency. The first frequency in the bandpass is chosen to be close to the first inversion in the frequency distribution, with each subsequent frequency approximately double the previous one. The dewow also consists of four frequencies chosen to compliment the amplitudes (0,0,1,1). This means that all data below the second frequency is removed, between the second and third frequency the proportion of data kept is progressively increased, and that all data above the fourth frequency is removed. The second frequency should be chosen so that it is close to the value of the first frequency in the bandpass filter. Each subsequent value should be approximately double the one before.

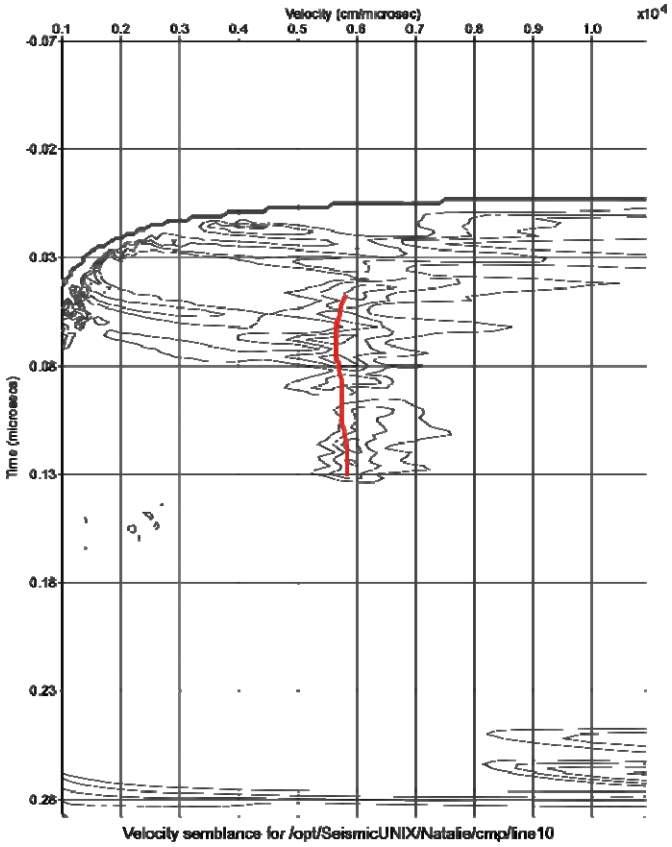

Figure 4.18. CMP velocity profile. Red line highlights velocity.

Postscript files were generated of the processed lines, and imported in to CorelDRAW Graphics Suite X3 which provided a platform for manual interpretation and quantification of the GPR data.

4.2. PHOTOGRAMMETRY

4.2.1 Theory

4.2.1.1 Introduction

Photogrammetry can be defined as "The art, science, and technology of obtaining reliable information about physical objects and the environment through processes of recording, measuring and interpreting photographic images and patterns of recorded radiant electromagnetic energy and other phenomena." Thompson (1966).

Photogrammetry has been of use in many disciplines for decades, with geomorphology often at the forefront in applications (Lane *et al.*, 2000). This has resulted in the gradual replacement of conventional methods of surface measurement based upon ground survey (Dixon *et al.*, 1998). Such methods as these are costly, time consuming, spatially constrained, invasive, and error prone (Winterbottom and Gilvear, 1997; Dixon *et al.*, 1998). Photogrammetry provides a more effective means of data collection and analysis, enabling the storage of 3D data in photographs which can be retrieved at any time (Lane *et al.*, 1993). Furthermore, developments in photogrammetry have facilitated the accurate representation of 3D topography, in the form of Digital Elevation Models (DEM) (Lane *et al.*, 1993). Further applications have been sought including the derivation of erosion and deposition volumes through the differencing of DEMs (Brasington *et al.*, 2000; Lane *et al.*, 2003) and the mapping of river bed topography through clear water (Winterbottom and Gilvear, 1997; Westaway *et al.*, 2003; Carbonneau *et al.*, 2006). Thus, photogrammetrically derived DEMs have an advantage when used in fluvial applications with submerged bed areas; attempts to map submerged beds using LiDAR (Light detection and ranging) have been unsuccessful (e.g. Charlton *et al*., 2003).

Photogrammetry is based upon the relationship between the surface of interest (3D

object), the imaging device (e.g. camera lens) and the 2D representation of the surface of interest on the recording medium (negative) (Lane *et al.*, 1993; Lane *et al.*, 2001). For an ideal photograph, it can be assumed that a straight line passes between a point on the surface (object point (X,Y,Z)), the perspective centre of the lens (X_0,Y_0,Z_0), and a point in the 2D image (x,y,z) (Lane *et al.*, 1993) (See Figure 4.19). The 2D representation of any object will have a constant value for the z coordinate which is the equivalent value of the camera's focal length (-c) (Lane *et al.*, 2001).

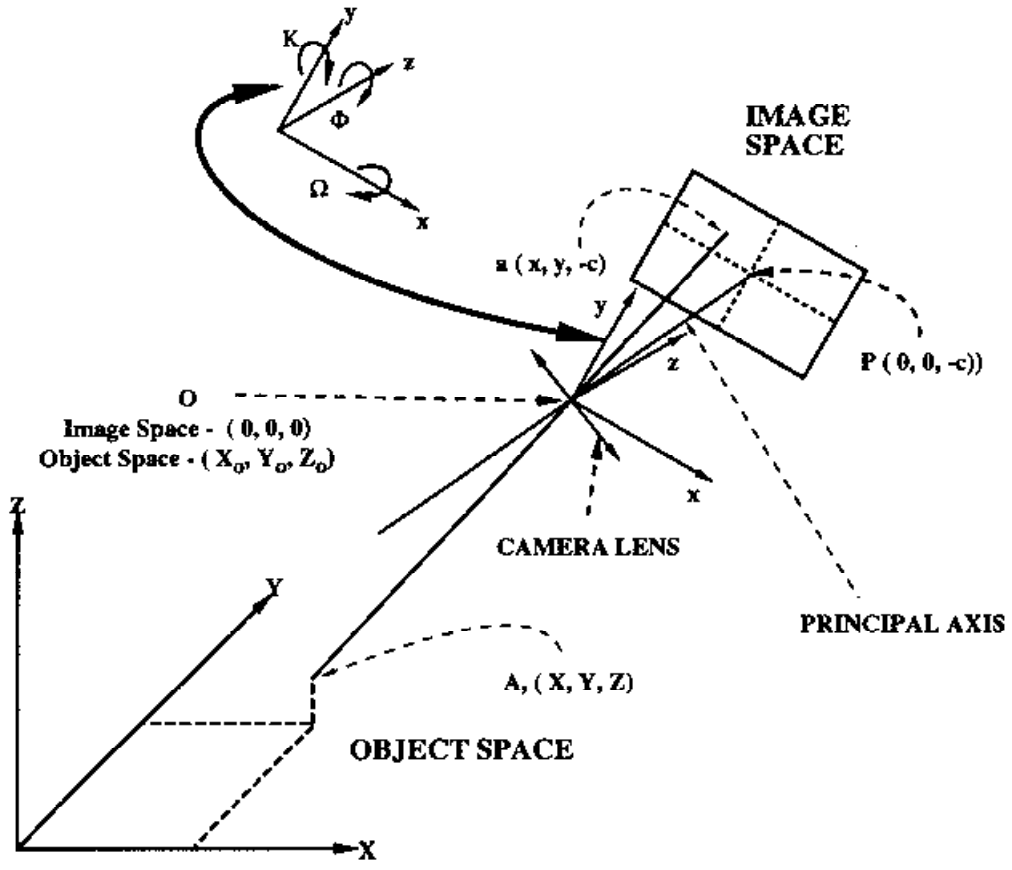

Figure 4.19. Relationship between the surface of interest (3D object), the camera lens and the 2D representation of the surface of interest on the recording medium. From Lane *et al.* (1993), p.314, Fig. 2.

This relationship is described by the projective transformation,

$$\begin{bmatrix} x \\ y \\ -c \end{bmatrix} = kM \begin{bmatrix} X - Xo \\ Y - Yo \\ Z - Zo \end{bmatrix} \qquad [4.4]$$

where k is a scale factor, and M is a rotation matrix with elements $m_{11}…m_{33}$ which are functions of ω, κ and φ (camera orientation parameters) (Lane *et al.*, 1993). The expansion of this equation yields two collinearity equations for each image point (Lane *et al.*, 1993).

$$x = \frac{-c\left[m_{11}(X - X_0) + m_{12}(Y - Y_0) + m_{13}(Z - Z_0)\right]}{\left[m_{31}(X - X_0) + m_{32}(Y - Y_0) + m_{33}(Z - Z_0)\right]} \qquad [4.5]$$

$$y = \frac{-c\left[m_{21}(X - X_0) + m_{22}(Y - Y_0) + m_{23}(Z - Z_0)\right]}{\left[m_{31}(X - X_0) + m_{32}(Y - Y_0) + m_{33}(Z - Z_0)\right]} \qquad [4.6]$$

These equations assume the special case of a perfect perspective projection, but due to factors such as imperfections in the camera lens, this is often not the case (Lane *et al.*, 2001). It is then necessary to correct for the effects of such distortion, which in a self calibrating bundle adjustment is performed simultaneously, or in the case of a metric camera with a stable internal geometry, may be corrected for before the application of collinearity equations, by modifying image coordinates (Lane *et al.*, 2001). To apply the collinearity equations, it is necessary to have a minimum of two overlapping photographs, and sufficient information on the variables and parameters in the equations; either known or calculable (Lane *et al.*, 1993). The way these parameters are determined is dependent on the photogrammetry approach

implemented (Lane *et al.*, 1993), which is discussed in the following section.

4.2.1.2 Photogrammetric approaches

Initially, photogrammetry utilised a mechanical approach, now known as analogue photogrammetry. Mechanical operations were applied using an analogue plotter to determine the relationships between the ground surveyed and camera parameters such as orientation and position (Lane *et al.*, 1993). However, limitations of the method were apparent. For example, only photography with a maximum tilt of 6 degrees from the vertical could be used; metric cameras were required in order to produce accurate results (Lane *et al.*, 1993; Dixon *et al.*, 1998). The development of analytical photogrammetry followed, utilising a mathematical approach to establish the relationship between the image space and the object space (Ghosh, 1979). A primary advantage of analytical photogrammetry is the interactive nature of the equations used (Lane *et al.*, 1993). By measuring the same point on two separate images (thus providing four image coordinates) and if the internal geometry, the camera orientations and positions are also known, then it is possible to calculate the object space coordinates of a point (Lane *et al.*, 1993; Dixon *et al.*, 1998). Conversely, if the internal geometry (e.g. focal length, displacement of the principal point) is not known, and there are many measured object space or image space coordinate sets, then it may be modelled simultaneously with the camera position and orientation in a self-calibrating bundle adjustment (Lane *et al.*, 1993, Dixon *et al.*, 1998). Bundle adjustment uses a simultaneous least squares method on a minimum of three object space coordinates (Lane *et al.*, 1993).

Therefore, analytical photogrammetry allows a greater flexibility in the use of camera media and image types, for example, oblique and historic photos can be analysed (Dixon *et al.*, 1998). Furthermore, data is captured in digital form which enables DEM production,

graphical display, and the opportunity for data transfer for manipulation in other software packages (Lane *et al.*, 1993; Lane *et al.*, 1994; Dixon *et al.*, 1998).

Recently, the development of digital photogrammetry has increased the adaptability of photogrammetry to close range work, e.g. flume studies (Lane, 2000; Butler *et al.*, 2002). Digital photogrammetry uses high resolution digital images, obtained from digital cameras or converted from aerial films through high resolution scanning, and utilises automated stereo-matching or manual matching of two images to identify paired points (Lane *et al.*, 2001). The availability of cheap stereo-matching packages for automated digital photogrammetry has increased the accessibility of photogrammetry with respect to cost, time and ease of use (Lane *et al.*, 2000). However, Lane *et al.* (2000) stress that because there are an increasing number of users lacking training in photogrammetry, the quality of data used and results obtained from automated photogrammetry are often not evaluated carefully. Also, there is often a large volume of data generated from such a process, making data handling and storage difficult.

4.2.1.3 Methods

Lane *et al.* (2001) state that project design is the critical first stage in any photogrammetry project, as the required precision of the end product (e.g. DEM) determines the coverage and scale of photographic images required. Figure 4.20 shows the suggested stages required to produce a DEM.

Ground control points (GCP) should be chosen so that they are visible on more than one photograph, and that they are located in positions which are easily identifiable (Dixon *et al.*, 1998). Elevation and horizontal positions must be established for these points, either prior to photographic survey or after images have been acquired so that optimum GCP locations can be determined (Dixon *et al.*, 1998). With respect to image acquisition, a basic photo pair

is required. However, knowing the camera positions is critical in order to achieve an optimum geometric configuration (Dixon *et al.*, 1998). In particular, it is advantageous to maximise the sine of the parallactic angle (the angle between two intersecting light rays focusing on a common point in stereoscopic view (Wolf, 1983)); and to minimise the distance between the objects and cameras (Lane *et al.*, 1993). However, too large an angle may prevent stereo-vision from being acquired, and similarly, too small a distance between object and camera may constrain the field of vision (Lane *et al.*, 1993).

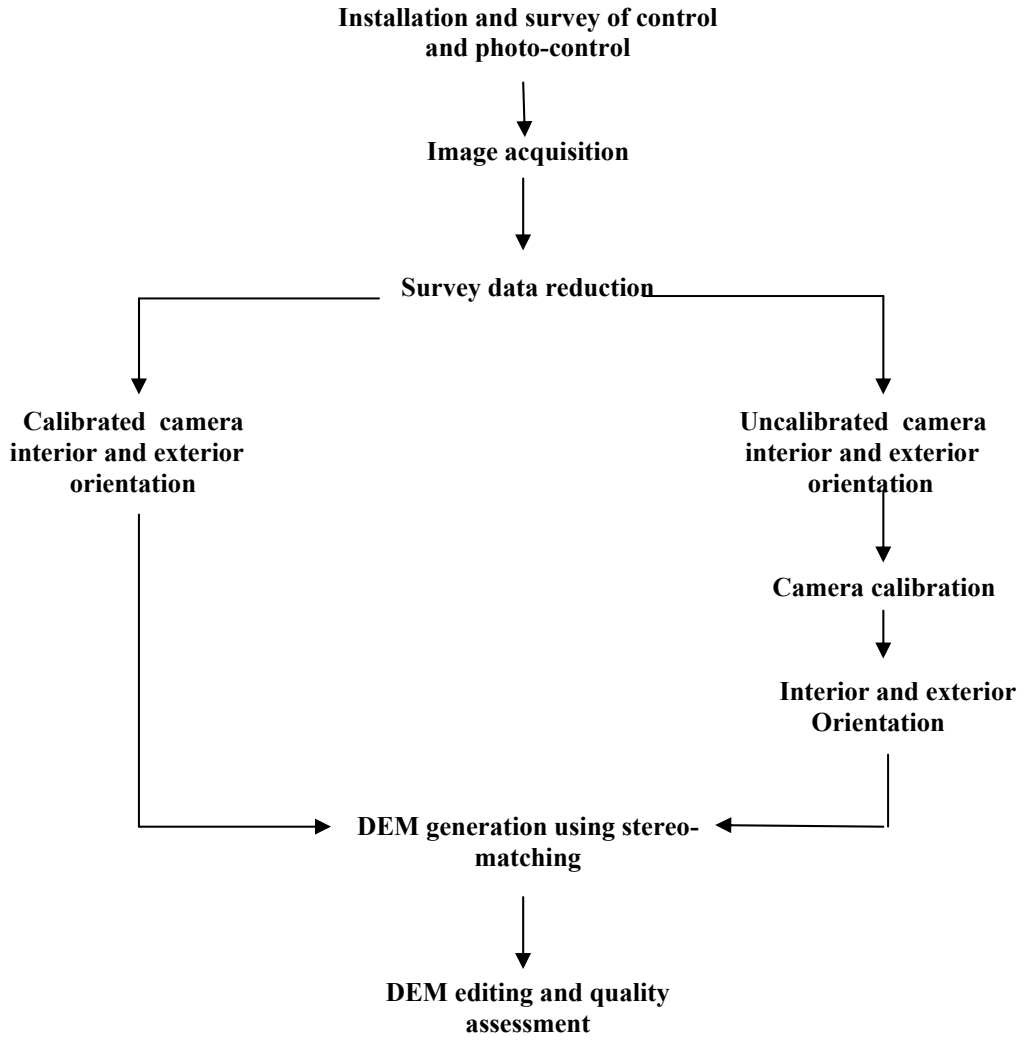

Figure 4.20. Stages required to produce a DEM using digital photogrammetry. From Lane *et al.* (2001), p.873, Fig. 2.

If images are required to be scanned, the resolution of scanning must also be considered carefully as it is an important control on surface resolution and data precision, since the pixel size will determine the highest density of a DEM (Lane *et al.*, 2000). The next major stage is to perform orientation procedures which allow the reconstruction of the original rays that were projected onto the negative (Dixon *et al.*, 1998). The process of simultaneous bundle adjustment achieves these orientations.

There are three types of orientation: inner (or interior), relative and absolute (or exterior) (Ghosh, 1979). Inner orientation utilises the fiducial marks on the photographs to restore the internal geometry of the camera at the time of exposure (Lane *et al.*, 2000). Relative orientation re-establishes the relationship between two images at time of exposure (Lane *et al.*, 2000) using the collinearity equations (Wolf, 1983). Finally, absolute orientation utilises GCPs to translate and rotate the stereo-model to the scale and orientation required (Dixon *et al.*, 1998). Wolf (1983) explains that errors in ground control values can also be taken into account, and adjusted in the process, resulting in a bundle adjustment that reduces the sum of squares of the weighted residuals for ground control and photogrammetric measurements.

With orientation performed, the next stage is elevation data generation using stereo-matching procedures. If more than one pair of photographs is used, then a continuous strip can be made through coordinate transformations performed on adjacent models (Wolf, 1983). Epipolar geometry can be employed in stereo matching which greatly reduces processing time (Wolf, 1983). For two photographs, left and right photo planes exist which are intersected by the epipolar plane (Wolf, 1983). Thus, for a given point location on the left photograph in the overlap area, the corresponding point on the right photo is known to lie on the epipolar line (Wolf, 1983). In digital photogrammetry, area-based or feature-based algorithms are

implemented to detect pixel pairs (Lane *et al.*, 2000). The area-based approach may involve epipolar geometry, but primarily correlates small windows of pixels on one gridded image with a corresponding image (Lane *et al.*, 2000). Feature-based approaches establish point matches through the structural information in the images, however, in some situations topography may not be sufficiently variable (Lane *et al*, 2000).

Point coordinates are then transformed into X, Y and Z model coordinates which provide the necessary data required for DEM generation (Wolf, 1983). Three major methods exist for DEM configuration; triangulated irregular network based, grid based and contour based, each having different processing requirements (Moore *et al.*, 1991). For modelling natural topography, the Delaunay Triangulation is the most popular method as it uses all data points provided to create the surface, and is flexible with respect to the distribution of data points (Lane *et al.*, 1994). However, if there is a high density of data points, as obtained through digital photogrammetric methods, then a grid based method is routinely applied.

The final stage in the photogrammetric process is to assess the quality of the DEM produced and to edit the DEM as necessary.

4.2.1.4 Quality assessment of DEMs

DEM quality is essentially dependent on data point quality; the distribution and density of data; and the surface reconstruction technique employed (Li, 1992). Lane *et al.* (1994) explain that error in data points can be separated into three forms: random, gross, and systematic. Random error controls the precision of data and arises in the measurement process (Lane *et al*, 2004). Gross errors, also known as blunders, result from erroneous data measurements due to human or equipment error (Lane *et al.*, 1994) and control data reliability (Lane *et al.*, 2004). Finally, systematic errors control the accuracy of data and result when

the functional model (collinearity equations) inaccurately represents the relationship between the photo-coordinates and object space points (Butler *et al.*, 1998). This may be due to factors such as lens distortion (Lane *et al.*, 1994).

The distribution and density of data points has an important control on the accuracy of topographic depiction since more points will result in a better representation of true surface form. Areas with a higher incident of topographic change would benefit from a higher number of data points. As always though, a trade off exists between computational time and the degree of surface representation attained. The method used to produce a surface from the data points also has a significant bearing on the DEM quality (Dixon *et al.*, 1998). For example, Lane *et al.* (1994) explain that during triangulation, errors may occur at boundaries of the data collection area such that surfaces may be formed between points that do not exist in reality. Limitations may also occur in the method of data collection over the surface. For example, photogrammetry software such as the CHEST version of ERDAS Orthomax does not allow for grid size to locally increase or decrease (Lane *et al.*, 2000). Furthermore, through developments in photogrammetry, increased reliance is placed on numerical algorithms for identifying corresponding points in a stereo photo pair, thus with no operator input, if the software cannot successfully match points, interpolation may be performed which could be a source of significant error (Lane *et al.*, 2000).

Butler *et al*. (1998) suggest a three stage procedure for assessing DEM quality. Firstly, the examination of ortho images allows a qualitative inspection. Secondly, statistics generated from the DEM processing stage allows the determination of the strength of correlation between matched pixels (Butler *et al.*, 1998). For example, matched points can be ranked into categories of good, fair and poor, depending on the user defined precision value (Butler *et al.*, 1998). Thirdly, the comparison of DEM derived points and corresponding

check points provides a reliable method of assessing DEM quality (Butler *et al.*, 1998; Westaway *et al.*, 2003). The standard deviation or root mean square error (RMSE) of height differences is traditionally used to evaluate this (Butler *et al.*, 1998). However, Lane *et al.* (2004) criticise the use of this statistic as it only allows the determination of precision if the mean error is zero. More reliable is a statistic that takes into account the measurement of mean error and standard deviation of error such as the variance of error:

$$\sigma_e^{\,2} = \frac{1}{n-1}\sum_{i=1}^{n}(e_i - \bar{e}_i)^2 \qquad [4.7]$$

Where σ_e is the standard deviation of error, n is the number of observations, *ei = zei – zci; zei* is the DEM estimated elevation of point *i, zci* is the independently measured elevation of point *i* (Lane *et al.*, 2004). This equation is reduced to the RMSE when mean error is zero (Lane *et al.*, 2004). Measures of error, however, may vary across a surface e.g. where blunders are present, so that global measures of error cannot be applied to the whole surface (Lane *et al.*, 2004). Removal of isolated significant errors will therefore allow the adoption of a more regional measure of data quality (Lane *et al.*, 2004).

Once errors have been identified, the next stage is to remove or reduce these. Lane *et al.* (2004) stress that the correction procedure utilised should have an empirical and theoretical foundation. In particular, re-collection of data points that are the cause of errors is favoured (Lane *et al.*, 2004). Furthermore, procedures must not introduce any new error into the data (Lane *et al.*, 2004).

4.2.1.5 Applications in fluvial geomorphology

4.2.1.5.1 DEMs of difference

Developments in analytical and digital photogrammetry have enabled the 4-dimensional study of topography through the differencing of DEMs (Brasington *et al.*, 2000). The subtraction of

DEMs representing different epochs allows a quantification of morphological change (Lane, 1998). As such it is of valuable use in fluvial geomorphology as the technique can be used to quantify volumes of erosion and deposition, and identify patterns spatially (Lane *et al.*, 2003). Furthermore, measures of change in process rates can be obtained by subtracting a DEM of difference from a successive DEM of difference (Lane *et al.*, 1993).

The methodology used to calculate such measures of change needs to be considered carefully in order to obtain reliable results (Lane, 1998). As discussed before, errors can arise in each stage of DEM production, thus they need to be taken into account. DEM grid size is a particularly important factor since sufficient topographic data is required to represent the DEM surfaces and therefore accurately derive any change in volume between the DEMs (Brasington *et al.*, 2000). Simple subtraction of grid nodes will allow surface comparison, providing the DEMs have the same grid spacing and origin (Lane, 1998).

Due to errors, there is a real need to asses the quality of the DEM of difference and hence derived parameters of volume change. In particular, thresholds are required so that statistically significant levels of change can be determined (Brasington *et al.*, 2000; Lane *et al.*, 2003). Lane *et al.* (1993) define the threshold value for elevation change on a DEM of difference as

$$\sigma_e = \left(\sigma_{e_1}^2 + \sigma_{e_2}^2\right)^{0.5} \qquad [4.8]$$

Where σ_e is the standard deviation of the error of the DEM of difference and σ_{e1} and σ_{e2} are the standard deviations of error of individual DEMs. A σ_e of 0.3 m would mean that any elevation change detected between -0.3 and 0.3 m was not significant.

Lane *et al.* (2003) produced DEMs of difference for a reach of the Waimakariri River, New Zealand. Thresholds for detection of significant change were applied to individual points based on their location (i.e. wet or dry area) and hence based upon the accuracy of the

point itself (Lane *et al.*, 2003). The resultant significant changes were then compared to their expected change, with respect to wet and dry bed areas of the reach (Lane *et al.*, 2003).

4.2.1.5.2 Bathymetric mapping

In fluvial environments, there is a necessity to represent submerged zones of river beds in DEMs. Depending on the water clarity, different methods can be used. Intensive ground survey of bed elevation e.g. tacheometric surveying, may be necessary where waters are of a high suspended sediment concentration, however, this method is costly and time consuming. Where waters are relatively clear, methods have been developed utilising digital photogrammetry.

Winterbottom and Gilvear (1997) and Westaway *et al.* (2003) have both utilised the reflectance properties of water and the river bed to determine water depth. This method is dependent on there existing a good correlation between water depth and reflectance levels (Winterbottom and Gilvear, 1997). Water colour is a function of the behaviour of light, and is influenced by suspended sediment concentration, water surface back scatter, river bed characteristics, and depth (Winterbottom and Gilvear, 1997; Westaway *et al.*, 2003). However, the level of light reflected is not linearly related to depth as an exponential decrease of light intensity occurs with distance (Winterbottom and Gilvear, 1997). This is demonstrated in Figure 4.21.

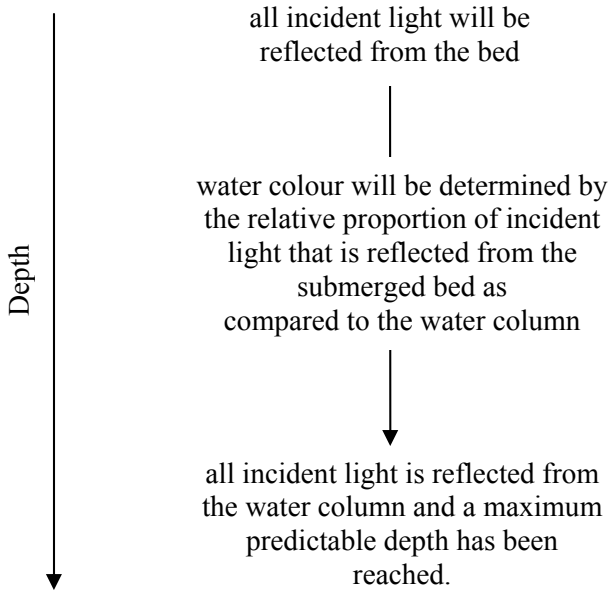

Figure 4.21. Variation of the colour spectrum of river water with depth. Adapted from Westaway *et al.* (2003).

An algorithm that describes this relationship in a linear form was proposed by Lyzenga (1981);

$$X_i = \ln L_i - Lw_{(i)} \qquad [4.9]$$

Where X_i represents the parameter linearly related to the depth of water (in band *i*), L_i is the water brightness and $Lw_{(i)}$ represents the deep water reflectance (Winterbottom and Gilvear, 1997). Applying this relationship in practice first requires the conversion of aerial photographs into digital images. The image can then be classified into wet and dry areas, and the wetted pixels red green blue (RGB) intensity values obtained by removing dry areas (Westaway *et al.*, 2003). Following Lyzenga (1981), a natural logarithmic transformation can be applied to the RGB values in order to establish a linear relationship between depth and water colour (Westaway *et al.*, 2003). Comparison with depth measurements yields a regression relationship which can be calibrated and validated through ground survey methods

(Westaway *et al.*, 2003). Furthermore, inspection of the curve produced by plotting estimated with surveyed depth allows the identification of maximum predictable depth (Westaway *et al.*, 2003). Estimated depths can then be subtracted from water surface elevation to produce a wet bed DEM, which can then be combined with a dry bed DEM to produce a surface for the whole river bed (Westaway *et al.*, 2003).

Carbonneau *et al.* (2006) determine water depths based on the same theory as Lyzenga (1981) but using the Beer-Lambert Law which describes the absorption effect on light as it passes through a media such as water. In this method however, the brightness of unsubmerged wetted clasts is used to provide a value for the incoming intensity of light, thus providing a correction for illumination variations (Carbonneau *et al.*, 2006).

Refraction correction is another method, which was developed by Westaway *et al.* (2000), for use on shallow gravel bed rivers with clear water and a submerged bed visible on photographs. Refraction of light causes a perceptible increase in bed elevation, thus by applying the refractive index (1.34) to the apparent DEM derived water depth; it can be corrected, and a more representative DEM produced (Westaway *et al.*, 2000).

Recently Lane *et al.* (In press) created DEMs for submerged areas of the South Saskatchewan River using 1:5000 scale grayscale imagery. Depths were determined for wet areas through calibration of the spectral signature (Lane *et al*., In press). Firstly, equal interval classification was applied to wet area points to select points with accurate depth estimates (based on elevation values) for pixel brightness (DN). The depths were then corrected for light refraction by applying the refractive index (Westaway *et al*., 2001). The corrected depths were then correlated with pixel values. This relationship was modelled and applied to all wet area points to obtain accurate depths. Wet and dry area DEMs were then merged to yield a complete DEM.

4.2.1.5.3 Archival image analysis

Lane *et al.* (In press) have developed a methodology which allows for archival and future imagery analysis. For one epoch, aerial images were acquired and specially set out targets (GCPs) were ground surveyed. The GCPs were used to produce a high quality bundle adjustment and subsequent DEM. From the bundle adjustment, a new set of GCPs were identified that could easily be viewed on both archival and future imagery e.g. building corners, large boulders, and bases of telegraph poles.

4.2.2 Methodology

DEMs were created for wet and dry areas of the study reach for October 2006 and July 2007 following the methodology of Lane *et al.* (In press) (Figure 4.22).

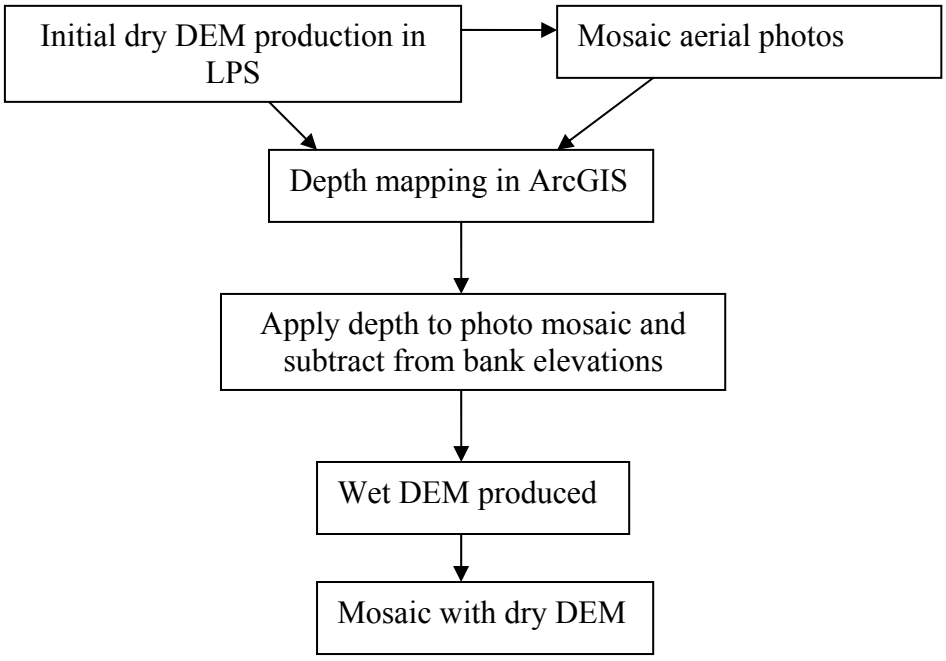

Figure 4.22. Main stages of DEM production for wet and dry areas.

4.2.2.1 Aerial photograph processing

Aerial photographs were flown of the reach at a 1:5000 scale in October 2006 (colour image) and July 2007 (grayscale image) by Geodesy Remote Sensing Inc., Calgary, and were scanned at a resolution of 7 μm by BKS Surveys Ltd, Co. Londonderry. The October 2006 photographs were converted to 0 to 255 grayscale in Erdas IMAGINE as required for the DEM process. Firstly, the RGB image is converted to an IHS (Intensity hue saturation) colourspace using *Image interpreter->spectral enhancement->RGB to IHS*. The IHS colourspace represents colour images in terms of the intensity of colour, the hue (colour), and the saturation (the amount of colour). By extracting just the intensity band, a greyscale image can be obtained which is scaled from 0 to 1 (*Image interpreter->utilities->subset*). Finally, this grayscale image is rescaled to an unsigned 8 bit image; resulting in a grayscale from 0 to 255 (*Utilities->rescale->unsigned 8 bit*).

4.2.2.2 Initial DEM production

ERDAS IMAGINE Leica Photogrammetry Suite 9.1 (LPS) was used for initial DEM production. Aerial images were imported into LPS and camera parameters were set including interior orientation through the location of fiducial points. Table 4.6 shows parameters set for block properties and triangulation properties. Using the ground point transfer methodology developed by Lane *et al*. (In press) (see section 4.2.1.5.3), ground control points were transferred from the September 2004 photogrammetric solution to the October 2006 and July 2007 images. This entailed importing known x, y, z coordinates of the 2004 GCPs, and manually locating them on 2 or 3 overlapping images for 2006 and 2007. Tie points were then added by manually identifying common points on paired images (e.g. boulders or building corners). A larger number of tie points were added to the 2007 images to aid

triangulation as only 11 GCPs could be located, compared with 14 in 2006. Triangulation was then performed. Results of the triangulation quantified the quality of the solution, through the total image unit-weight root mean square error (RMSE) (the quality of the entire solution based on image coordinate residuals) and control point RMSE for X, Y and Z coordinates (individual RMSEs for ground control points) (ERDAS IMAGINE 9.1 online help). The triangulation report also contained information on the quality of individual ground control points. Ground control points and tie points were manually adjusted at the pixel scale in order to improve their positions on paired images and thus to decrease root mean square errors (see Table 4.6 for Triangulation results). The ideal RMSEs of ground control points correspond to the dimensions of pixels in the surface (= scan resolution ÷ scale of imagery) (Lane *et al*., 2001). Thus, with an imagery scale of 1:5000 and a scanning resolution of 7 μm, DEM precision is approximately 0.035 m (5000 m * 0.000007 m). Thus, ideal RMSE values

Table 4.6. Parameters and results for Triangulation and DEM extraction from final versions of October 2006 and July 2007 DEMs.

		October 2006	**July 2007**
Triangulation	# GCPs	14	11
	# Tie points	47	87
	Total image unit-weight RMSE	1.58	0.71
	GCP RMSE (m)	X=+/-0.0401 Y=+/-0.050 Z=+/-0.224	X=+/-0.033 Y=+/-0.032 Z=+/-0.120
DEM parameters	Cell size	0.5x0.5 m	0.5x0.5 m
	Search window, correlation limit, correlation size	5x5, 0.7, 7x7	5x5, 0.7, 7x7
DEM results	Mass point quality	Excellent 13.7%, Good 72.4%, Suspicious 13.9%	Excellent 5.5%, Good 79.1%, Suspicious 15.4%
	Vertical accuracy (VA) RMSE	0.71	1.80
	Block GCP to DTM VA	0.93	1.10
	Block tie point to DTM VA	0.63	1.80

for X and Y are around +/-0.04 m. The resolution (i.e. the frequency with which heights may be determined) is ~5 * precision (Lane *et al.*, 2001). Thus, the ideal RMSE for Z is around +/-0.20 m.

DEM extraction was then performed (see Table 4.7 for extraction parameters) and a DEM extraction report produced detailing mass point quality and global accuracy statistics including RMSE values. Mass point quality detailed the percentage of points in each class of excellent (points matched in 2 images with a certainty of 85 to 100%), good (points matched in 2 images with a certainty of 70 to 85%), fair (points matched in 2 images with a certainty of 0 to 70%), isolated and suspicious points (Figure 4.23). To improve the percentages of excellent and good points and to decrease the RMSE, triangulation and DEM production stages were re-run until an improved result was found (see Table 4.6 for final results). This included adding extra tie points, and further adjustment of GCPs and tie points to improve their matching on paired images.

Two DEM outputs for each epoch were created for use in ArcGIS. Firstly an ASCII file containing X and Y coordinates, elevation values, and data quality information for each point. The ASCII file was imported into ArcCatalogue, converted into a shape file, and then imported into ArcMap in ArcGIS. Secondly an orthophoto was generated in LPS from the aerial images. Using the information from the DEM production, images are orthorectified i.e. corrected for terrain displacement (ERDAS IMAGINE 9.1 online help). The aerial images were then mosaiced (i.e. stitched together) using the mosaic tool in ERDAS IMAGINE. The aerial images were cropped prior to mosaicing in order to remove fiducial marks and black areas bordering the images, preventing remnants of these features appearing in the mosaiced image. Cutlines were manually drawn across overlapping image areas, and feathering was applied in the mosaic process to blend pixel information in the overlap area. Convolution

	Class Names	Color
0	Background	
1	Excellent	
2	Good	
3	Fair	
4	Isolated	
5	Suspicious	

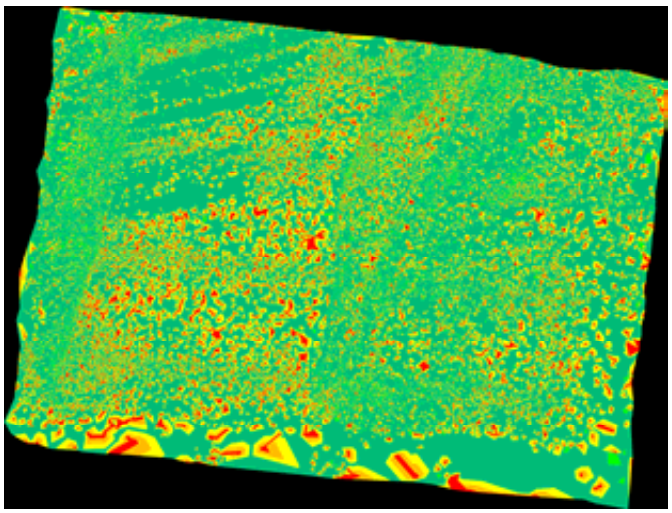

Figure 4.23. A DEM point quality output

filtering was then applied to the mosaiced image using a 7x7 low pass filter. This process averages pixel values across a 7x7 pixel window to produce a smoothed image, and therefore remove any noise in the data. The image was then cropped to include only the channel and bank areas and imported into ArcMap.

4.4.2.3 Depth of wetted area

The depths of submerged areas were determined using the methodology developed by Lane *et al.* (In press) to calibrate the spectral signature of the imagery (see section 4.2.1.5.2). In greyscale imagery, pixel values (DN) range from 0 to 255, where 0 is black and 255 is white. Therefore, lower pixel values represent higher depths and vice versa.

Firstly, DEM data points suitable for calculating the depth of the river channel were selected. The criteria was that points had an elevation lower than 473 m (maximum bank elevation in the reach), and a quality of 1 (excellent) or 2 (good). These points were exported into a new shape file in ArcGIS, and the point file was clipped to remove emergent bar areas within the channel. Any dry points left over were also deleted manually.

Secondly, in ArcMap, using *Spatial Analyst->Extraction->Extract values to points*, pixel values (DN) were extracted from the mosaic and appended with elevation data from the modified DEM shape file. This produced a dBase File containing X, Y, elevation data, DN, and quality information for each point in the channel area. A shape file of this was produced and imported into ArcMap. The attributes elevation and DN were then classified into equal interval groupings of 10 classes (see Table 4.7) and data fitting this depth-brightness distribution were selected.

Table 4.7. Equal interval classification for Z and DN values, July 2007.

Equal Interval Class	Z	DN
1	469.9-470.3	9-29
2	470.4-470.6	30-49
3	470.7-470.9	50-69
4	471.0-471.2	70-89
5	471.3-471.5	90-110
6	471.6-471.8	111-130
7	471.9-472.1	131-150
8	472.2-472.4	151-170
9	472.5-472.7	171-190
10	472.8-473.0	191-210

Points that fell into a class were exported as a new dBase file and imported into an Excel spreadsheet. Water surface elevation was calculated for each point based on the left bank elevation values. Apparent depth was then calculated by subtracting point elevation from water surface elevation. Depth values were then corrected for light refraction by applying the refraction index (multiplying by 1.34) (Westaway *et al*., 2000). The resulting depth values were taken as representing real depth. Depth brightness modelling was then carried out in order to predict depth based on pixel DN. Real depths and their corresponding pixel values were sorted with depth to find DN values at the highest depths. An extinction depth pixel was chosen from the highest depths to represent the depth at which light could no longer penetrate

the water column. The extinction depth and corresponding DN were then modelled into depth equations (Lane *et al*., In press) where

For DN values > extinction depth DN

$$\textbf{Predicted depth} = (G * \ln(DN - \text{extinction DN})) + I \quad [4.10]$$

And for DN values <= extinction depth DN

$$\textbf{Predicted depth} = \text{extinction depth} \quad [4.11]$$

Where G is the gradient, and I is the intercept calculated from linear regression analysis between real depth and ln(DN – extinction depth). The resulting predicted depth was then correlated with real depth to assess the fit of the relationship. Depth was then modelled with alternative extinction depths and corresponding DN values until the best predictor was found (see Table 4.8 for final results).

4.2.2.4 Bed elevation

The depth equation was applied in Arc GRID to the mosaic which had been clipped free of dry areas. This resulted in depth values for every wet point in the reach (Table 4.8). A raster containing values of water elevation for the whole reach was then produced in ArcMap by applying natural neighbourhood interpolation to elevation values from the left bank (*Spatial analyst->Interpolation->Natural neighbourhood*). To produce the bed elevation values, the

Table 4.8. Final results for depth mapping procedure.

	October 2006	**July 2007**
Extinction depth (m)	2.33	2.46
Extinction pixel value (DN)	40	65
Intercept value, Gradient value	4.404, -0.818	3.782, -0.721
Predicted depth v Real depth: Correlation coefficient, mean error, standard deviation	0.67, 0.01, +/-0.24	0.74, 0.00, +/-0.23
Predicted depth range (m)	0.09-2.33	0.01-2.46

depth raster was subtracted from the water elevation raster in Arc GRID. This created a DEM for the channel area.

4.2.2.5 Complete DEM

The wet area DEM was mosaiced with the original DEM produced in ERDAS IMAGINE. This was done in Arc Map using *Data management->Raster->Mosaic to new raster,* with the wet DEM inputted prior to the original DEM. The mosaic method FIRST is used to ensure that only wet DEM values are chosen in the overlap area. The resulting mosaic is a complete DEM of the channel and bank areas of the reach.

4.2.2.6 Deriving geomorphological variables from DEMs

DEMs of difference were derived to quantify morphological change between epochs. In addition to the 2006 and 2007 DEMs, DEMs were obtained for 2004 and 2005 (Lane *et al*., In press). In order to produce a DEM of difference, cell size and area of coverage is required to be the same for each DEM. The 2004 and 2005 DEMs had a cell size of 1.0 x 1.0 m, so resampling was performed on the 2006 and 2007 DEMs to obtain the same cell size (from 0.5 x 0.5 m). A template of the study area excluding banks was manually digitised in ArcMap and was used to clip all of the DEMs to the same area. DEM grids were then subtracted from each other in ArcGRID to produce a DEM of difference.

4.2.2.7 Errors apparent in DEMs

With both the October 2006 and July 2007 dry DEMs, 'banding' occurred where individual DEMs overlapped. These are erroneous points, thought to be caused by random errors in estimating camera orientation and precision, which propagate into systematic errors in overlap

areas (Lane *et al*., 2004). To reduce the error, a method was adopted from Lane *et al.* (2004). Individual DEMs were stitched together using a distance-weighting algorithm which averaged the points between the two DEMs based upon distance from the overlap centre (where error is worse). This removed the banding for both DEMs.

The October 2006 images were transformed into greyscale from colour for the DEM process. Unfortunately, this resulted in the transformed images containing a small range of very low pixel values (i.e. darker pixels) in the channel areas and relatively little detail could be made out on the channel bed in comparison with the 2007 aerial images (see Figure 4.24). In the depth mapping stage, this resulted in many of the pixels being at or below that of the extinction depth. The final DEM shows a lack of elevation variability on areas of the primary channel, and a distinct lack of submerged unit bars compared with 2005 and 2007. Based on knowledge of the study reach it is concluded that the lack of morphological units is inherent from the depth mapping of the aerial image and not a real representation of the channel bed. This will be taken into account when analysing the 2006 DEM in the following chapter.

Streaks were noticeable on the July 2007 images, which appear as feint light coloured lines present along the channel length. In the depth mapping procedure they have been interpreted as areas of higher elevation (see Figure 4.25). These areas, whilst having erroneous elevation values, only account for a very small proportion of data points on the DEM so are not a significant source of error.

On all DEMs, there were a number of points that the depth mapping had over estimated; this may be due to the presence of silt on the channel bed. Thomas (2006) explains the limitation of the depth mapping method as not being able to accurately calculate the depth of all pixels due to differences across the river in illumination, substrate type, turbidity and water surface state. Thomas (pers. comm., 2009) encountered these problems with the

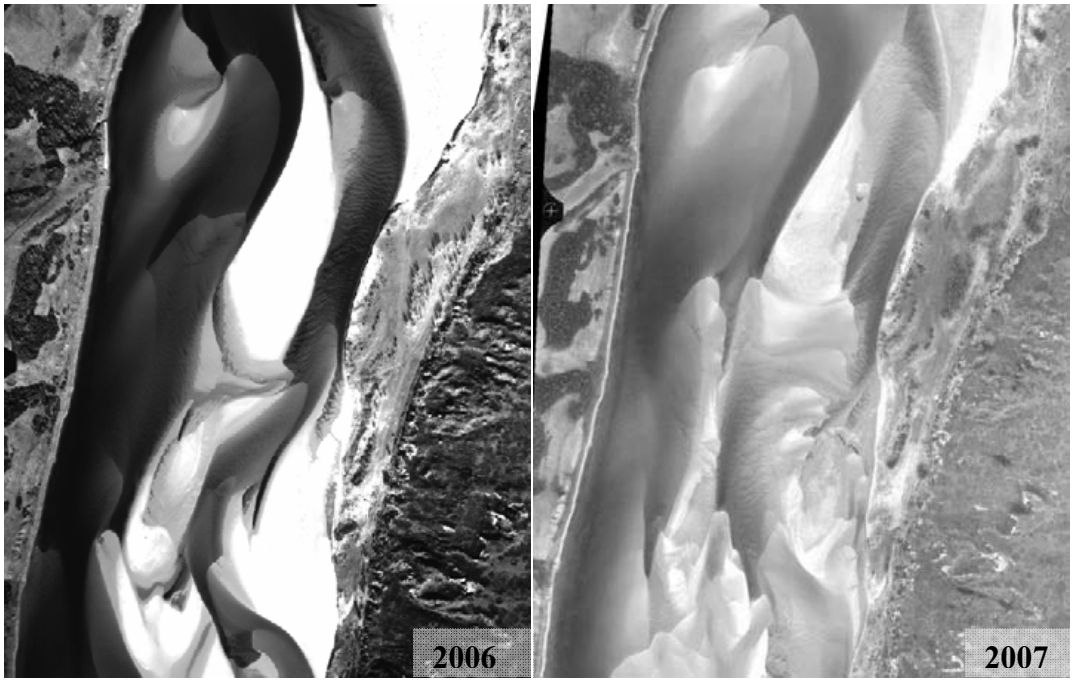

Figure 4.24. Grayscale aerial images for 2006 and 2007. Note the darker pixels in the primary channel in 2006.

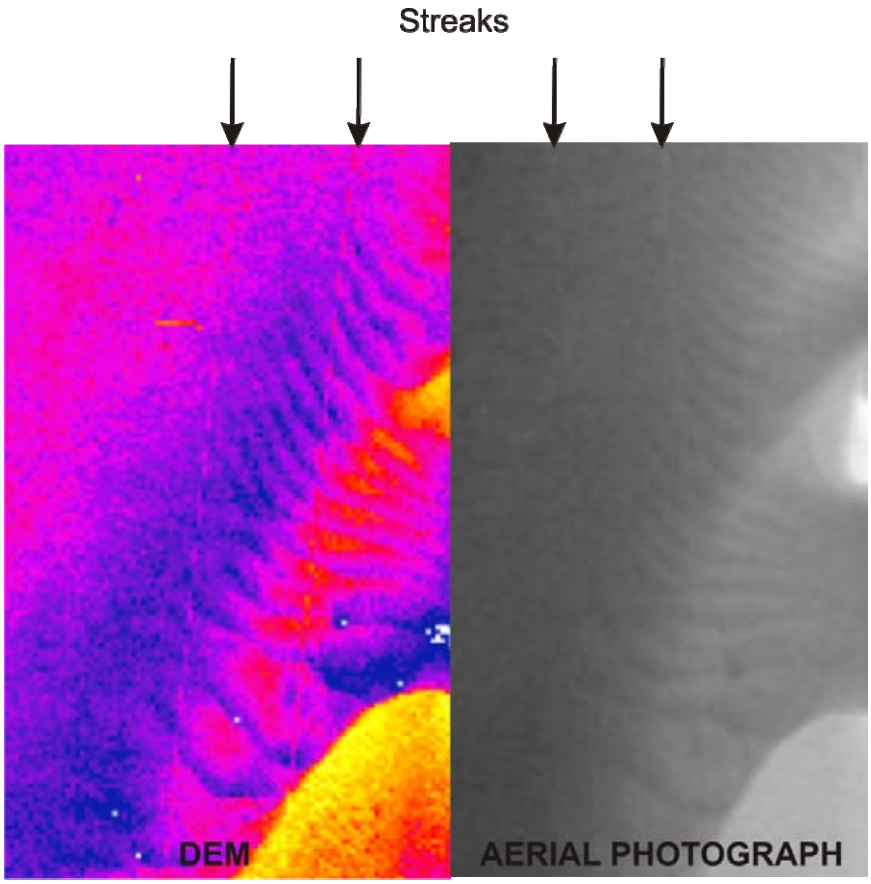

Figure 4.25. Streaks in the aerial photograph and their representation in the DEM for July 2007.

September 2004 and August 2005 DEMs, and removed points that were 'too deep' due to the presence of silt or clay. The silt or clay substrate had resulted in a different relationship between depth and light intensity compared to sandy substrate (Thomas, pers. comm., 2009). It was thus decided to remove points that were 'too deep' from the 2006 and 2007 DEMs.

Furthermore, some data points had been underestimated in the depth mapping process and given the maximum depth value (extinction depth). Thomas (pers. comm., 2009) quantified that only 2 % of points were underestimated, and that these were spread out across the reach. Therefore, it is unlikely that there has been a significant loss of morphology as, for example, if the elevations of a deep channel have been underestimated then their data points would be clustered along the channel path.

4.2.2.8 Assessing DEM accuracy

GPS surveys were conducted in July 2006 and August 2007 on exposed bar areas on the study reach to aid GPR data collection. The GPS data were used as check data for the elevation values that the October 2006 and July 2007 DEMs predicted. In ArcMap, using *Spatial Analyst -> Extraction -> Extract values to points*, DEM derived elevations were extracted for each location a GPS elevation value had been obtained for. Mean error was then calculated (GPS elevations minus DEM elevations) as a measure of the accuracy of the DEM. The standard deviation of the error was also calculated as a measure of the DEM precision (Table 4.9). The mean error for October 2006 is fairly small at -0.05 m, and suggests that the DEM elevation values are slightly overestimated based on the July 2006 data. However, deposition may have occurred on the bar surfaces due to aeolian reworking between July and October 2006, and thus may account for the mean error. Standard deviation is +/-0.53 m, which is fairly high; however, it is acceptable for dry areas on this reach, which are expected to have

higher errors due to the lack of surface texture. For July 2007, mean error was greater at 0.64 m, with a standard deviation of +/-0.28 m. This suggested that systematic errors were present in the DEM model and that the DEM underestimated elevations by 0.64 m on average. The systematic errors were thus corrected for by the addition of 0.64 m to the DEM. The residual mean error (assessed by using extra check points not used in the initial error assessment) is 0.15 m with a standard deviation of +/-0.44 m.

Lane *et al.* (In press) calculated the mean error for the September 2004 DEM as -0.08 m, with a standard deviation of +/-0.31 m. Following Lane *et al*. (2003), the standard deviation of error can be propagated to identify a minimum level of detection in DEMs of difference. Thus using equation 4.7 (section 4.2.1.5.1), and assuming the standard deviation is similar for August 2005, the minimum levels of detection for dry areas on DEMs of differences are +/-0.44 m (2004 - 2005), +/-0.61 m (2005 - 2006) and +/-0.69 m (2006 - 2007). Therefore any change in elevation within these limits may be due to random noise. Furthermore, this means that any bedforms apparent on the dry areas of the DEM which have heights less than the levels of detection may be due to random error (Thomas, 2006).

For inundated areas no check data exists for October 2006 and July 2007. However, in the depth modelling stage, 'real' depth values were obtained by applying the refraction index to depths calculated by subtracting the elevation of excellent quality points from water surface elevation. These 'real' depth values were compared with predicted depth values. Mean errors and standard deviation of errors were thus calculated (Table 4.8). Mean errors relate to systematic errors in the DEM and are very low in both cases (0.01 and 0.00 m). The standard deviation of the error relates to random error and measures +/-0.24 and +/-0.23 m respectively.

However, Lane *et al.* (In press) determined the accuracy of inundated areas for the September 2004 DEM using dGPS data. They concluded that generally, errors for wet areas were less than those for dry areas. They suggested sources of error as the presence of silt or clay on the bed (see section 4.2.2.7) and also error being propagated from the dry DEM through the use of dry DEM water surface elevations in the depth modelling. Following Lane *et al*. (2003), the minimum level of detection in DEMs of difference for wet areas is +/-0.39 m (based on a standard deviation of +/-0.279 m for September 2004). Thus, any change in elevation between -0.39 and 0.39 m may be due to random noise.

All of the error values calculated above relate to maximum possible error. In order to determine the extent of errors with respect to DEM interpretation, bedforms were identified from the DEMs and their dimensions quantified and compared to bedforms identified from other sources. Dunes identified on the channel bed had similar mean heights to those quantified by Lunt *et al.* (In prep.) through echo-sounding and GPR techniques. Lunt *et al.*(In prep.) measured mean dune heights of 0.15 m for flows less than 100 m^3s^{-1}, and 0.49 m for flows > 600 m^3s^{-1}. This compares with mean dune heights of 0.15 m for 57 m^3s^{-1} (from the 2004 DEM) and 0.43 m for 292 m^3s^{-1} (from the 2005 DEM). The similarity in measurements suggests confidence in the DEMs, and in the identification of bedforms, in spite of the possible random errors. Furthermore, dunes and unit bars identified from the DEMs display typical geometries for their bedform type, and have been identified from DEMs in the same locations as they have been observed in the field and from aerial photographs.

With respect to the DEMs of difference, the error margins encompass morphological changes arising from small bedforms such as the migration of dunes, but also unit bar migration and channel incision across bar tops. However, the patterns of erosion and deposition associated with such changes, especially unit bar growth, appear to be accurately

represented on the DEMs of difference, and demonstrate that these changes represent real processes on the reach.